



**Politecnico
di Torino**

Politecnico di Torino

DEPARTMENT OF MECHANICAL AND AEROSPACE ENGINEERING (DIMEAS)

Master's in Mechanical Engineering

2020/2023

Modeling and Experimental Characterization of a Stockbridge Damper

Master's thesis

December/2023

Supervisors:

Prof. Dario Anastasio

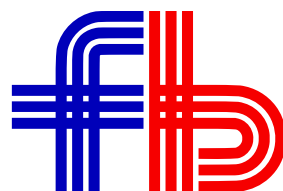
Prof. Alessandro Fasana

Company Supervisor:

Eng. Mattia Passuello

Student:

Kodanda Challa



Abstract

An aeolian vibration damper plays a vital role in overhead electrical power transmission lines by mitigating the vibrations caused by wind-induced excitation, thereby ensuring the durability of the conductor wires.

Among the various aeolian vibration dampers available, a Stockbridge-type damper consists of a wire, known as the messenger cable, with three lumped masses. Two of these masses are positioned at the endpoints of the wire, while the third mass acts as a clamp. This setup enables the damper to be easily installed on the conductor. This kind of damper gets the excitation from the clamp that is in contact with the conductor and it is typically designed to exhibit a specific response within a frequency range that varies based on factors such as the conductor type, wind conditions, and various environmental parameters.

This thesis has the aim of investigating the behavior of such a damper experimentally and the implementation of a mathematical model that fits the collected data.

The first part of the activity consists of testing a damper prototype on a shaker, to measure its response to many kinds of controlled input profiles. The damper is always mounted on the placement with the same tightening torque: what changes is the excitation profile of the shaker base, which is always controlled in amplitude within a frequency range from 4 to 40 Hz. The datasets contain the measured amplitude and force given to the base and, thanks a certified software that process this data and gives out the dynamical stiffness and phase of the damper.

The second part of the activity consists in implementing a basic finite element model (FEM) of the damper, which is capable of computing the response at each node to the excitation of the base. This is a plane model with 6 degrees of freedom having only rotation and displacement in the vertical plane of the masses. Hysteretic damping is considered and flexural stiffness is assumed as constant for the entire messenger cable as an initial guess.

Among the several different parameters entering the model, a vector containing the most uncontrolled ones is used to set a cost function to be minimized in order to estimate the values that give the best fit with the data. Generally, the geometry of the damper is known, so inertial properties and lengths are considered with a very small possible variation. On the other side, the stiffness and damping properties of the messenger cable, that is the kernel of the damper, are very difficult to estimate because the nominal value known from formula in the literature can be reduced of orders of magnitude while the cable is working: this happens mainly because the single ropes of the messenger wire can displace and slide one over the other.

The fitting method leaves a certain freedom in the choice of the cost function. Different cost functions are tried using the powerful tool of a genetic algorithm, searching for the one that better minimizes and at the same time better represents the shape of the system experimental response. To do so, common sense limits are set to the parameters of the cost function in order to avoid a parameter being dominant (absorbing all the error) even if it is not in the realm. With

the same scope, geometrical and inertial parameter are set to be from 95% to 105% of the real very well-known value.

The final result of the entire activity is having a map for both flexural stiffness and loss factor of the damper – the messenger wire - both in amplitude and in frequency. This map is useful to predict the behavior of the same messenger cable used in different configuration of the damper, for example with different cable lengths or masses. This is important to tune the damper to different conductors, giving a certain elasticity to the system and to give a tailor-made solution for different customers.

The third part of the activity considers the fitting of the same FE model, but including a non-constant bending stiffness to take into account geometrically nonlinear effects. This should be considered as a first step towards the development of a fully nonlinear model of the Stockbridge damper.

Eventually, all the previous steps are repeated on a second damper prototype to ensure the analysis's accuracy and reliability.

Table of contents

<i>Introduction</i>	1
1.1 Aeolian vibration	3
1.2 State of the art	4
1.3 Application to the study case	5
<i>Experimental analysis</i>	7
2.1 Experimental setup	7
2.2 Input excitation	10
2.3 Calibration	13
2.4 Collected datasets	14
2.5 Datasets quality check	17
2.6 Outliers removal	21
2.7 Conclusion from different tests	24
<i>Finite element model</i>	27
3.1 Scheme of the damper (FEM)	27
3.2 Element 1	29
3.3 Element 2	34
3.4 Assembly	36
3.5 Equation of motion	39
3.6 Damping matrix	40
3.7 Dynamic stiffness and phase (Master/slave method)	41
<i>Model fitting</i>	45
4.1 Introduction to genetic algorithm	45
4.2 Euclidean fitness function	49
4.3 Parameters of Stockbridge damper	51
4.4 Curve fitting with different sets (θ_1, θ_2 and θ_3) of parameters	56
4.5 Optimized parameters from all tests	61
4.6 Conclusion on curve fitting	62
4.7 Comparison of between different samples	66

<i>Improved model</i>	69
5.1 Non-constant flexural rigidity	69
5.2 Curve fitting with θ_1 parameters (improved model).....	70
5.3 Optimized parameters for improved model.....	75
5.4 Conclusion on improved model.....	76
<i>Appendix</i>	77
A. Tests on dampers	77
B. Lumped mass contribution.....	78
C. MATLAB - 6 DOF model	82
References	84

List of figures

Figure 1.1. Stockbridge nomenclature	2
Figure 1.2. Different types of messenger cable.....	2
Figure 1.3. Birth mechanism of aeolian vibration.....	3
Figure 2.1. Experimental setup for Stockbridge analysis (Layout).....	8
Figure 2.2. Load cells and accelerometer.....	8
Figure 2.3. Experimental setup for Stockbridge analysis (Lab).....	9
Figure 2.4. Input vs frequency	10
Figure 2.5. Calibration curve.....	13
Figure 2.6. Dynamic stiffness & phase vs frequency.....	16
Figure 2.7. Deviation in dynamic stiffness and phase data.....	19
Figure 2.8. Dynamic stiffness and phase vs frequency (Test2-1).....	20
Figure 2.9. Mean curves for different Z score.....	23
Figure 2.10. Comparison of Test1-1 and Test2-1	24
Figure 2.11. Comparison of Test1-1, Test2-1 and Test2-2	24
Figure 2.12. Comparison of tests	25
Figure 2.13. Comparison of Test1-1 after lubrication.....	25
Figure 3.1. Stockbridge damper parameters.....	28
Figure 3.2. Stockbridge damper scheme	28
Figure 3.3. Local co-ordinate system	29
Figure 3.4. Scheme diagram for element 1	29
Figure 3.5. Free body diagram for mass 1.....	30
Figure 3.6. Free body diagram for the element 1	30
Figure 3.7. scheme diagram for element 2	34
Figure 3.8. Dynamic stiffness and phase vs frequency plot from model.....	43
Figure 4.1. Genetic algorithm flowchart	46
Figure 4.2. Frequency step	50
Figure 4.3. Stockbridge damper dimensions	51
Figure 4.4. Stockbridge damper (3D).....	54
Figure 4.5. Output of genetic algorithm (Damper1, Test1-1, Set θ_1 parameters)	58
Figure 4.6. Output of genetic algorithm (Damper1, Test1-1, Set θ_2 parameters)	59

Figure 4.7. Output of genetic algorithm (Damper1, Test1-1, Set θ_3 parameters)	60
Figure 4.8. Number of parameters vs computational time	62
Figure 4.9. Flexural stiffness vs input displacement at the clamp (Damper1).....	64
Figure 4.10. Loss factor vs displacement with set θ_1	65
Figure 4.11. Flexural stiffness vs displacement (Damper1 and damper2).....	66
Figure 4.12. Loss factor vs displacement (Damper1 and damper2).....	67
Figure 5.1. Output of genetic algorithm (Damper1, Test1-1, Second order polynomial).72	
Figure 5.2. Output of genetic algorithm (Damper1, Test1-1, Third order polynomial)....	73
Figure 5.3. Output of genetic algorithm (Damper1, Test1-1, Fourth order polynomial)..	74
Figure 5.4. Flexural rigidity (EJ) vs frequency	76

List of tables

Table 2.1. Tests and displacements	11
Table 2.2. Frequency step increment	12
Table 4.1. Inertial properties of masses.....	52
Table 4.2. Inertial and stiffness properties of the messenger cable.....	53
Table 4.3. Parameters sets to optimize	55
Table 4.4. Limit box for the parameters.....	55
Table 4.5. Optimized parameters for different sets	61
Table 4.6. Flexural stiffness for different input displacement at the clamp.....	63
Table 5.1. Optimized parameters from improved model	75

Chapter 1

Introduction

The Stockbridge damper is a device used in power lines to suppress wind-induced vibrations, which can cause fatigue damage and ultimately lead to the failure of the lines. This simple and effective device has become instrumental in reducing the need for maintenance and repairs. It was invented by George H. Stockbridge, who received a patent for it in 1926 [1].

A sample Stockbridge damper is shown in Figure 1.1, and consists of two weights attached to either ends of a messenger cable, which is clamped around the conductor of the power line. It is designed to vibrate at the primary frequencies at which the power line vibrates, like a tuned-mass-damper.

At low frequencies, the whole damper swings as a pendulum with the weights providing the inertia. At high frequencies, the damper cable oscillates with a wave-like motion. Due to their inertia, the weights try to remain stationary while the damper cable moves, causing bending strain in the cable and friction between the wires of the messenger cable and so reducing the amplitude of the vibration of the power line.

The greater the relative friction between the wires, the higher the energy that is dissipated. Figure 1.2 shows different configuration of messenger cable.

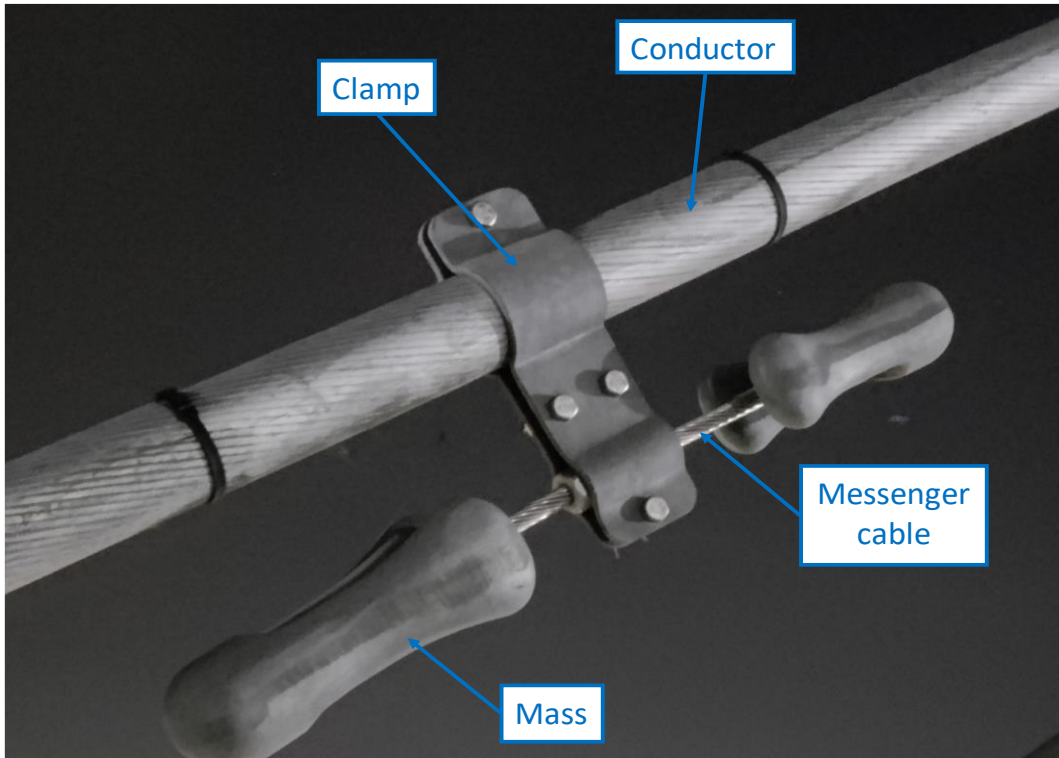


Figure 1.1. Stockbridge nomenclature

As wind speeds fluctuate, the frequency of the vibrations induced by the wind also changes. To counteract this, the damper's mass and length are selected to accommodate a wide spectrum of frequencies, based on the modes of vibration of the conductor.

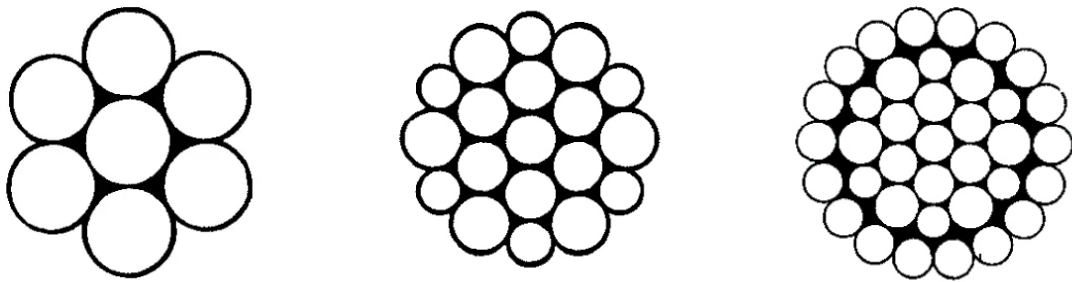


Figure 1.2. Different types of messenger cable

1.1 Aeolian vibration

Aeolian vibration is a high-frequency and low-amplitude type of motion caused by wind acting on conductors and overhead ground wires of transmission and distribution lines. It is generally linked with non-turbulent winds ranging from 1 m/s to 7 m/s, and it can be a daily occurrence. The conductor oscillates due to the transverse wind as shown in Figure 1.3.

The frequency of aeolian vibration is determined by the wind speed and the dimensions of the conductor cable, with the experimental formula [2] [6]:

$$f = S \cdot \left(\frac{v}{d}\right)$$

where:

- S is the Strouhal' number [3] (between 0.185 and 0.2)
- v is the wind speed (m/s)
- d is the conductor diameter (m)

Under severe aeolian vibrations, the maximum vibration amplitude typically equals the conductor diameter. This is most likely to occur in long spans with high conductor tensions under steady winds.

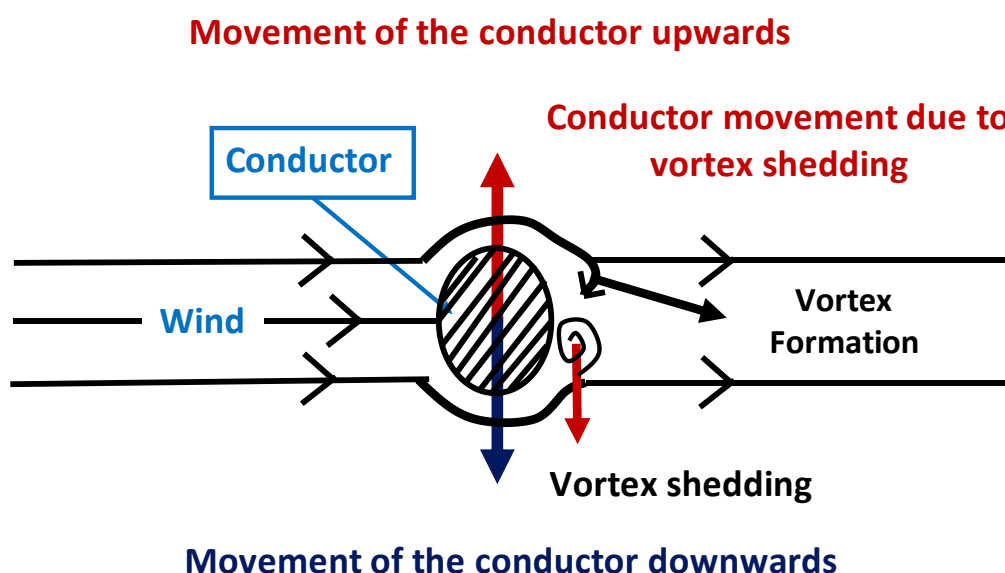


Figure 1.3. Birth mechanism of aeolian vibration

1.2 State of the art

The first investigations and studies on conductors used for the transmission and distribution of electrical energy were carried out by Claren and Diana [4], who hypothesized a model based on the assumption of the messenger cable treated as a Bernoulli Euler beam. The experimental validation of Claren and Diana's model [4] came from Barbieri et al. [5] who compared the free response of the cable analytically with the experimental response based on its length and pre-tensioning.

Subsequently, research focused on the dynamic response of the conductor, considering the influence of wind action. Diana et al. [6] demonstrated that the force was proportional not only to the flow velocity hitting the cable but also to its diameter and length.

Initially, many models were developed with assumption of treating the mass as a 2-degree-of-freedom system, one for vertical translation and one for rotation. It was then connected to an element representing the clamp through the messenger cable modeled as a rod. All these models were based on the assumption that the mass of the messenger cable was very small and therefore negligible.

Among these, Kim [7] presented a parametric analysis of the resonance frequencies of the device based on its characteristic dimensions, such as length, total mass, and stiffness of the messenger cable. Leblon et Hardy [8], on the other hand, derived an analytical expression for the four elements of the impedance matrix, which expresses the proportionality between the clamp's movement (translation and rotation) and the force and moment exerted by it on the conductor.

The most noticeable evolution over time of the Stockbridge damper, more than in material or form, lies in the transition from a symmetric to an asymmetric appearance, in terms of cable dimensions and weight of masses at the ends. This change has allowed increasing resonance frequencies from two to four, thus expanding the working frequency range when well-designed. This shift has led to the need to develop new models considering both the right and left parts. Diana et al. [9] developed a six-degree-of-freedom analytical model to simulate the behavior of the Stockbridge at low frequencies.

The analysis conducted by Onore [10] to understand the operation of dampers was focused on developing an analytical model. This model aims to simulate the real behavior of dampers and evaluate their effectiveness using various Stockbridge parameters. It will serve as the foundation for this thesis and efforts were made to enhance the model through the utilization of a genetic algorithm.

1.3 Application to the study case

In the present study case, all the experimental investigation is made on a damper prototype designed to hold conductor of diameter 28÷34 mm subjected to wind velocity in the range 1÷6 m/s. Hence the frequency range is between [5.44, 42.8] Hz by applying the experimental formula.

Chapter 2

Experimental analysis

2.1 Experimental setup

The prototype is tested on an electromagnetic shaker, its clamp is fixed on the base of the shaker at the prescribed tightening torque. The test consists in feeding an excitation profile to the device (i.e., the shaker base) in terms of amplitude over a specific range of frequencies. The shaker is governed in closed loop by a certified control software and the adopted sensors are all calibrated: the entire test bench is called DTS (Damper testing system). The logged signals are post processed by the same software that can produce many types of diagrams like dynamic stiffness, power dissipated, impedance.

The displacement of the clamp is logged thanks to an accelerometer solid with the shaker base. The damper's response in terms of force is logged with two load cells.

A schematic diagram can be seen in Figure 2.1, while two photos of the experimental setup are shown in Figure 2.2 and Figure 2.3.

The DTS software operates as follows:

1. Stabilization at target frequency (tolerance $\pm 0.01\%$)
2. Stabilization at target amplitude (tolerance $\pm 5\%$)
3. Recording and FFT (Fast Fourier Transform)
4. Change frequency and restart from step 1

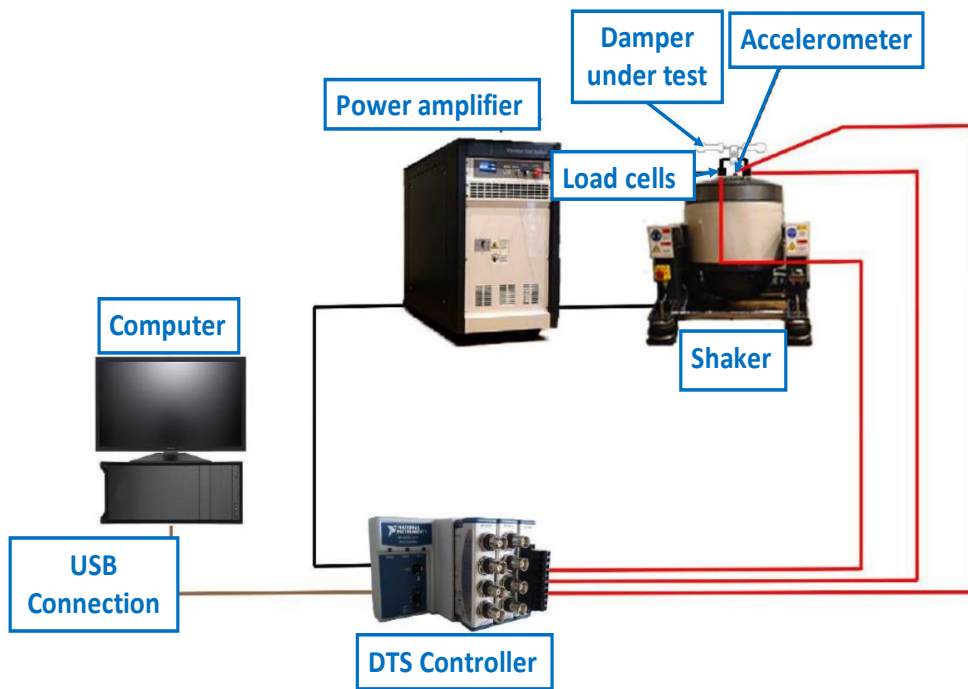


Figure 2.1. Experimental setup for Stockbridge analysis (Layout)

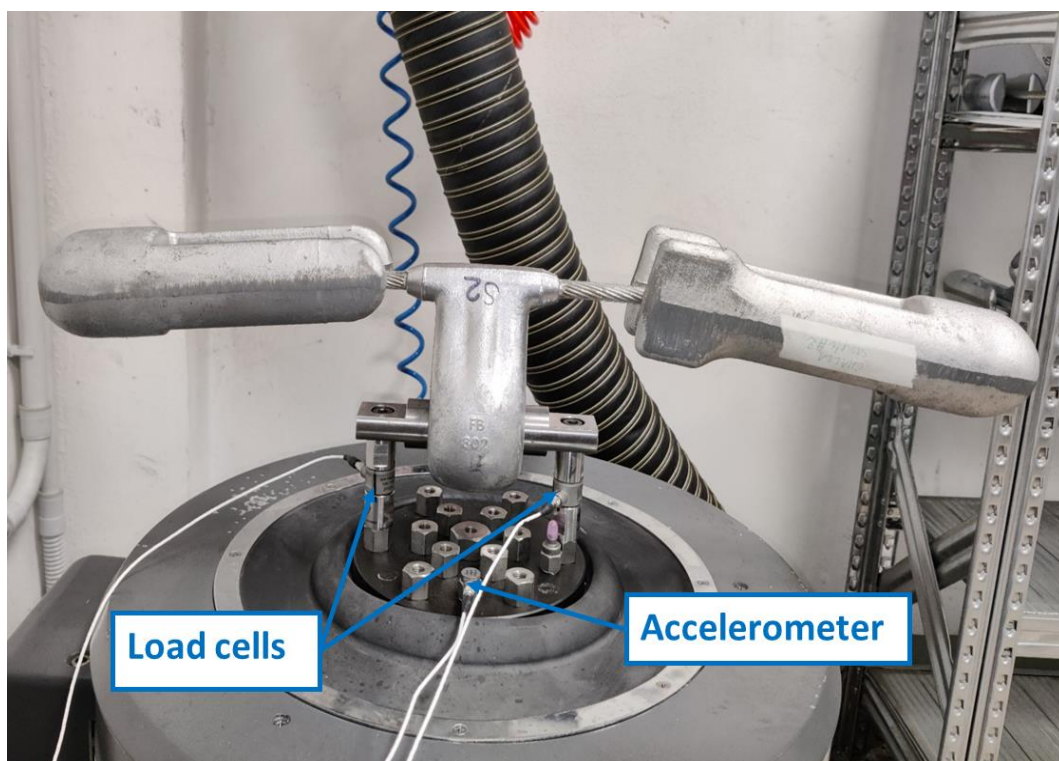


Figure 2.2. Load cells and accelerometer



Figure 2.3. Experimental setup for Stockbridge analysis (Lab)

2.2 Input excitation

The experiments on the damper consisted of sine tests with constant amplitude over a certain frequency range.

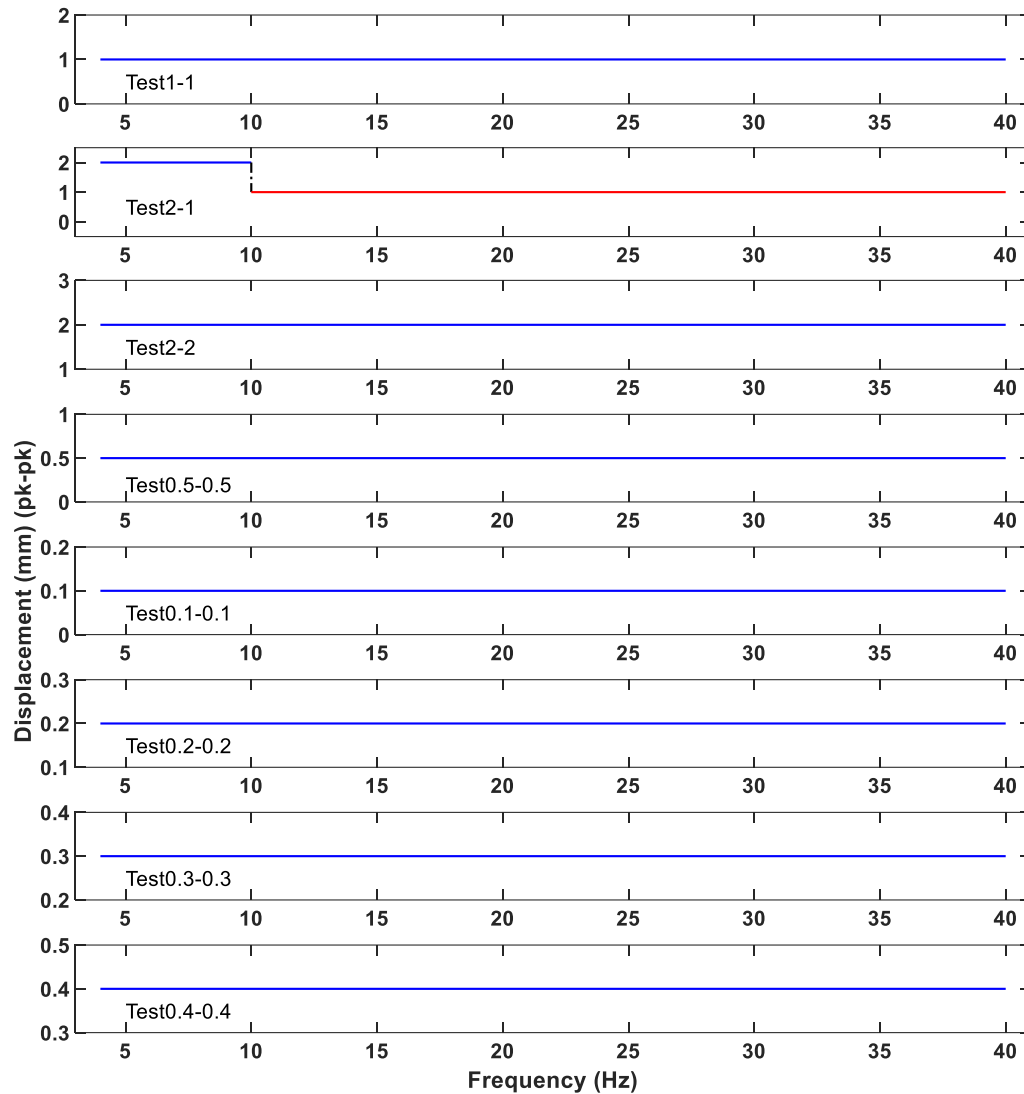


Figure 2.4. Input vs frequency

Eight different tests are conducted as shown in Figure 2.4. A summary is here reported.

- **Test1-1:** Constant amplitude of 1mm over frequency range 4-40Hz.
- **Test2-1:** Constant amplitude of 2mm over frequency range 4-10Hz and constant amplitude of 1mm over frequency range 10 - 40Hz.
- **Test2-2:** Constant amplitude of 2mm over frequency range 4-40Hz.
- **Test0.5-0.5:** Constant amplitude of 0.5mm over frequency range 4-40Hz.
- **Test0.1-0.1:** Constant amplitude of 0.1mm over frequency range 4-40Hz.
- **Test0.2-0.2:** Constant amplitude of 0.2mm over frequency range 4-40Hz.
- **Test0.3-0.3:** Constant amplitude of 0.3mm over frequency range 4-40Hz.
- **Test0.4-0.4:** Constant amplitude of 0.4mm over frequency range 4-40Hz.

Test1-1 is re-conducted after lubrication to analyze the behavior of damper after lubrication. The reader can refer to Appendix A for more details.

Test	Displacement p-p (mm)
Test1-1	1
Test2-1	2(4-10Hz) & 1(10-40Hz)
Test2-2	2
Test0.5-0.5	0.5
Test0.1-0.1	0.1
Test0.2-0.2	0.2
Test0.3-0.3	0.3
Test0.4-0.4	0.4

Table 2.1. Tests and displacements

The frequency increments on each test are not constant, as listed in Table 2.2. These frequency increments are kept equal for all the tests.

Frequency (Hz)	Step (Hz)
4-9	0.5
10-30	1
32-40	2

Table 2.2. Frequency step increment

2.3 Calibration

Prior to commencing experiments on a damper within a shaker, a calibration test is conducted without the damper to mitigate errors arising from factors such as friction and temperature. Calibration is a critical process in the utilization of laboratory shakers, and the following are some reasons underlying the necessity of calibration preceding experimentation:

- **Accuracy and Precision:** Calibration is the act of testing and adjusting the precision and accuracy of an instrument. It reduces the bias in an instrument's readings, ensuring that the data collected is both precise and accurate.
- **Standard Compliance:** A routine shaker validation test ensures that the laboratory shaker is performing according to standard. This is important for maintaining the integrity of the experimental results and ensuring they are reliable and reproducible.
- **Longevity of Instruments:** Instruments can degrade for several reasons, including usage frequency and the environment in which they are used. Calibrating the equipment and keeping it up to standards can help extend its usage life.

In Figure 2.5, the red line and green line respectively denote the upper and lower limits for dynamic stiffness calibration. Following the calibration of the shaker, the validity of its calibration is determined by assessing whether the calibration curve (depicted in blue) falls within these limits. A shaker is deemed suitable for experimentation with a damper only if the calibration curve conforms to the specified limits.

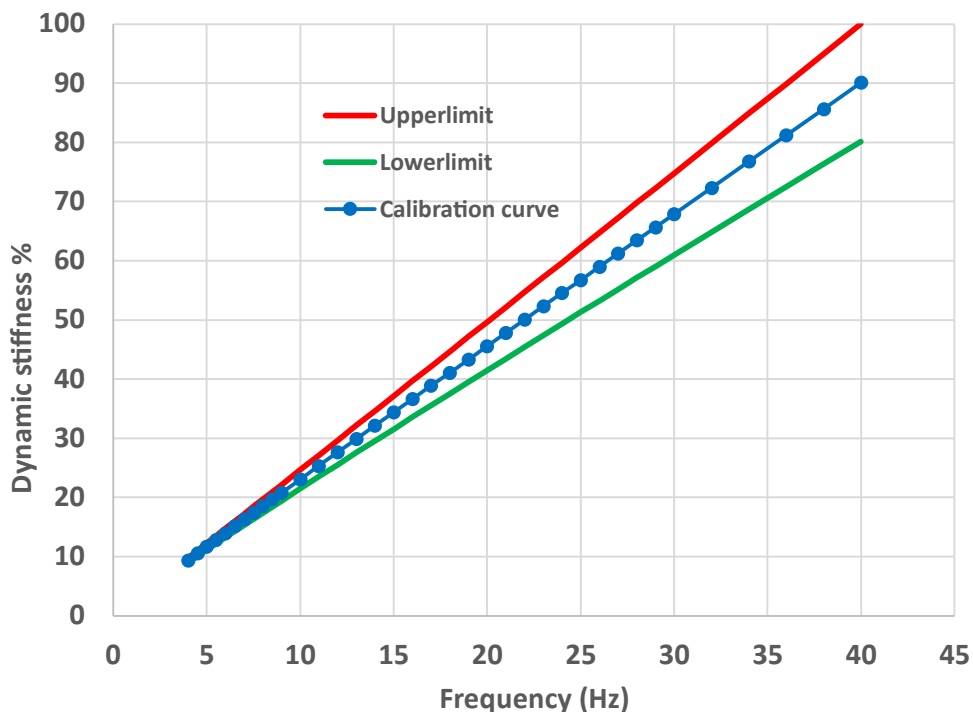
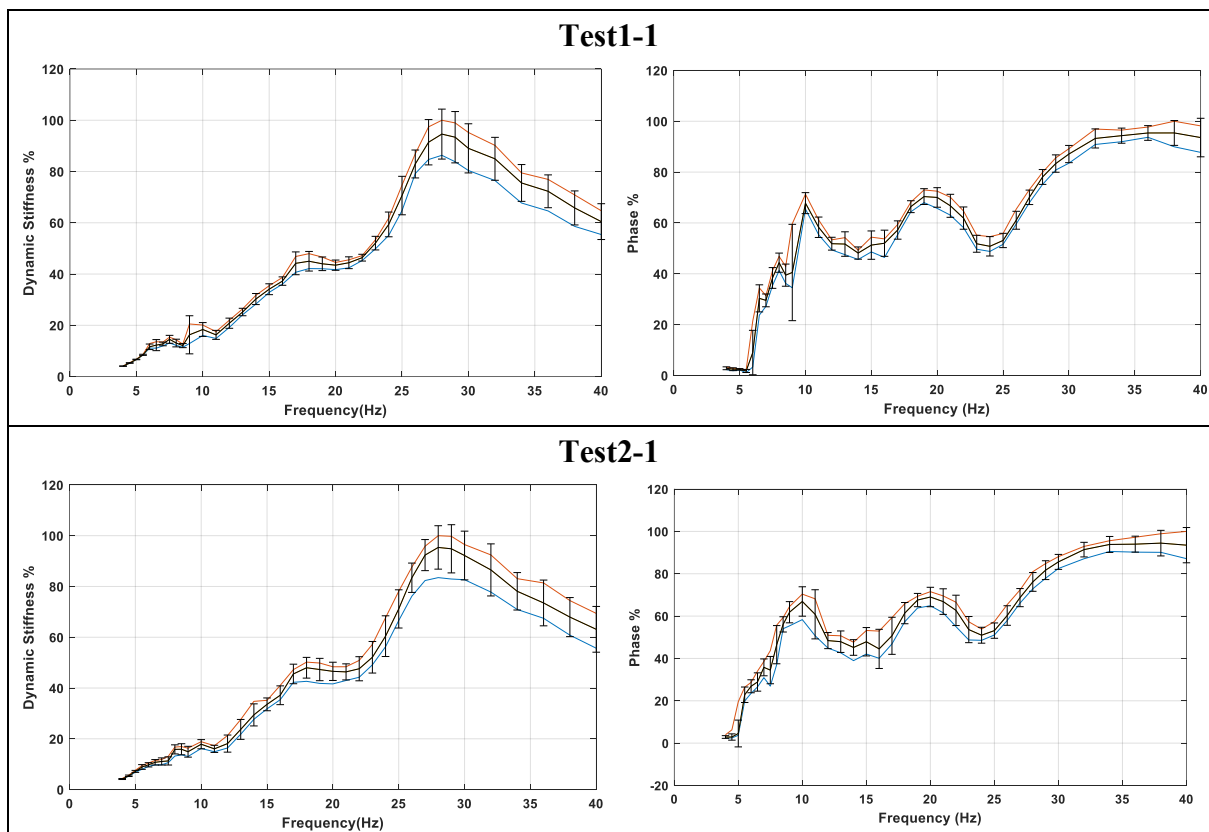


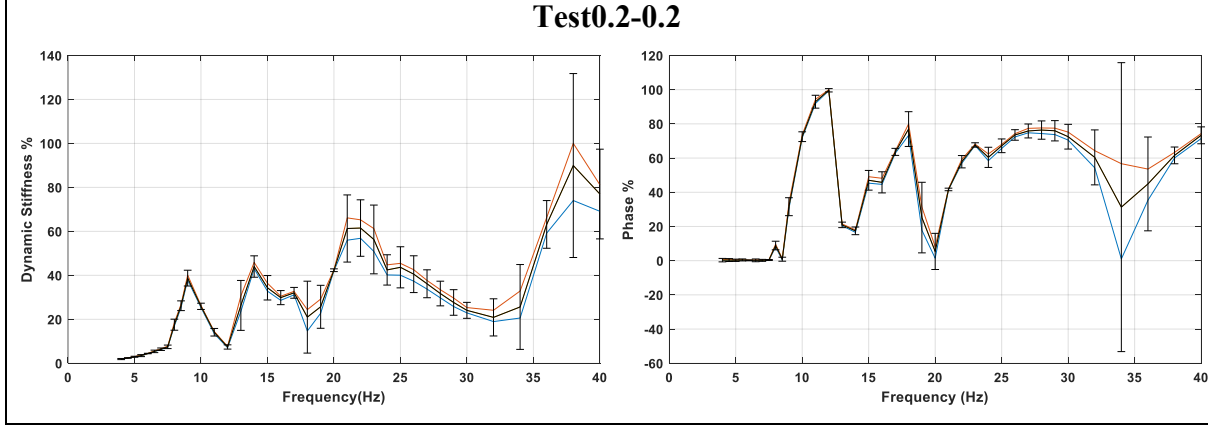
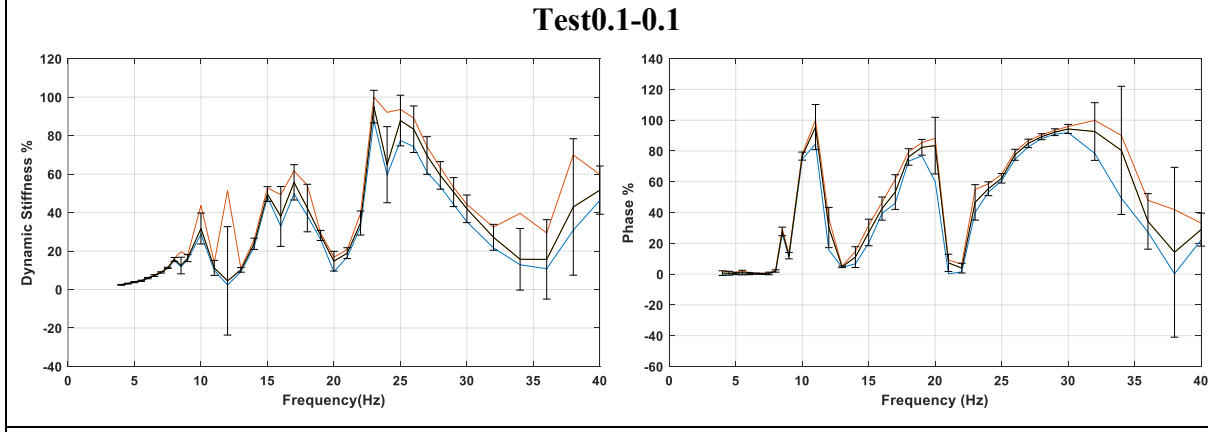
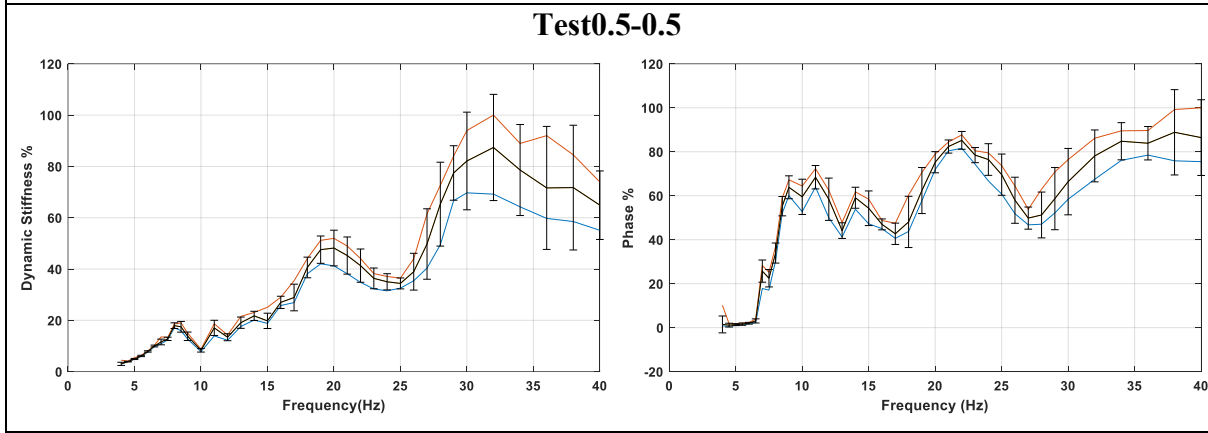
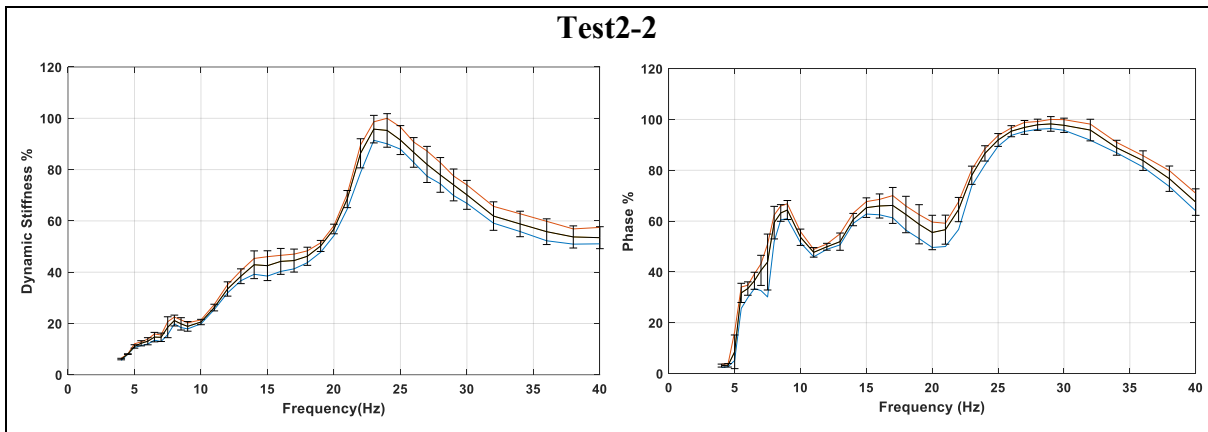
Figure 2.5. Calibration curve

2.4 Collected datasets

The main output of the dynamic tests performed on the Stockbridge damper is the force transmitted to the moving base of the shaker per unit of base displacement and for each excited frequency. Since it is expressed in $[N/m]$, it will be referred to as “dynamic stiffness” in the following chapters of the thesis and it will be generally represented in magnitude and phase. The Data Acquisition System (DAS) returns the dynamic stiffness of the system automatically through an Excel file.

The magnitudes and phases of the dynamic stiffnesses for the different tests are depicted in Figure 2.6. For each set of tests (Test1-1, Test2-1, ...) the red line represents the locus of maxima of all experiments, the black line indicates the average curve of all experiments, and the blue line shows the locus of minima values of all experiments. Additionally, a representation of variability is incorporated by including three standard deviations around the mean value (I). The graphs are shown in percentage values with respect to the maximum value due to company policy.





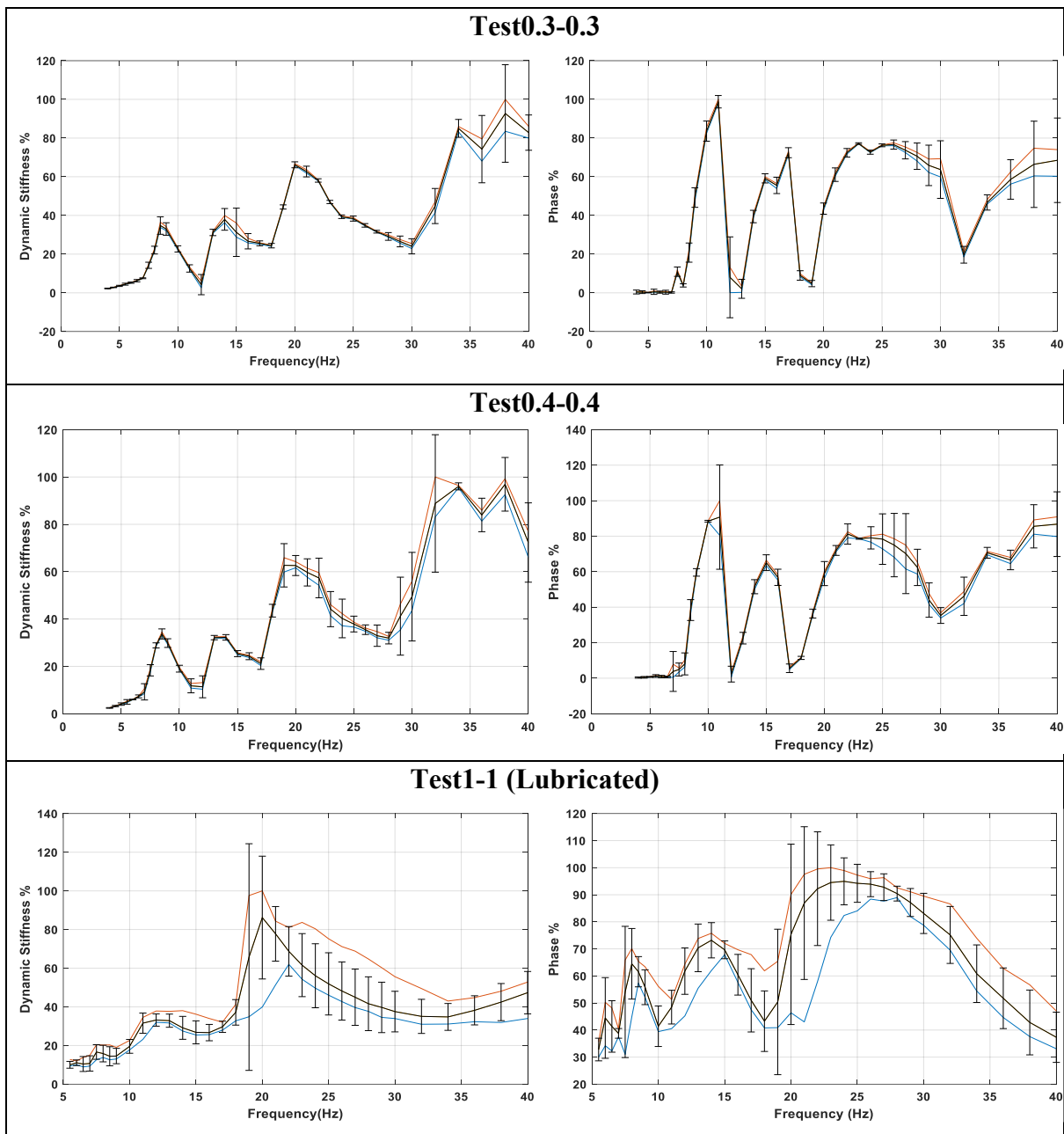


Figure 2.6. Dynamic stiffness & phase vs frequency. Black line: mean curve; blue line: locus of the minima; red line: locus of the maxima; bar: three standard deviations around mean.

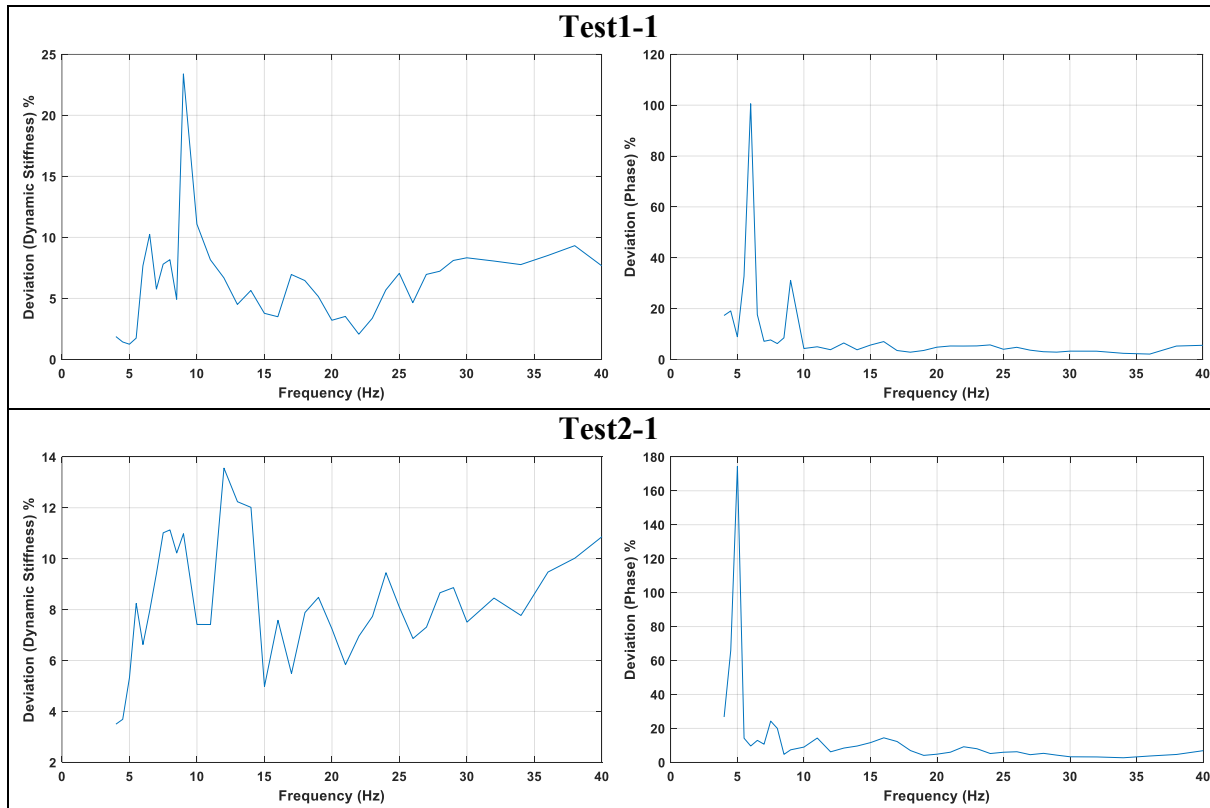
2.5 Datasets quality check

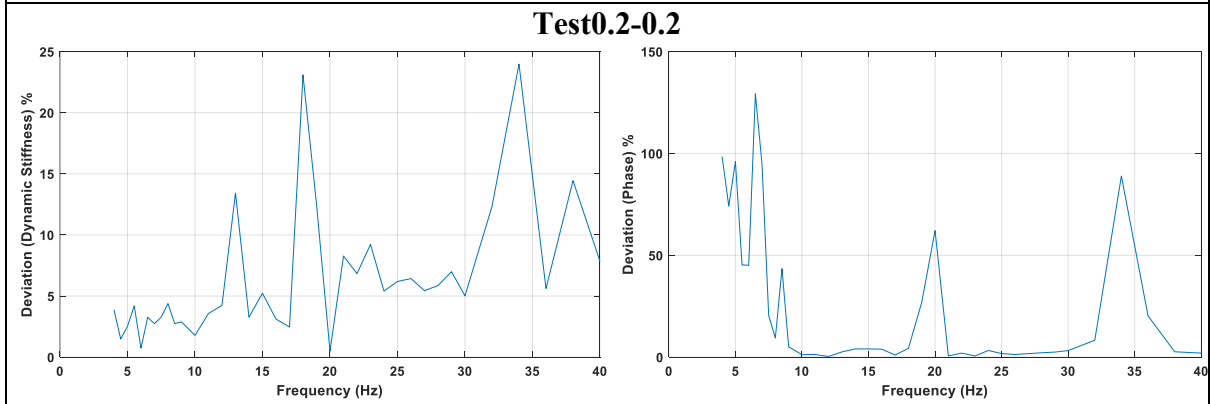
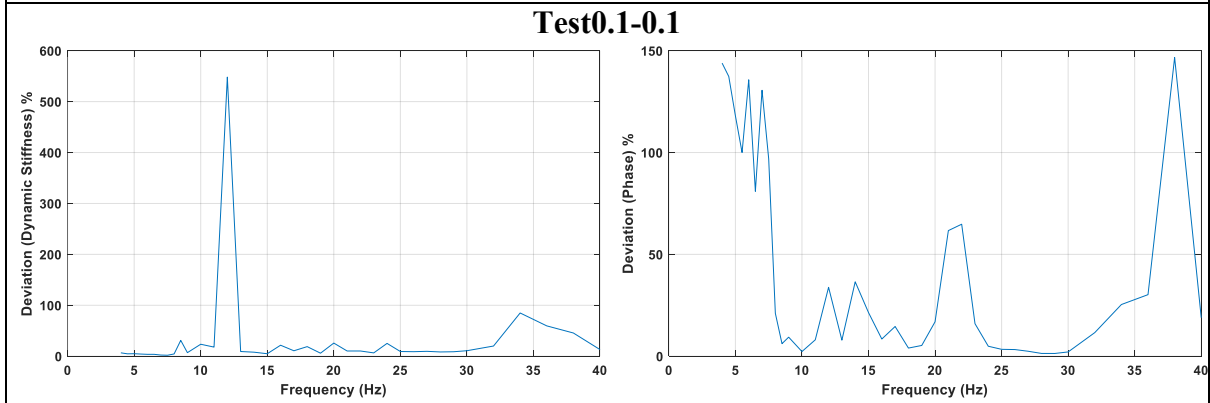
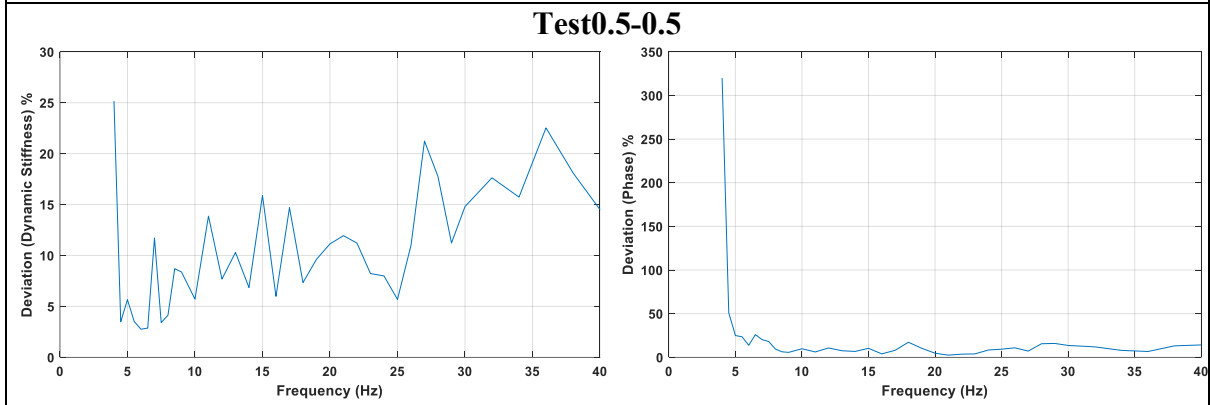
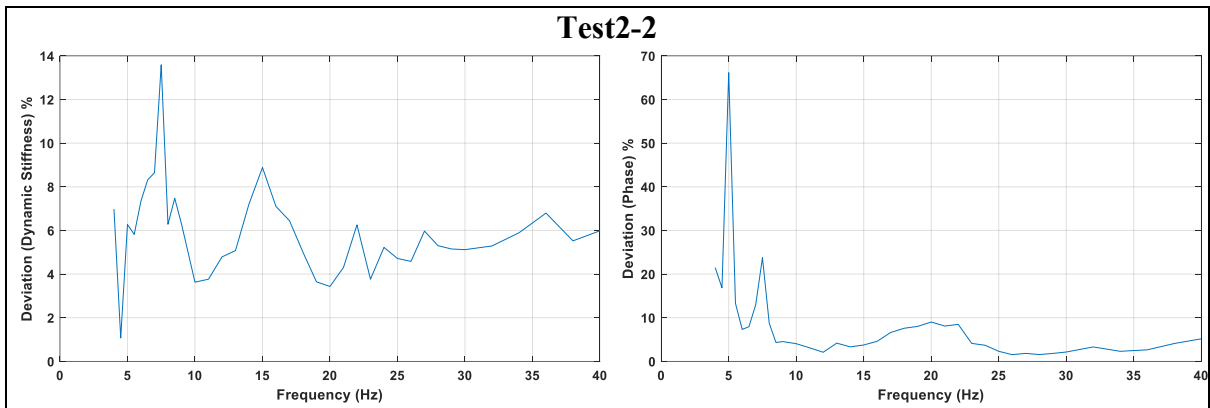
Outliers are extreme data points that deviate significantly from most of the data. They can result from noise, errors, natural variation, or sampling issues. Outliers distort summary statistics, affect data distributions, mislead visualizations and can model fitting on data.

The coefficient of variation (CV) is a statistical measure of the dispersion of a set of data points around their mean value. It is expressed as a percentage and is calculated by

$$CV = 100 \frac{(\max - \min)}{(2 \cdot \text{mean})}$$

In this formula, max and min are the maximum and minimum values in the dataset, respectively, while the mean is the mean value of the dataset.





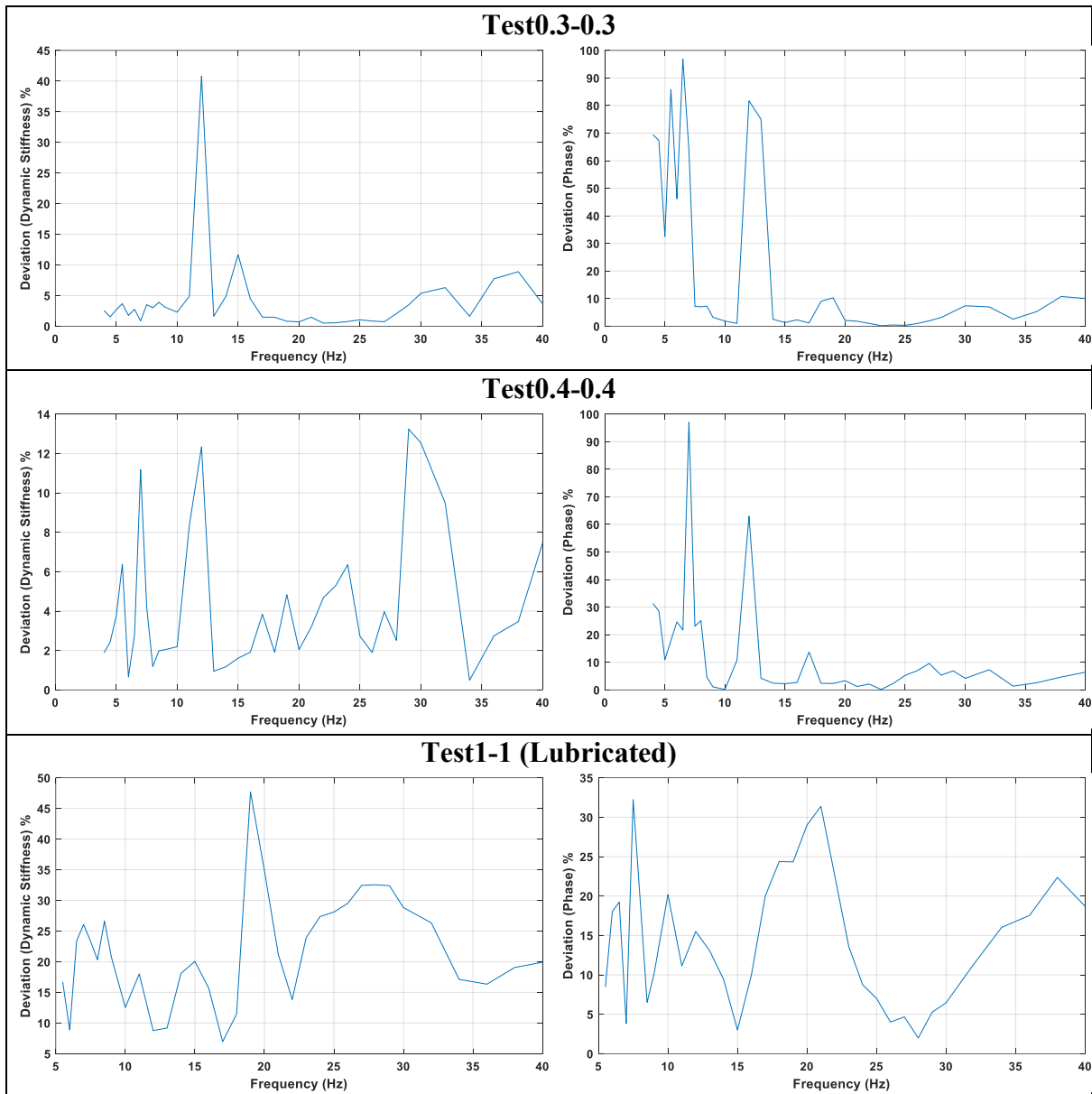


Figure 2.7. Deviation in dynamic stiffness and phase data

The investigation on deviation graphs Figure 2.7 has uncovered that errors in dynamic stiffness and phase are not minimal in the analyzed datasets at a low-frequency range (4-15 Hz), indicating the necessity for data optimization and refinement. This inaccuracy holds the potential to distort possible analytical conclusions. Hence an in-depth data cleaning procedure is carried out to rectify this issue: this procedure involves identifying and removal of outliers. Such a thorough approach is geared towards improving data quality, thus guaranteeing more robust outcomes in subsequent analyses.

In the analysis of experimental data, it is common to encounter curves that exhibit larger deviations from the rest of the data. An example is reported in Figure 2.8. Various outliers removal techniques can be employed to address this issue, one of such technique is Z-score method. This technique is used to identify and remove outliers, which are data points that significantly deviate from the mean of the dataset.

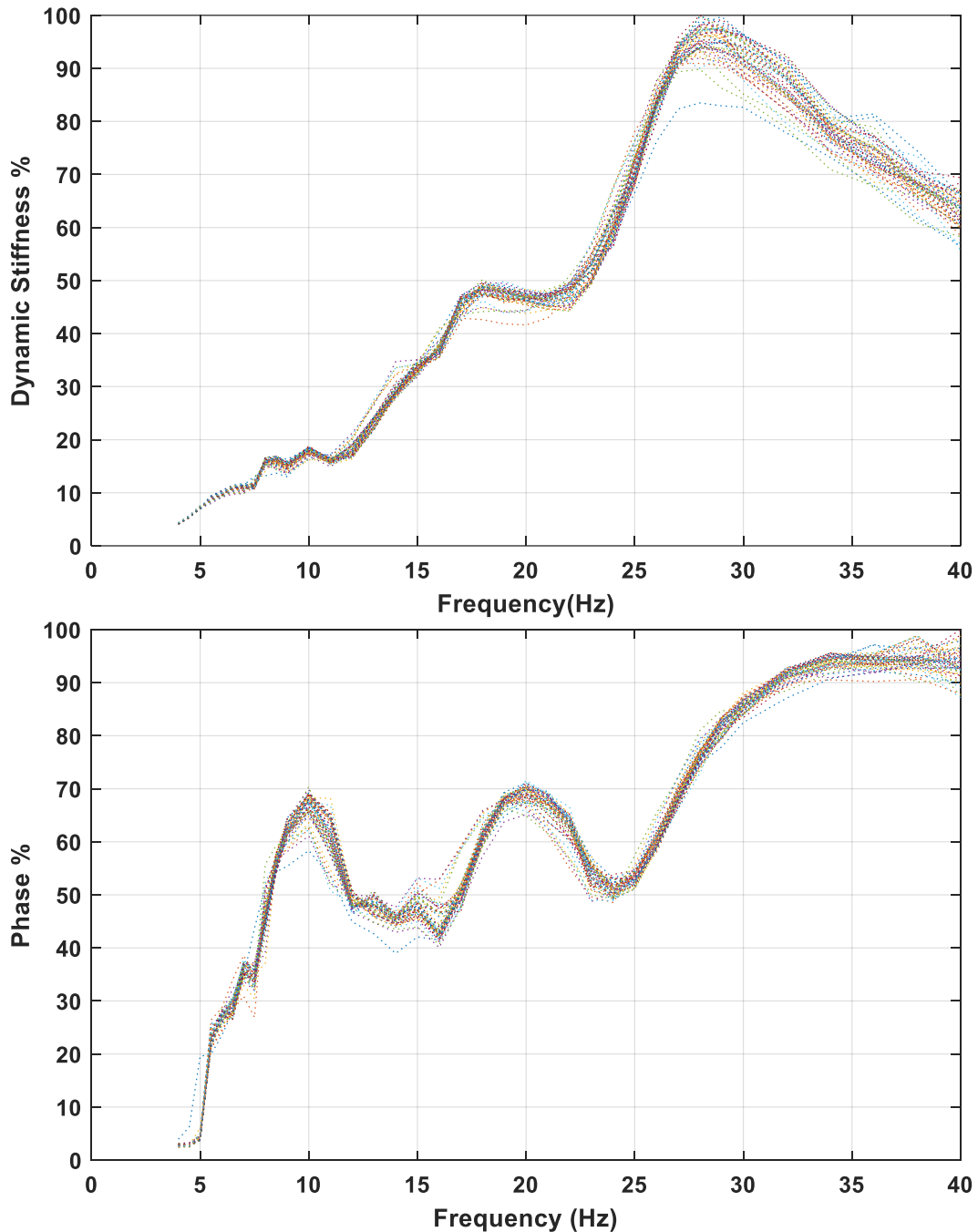


Figure 2.8. Dynamic stiffness and phase vs frequency (Test2-1)

2.6 Outliers removal

To ensure data integrity and address anomalies in the curves, the Z-score method was employed for outlier detection and removal. This statistical technique facilitated the identification of outliers, and curves that significantly deviated from the mean were eliminated, thereby enhancing the accuracy of the curve analysis. Mathematically, the Z-score formula is

$$Z_i = \frac{X_i - \mu}{\sigma}$$

where:

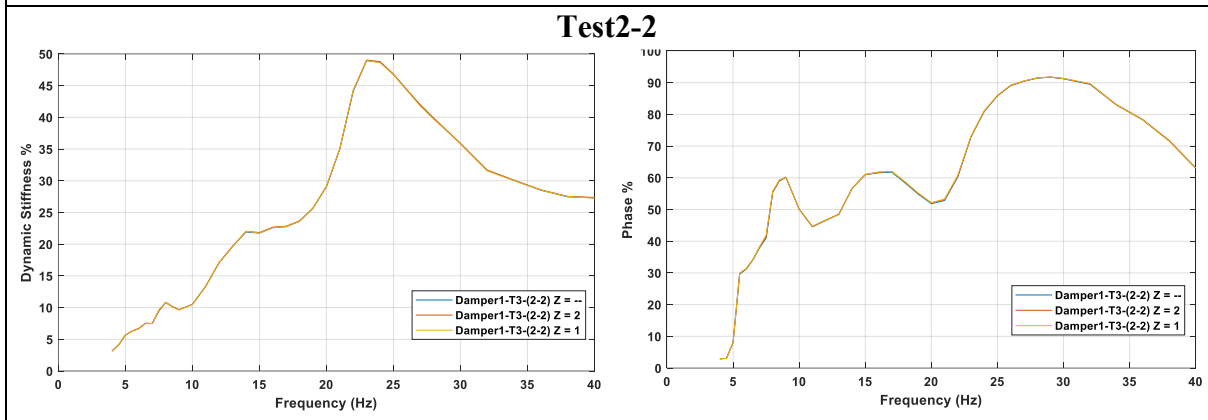
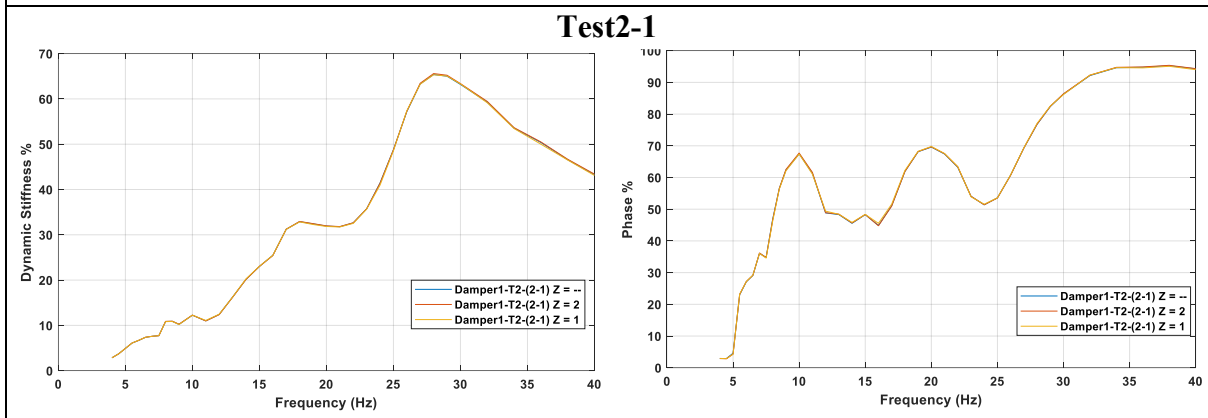
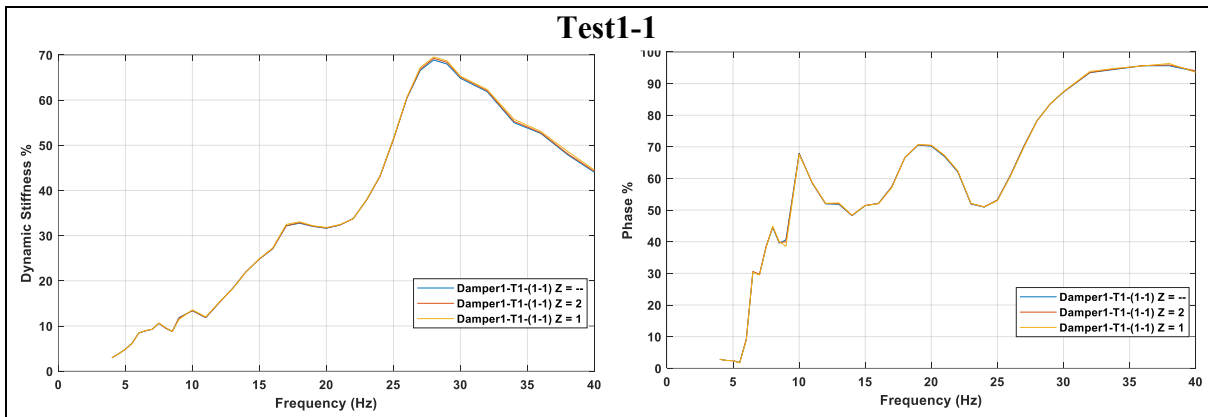
- Z_i is the Z-score of the i-th data point
- X_i is the value of the i-th data point
- μ is the mean of the dataset
- σ is the standard deviation of the dataset

Positive Z-scores indicated values above the mean, while negative Z-score values were below the mean. Data points with Z-scores exceeding ± 2 or ± 3 standard deviations from the mean are typically considered as outliers. As can easily be seen, Z-scores may differ between tests or datasets because they are based on the unique properties of each dataset, such as mean, standard deviation, and data distribution.

Figure 2.9 illustrates the mean curve across various Z-score values for the considered damper in different tests. It includes plots without outliers (legend $Z = --$), as well as plots with outliers removed for Z-scores of 2 (legend $Z = 2$) and 1 (legend $Z = 1$).

When outliers are removed from a dataset using the Z-score method, the mean has not shown significant changes due to several reasons:

- *Proximity to Mean*: If the outliers are not too far from the mean, their removal will not alter the mean value.
- *Dataset Size*: In a large dataset, a few outliers have a diluted effect. So, even if they are removed, the mean remains relatively stable.
- *Data Concentration*: If a majority of the data points are clustered around the mean, then the outliers have less influence on the mean. Thus, their removal has a minimal impact.
- *Outlier Magnitude*: Outliers that are not substantially larger or smaller than the other data points won't significantly shift the mean.
- *Compensating Outliers*: Sometimes, outliers on both ends (high and low) can offset each other's impact on the mean.



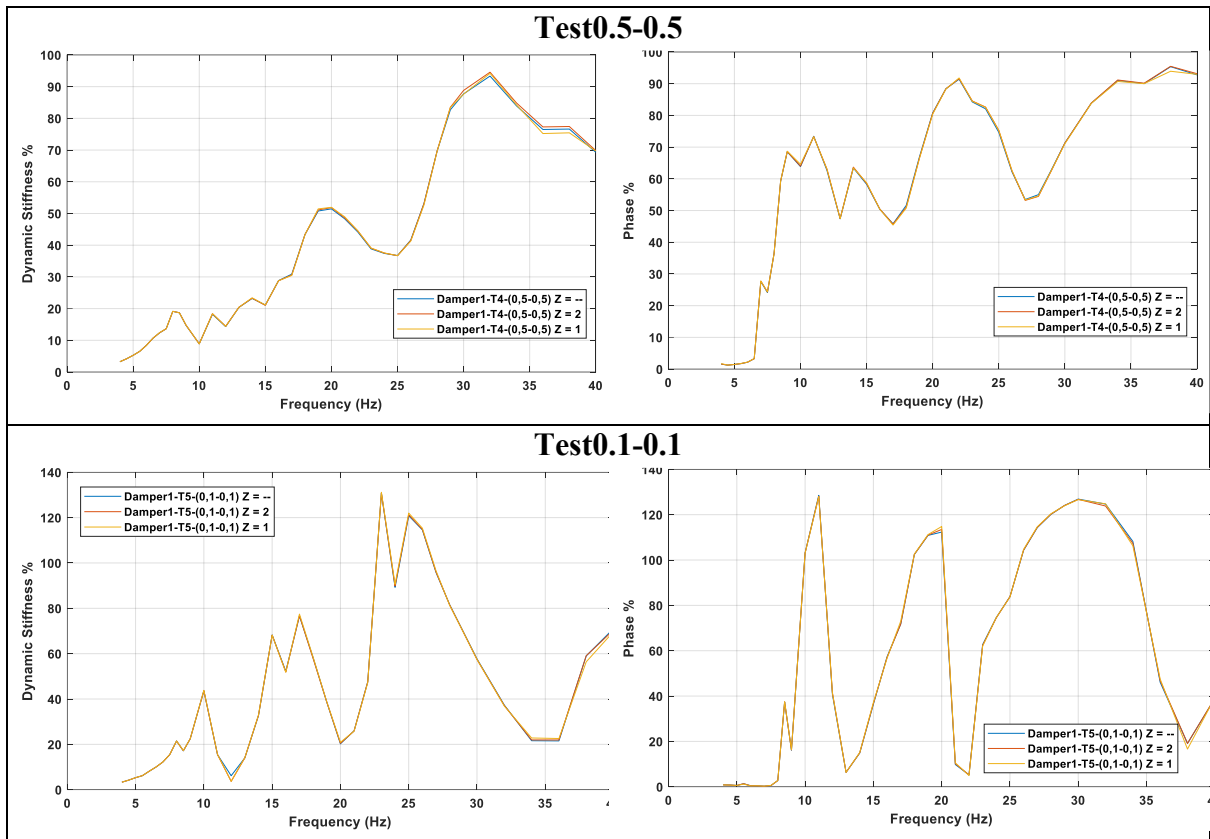


Figure 2.9. Mean curves for different Z score

The mean curves for different Z-score for Test0.2-0.2, 0.3-0.3, and 0.4-0.4, is not plotted due to the limited number of conducted experiments, which precluded their graphical representation.

2.7 Conclusion from different tests

The dynamic stiffness and phase vs frequency curves for Test1-1 (blue curve) and Test2-1 (red curve) shows similar behavior (Figure 2.10), indicating consistent response characteristics across the frequency range.

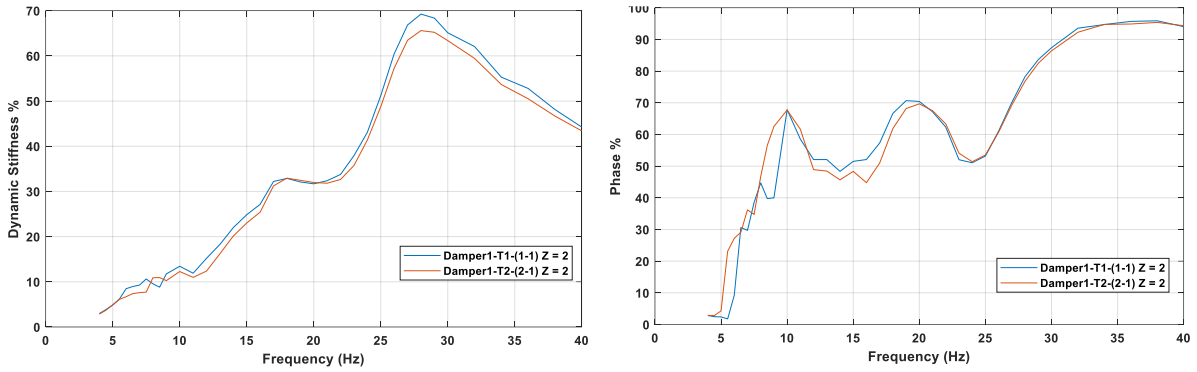


Figure 2.10. Comparison of Test1-1 and Test2-1

At higher frequencies above 15 Hz, Test2-2 (yellow curve) in Figure 2.11 totally deviates from Test1-1 (blue curve) and Test2-1 (red curve). The dynamic stiffness and phase response appear to deviate from the expected trend, suggesting possible nonlinear phenomena influencing the dynamic stiffness and phase measurements in this frequency region and for this level of excitation.

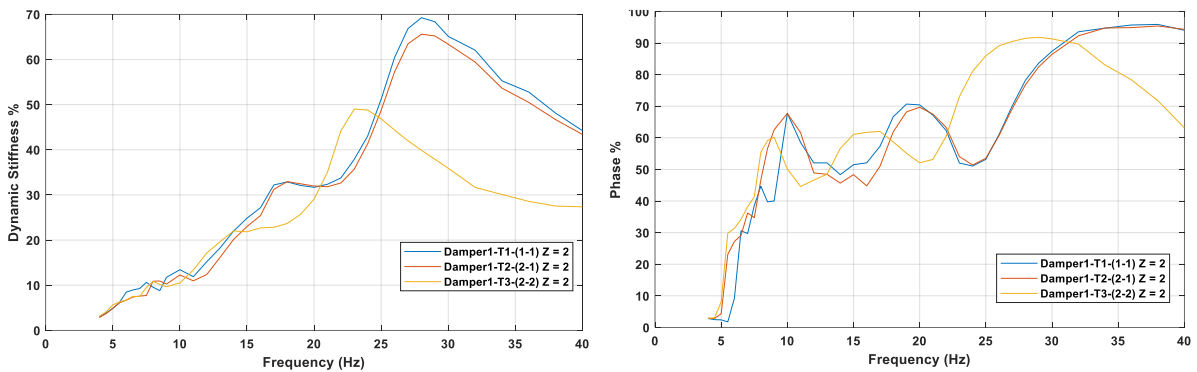


Figure 2.11. Comparison of Test1-1, Test2-1 and Test2-2

This phenomenon is more evident by looking at Figure 2.12, including the results of Test0.5-0.5. The system seem to exhibit a softening behavior, which is visually represented by the mean curves shifting to towards lower frequencies when the excitation level increases. Additionally, there is a discernible decrease in dynamic stiffness as the amplitude increases.

This observed behavior can be attributed to the presence of inherent nonlinearities within the material or the system itself. These nonlinearities can manifest as alterations in the system's response to varying levels of vibration amplitude. As the vibration amplitude changes, the system's inherent nonlinear properties come into play, resulting in a modification of the dynamic stiffness. Understanding and characterizing these nonlinearities is crucial for accurately modeling and predicting the behavior of such systems under varying vibrational conditions.

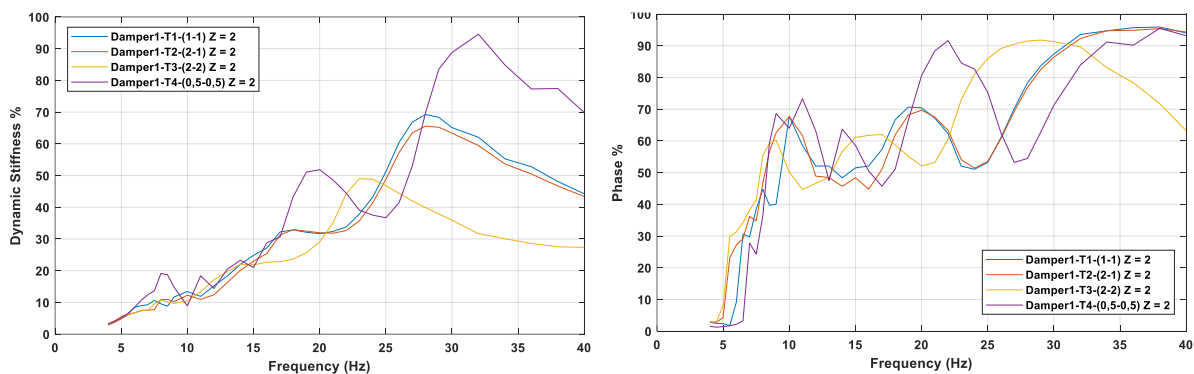


Figure 2.12. Comparison of tests

In Figure 2.13 the blue curve represents the mean curve of Test1-1, and the red curve represents Test1-1 after applying lubrication to the messenger cable. A clear reduction in the stiffness is observed after applying lubrication, with a decrease of damping.

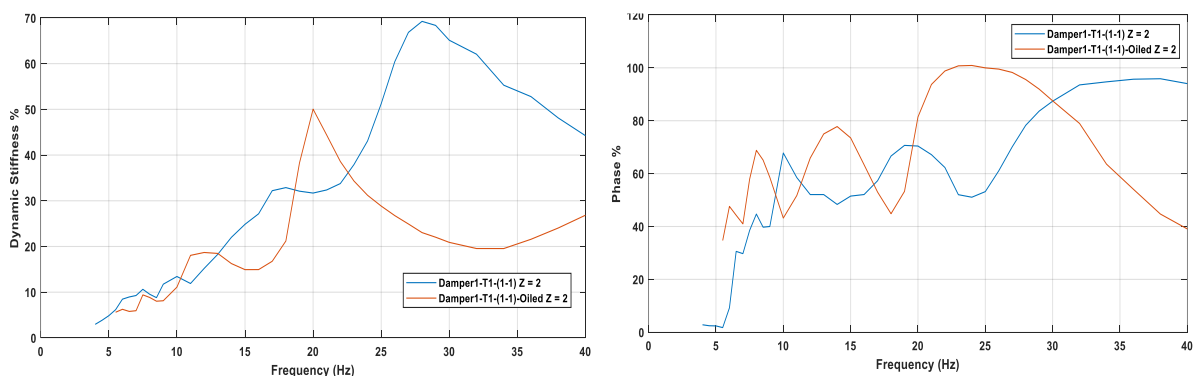


Figure 2.13. Comparison of Test1-1 after lubrication

Chapter 3

Finite element model

The following procedure is adopted to construct the finite element model of the damper:

1. Identification of inertial and stiffness contributions
2. Distribution of inertial and the stiffness properties with shape functions for each element in local (element) coordinates frame
3. Projection (rotation) of local matrixes into global reference frame
4. Assembly

3.1 Scheme of the damper (FEM)

The damper under analysis (Figure 3.1) can be schematized as a three-nodes Euler-Bernoulli beam with lumped masses connected through rigid links.

For simplicity of description, the motion is assumed to be in the vertical plane with no horizontal displacement, so each node has two degrees of freedom: one corresponding to the vertical motion and the other to rotation, as shown in Figure 3.2. By this representation, the Stockbridge damper has 6DOF:

- x_1, x_c and x_2 are the vertical displacements
- φ_1, φ_c and φ_2 are the rotation

The parameters entering the dynamics of the system are (see Figure 3.1):

- The end masses m_1 and m_2 , the mass of the clamp m_c , the linear density of the messenger cable μ (kg/m).
- The moment of inertia of the end masses around their center of mass J_{G1} and J_{G2} , and the moment of inertia of the clamp around its center of mass J_{GC} .
- The flexural rigidity EI (Nm^2) of the messenger wire. This is the product of the Young's modulus E (N/m^2) and of the area moment of inertia I (m^4) of the wire section.
- Distances between the rotation axis and the center of mass of each of the masses a_1, a_2, a_c
- The free lengths of the cable between the clamp and the attach points of the end masses L_1, L_2 .

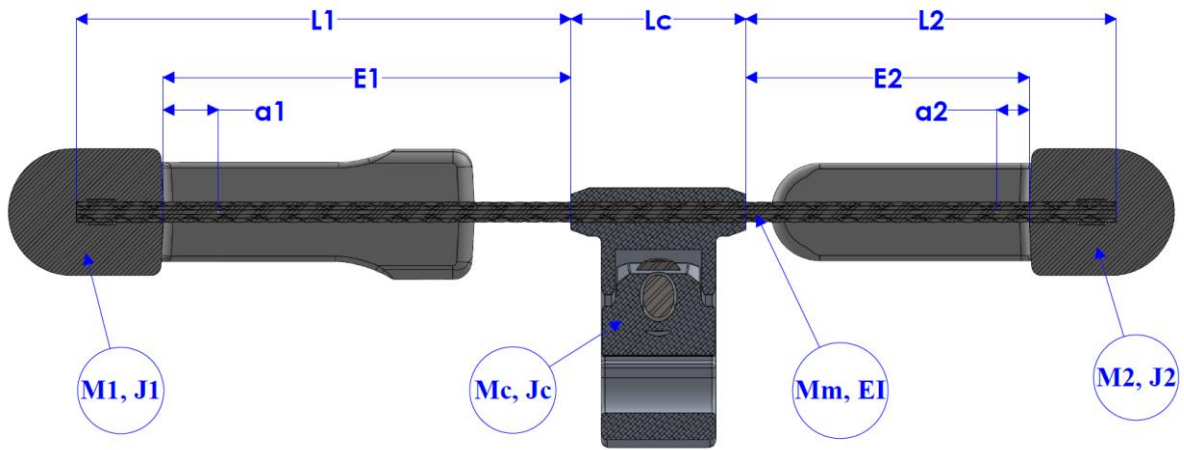


Figure 3.1. Stockbridge damper parameters

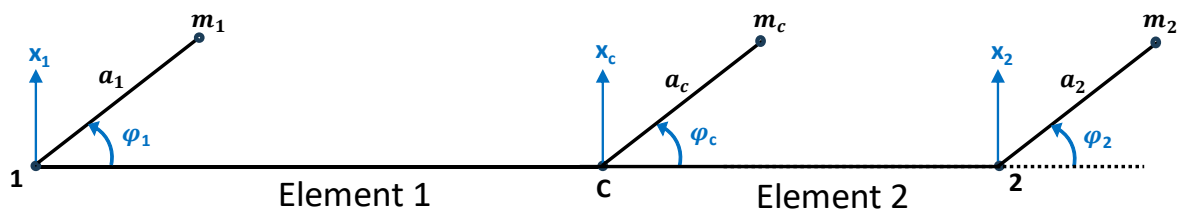


Figure 3.2. Stockbridge damper scheme

3.2 Element 1

Figure 3.3 shows the local reference frame for element 1, and its scheme is shown in Figure 3.4. The 4 degrees of freedom are x_1 , x_c , φ_1 , φ_c .

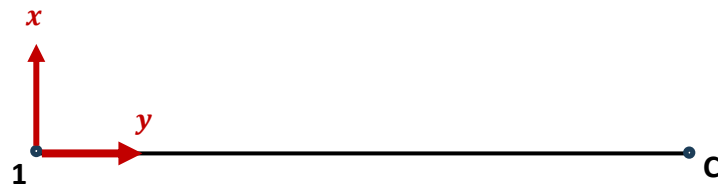


Figure 3.3. Local co-ordinate system

The mass matrices for element 1 and element 2 incorporate contributions from both wire and lumped masses. Consequently, the mass matrix of the system is obtained by assembling the single mass contributions.

For element 1, the two masses m_1 and m_c are considered. For convenience, the inertial contributions of the clamp are attributed exclusively to element 1, rather than split between element 1 and element 2.

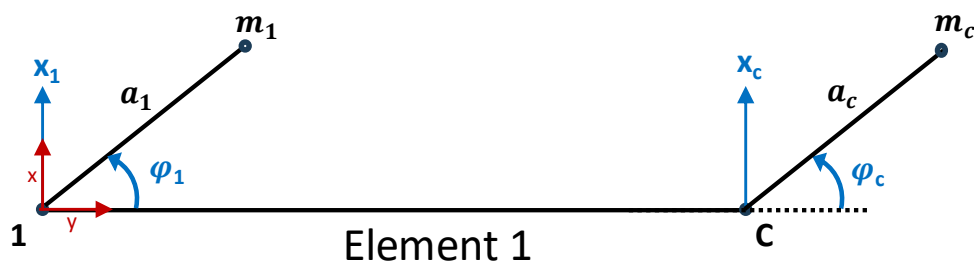


Figure 3.4. Scheme diagram for element 1

Figure 3.5 and Figure 3.6 show the free body diagrams of mass 1 and element 1, respectively. Inertial forces are represented in red color, reactions in blue and external forces in green.

In the Figure 3.5 H_1 , V_1 and M_1 are the reactions on mass m_1 at node 1. $J_{G1}\ddot{\phi}_1$, $m_1 a_1^2 \dot{\phi}^2$, $m_1 a_1 \ddot{\phi}_1$, $m_1 \ddot{x}_1$ are the inertial forces due to mass m_1 .

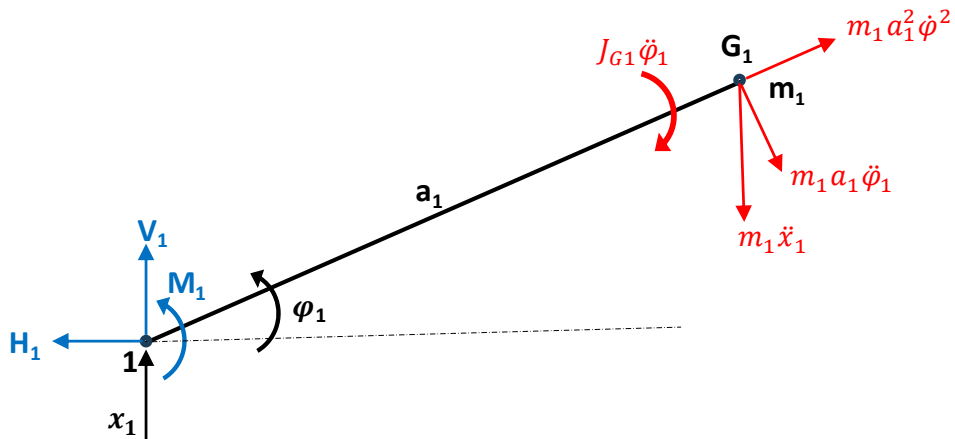


Figure 3.5. Free body diagram for mass 1

In the Figure 3.6 H_1 , V_1 and M_1 are the reactions on messenger cable at node 1, H_2 , V_2 and M_2 are the reactions on messenger cable at node c. F_c and M_c are external force and moment at node c.

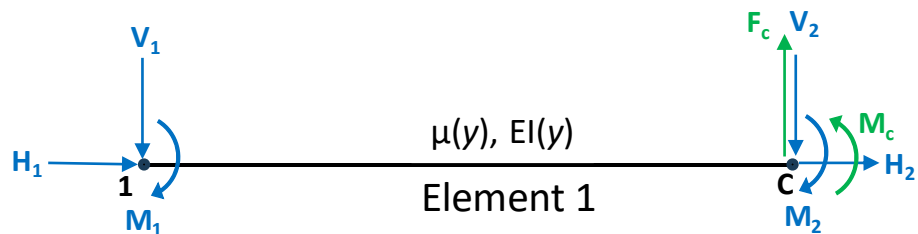


Figure 3.6. Free body diagram for the element 1

The wire is represented using the Euler-Bernoulli beam theory [4][11]. Here below are recalled the basic formula useful for the beam deformation.

Curvature of the beam

$$\frac{\partial^2 x(y)}{\partial y^2} = \frac{M(y)}{EI}$$

- $x(y)$ represents the transverse displacement of the beam at position y
- $\frac{\partial^2 x(y)}{\partial y^2}$ is the second derivative of $x(y)$ with respect to y , which gives the curvature of the beam
- $M(y)$ is the bending moment along the beam at position y

Vertical displacement field (separate variables):

$$x(y, t) = \{N(y)\}^T \{X(t)\}$$

- $x(y, t)$ is the vertical displacement of the beam at position y and time t .
- $N(y)$ is a vector containing functions that describe the spatial distribution of displacement (shape functions)
- $X(t)$ is a vector containing functions that describe the time-dependent behavior

Angular displacement equation:

$$\varphi(y, t) = \frac{\partial x(y, t)}{\partial y} = \{N'(y)\}^T \{X(t)\}$$

Shape functions:

Shape functions are mathematical functions used in finite element analysis (FEA) to describe the spatial variation of a physical quantity (displacement) within an element [11]. These functions play a crucial role in approximating the behavior of the physical system under consideration.

$$N_1 = 1 - \frac{3y^2}{l^2} + \frac{2y^3}{l^3}$$

$$N_2 = y - \frac{2y^2}{l} + \frac{y^3}{l^2}$$

$$N_3 = \frac{3y^2}{l^2} - \frac{2y^3}{l^3}$$

$$N_4 = -\frac{y^2}{l} + \frac{y^3}{l^2}$$

$$\{N\} = \{N_1, N_2, N_3, N_4\}^T$$

Displacement vector:

$$\{x\} = \{x_1, \quad \varphi_1, \quad x_c, \quad \varphi_c\}^T \quad (3.1)$$

The mass matrix for the messenger wire (element 1) can be obtained from the expression representing the kinetic energy of the beam [11]

$$[m_{\text{wire},e1}] = \int_0^{l_{e1}} \mu(y) \{N(y)\} \{N(y)\}^T dy$$

- $\mu(y)$ is the mass per unit length along y

assuming $\mu(y)$ as constant μ

$$[m_{\text{wire},e1}] = \frac{\mu l_{e1}}{420} \begin{bmatrix} 156 & 22l_{e1} & 54 & -13l_{e1} \\ 22l_{e1} & 4l_{e1}^2 & 13l_{e1} & -3l_{e1}^2 \\ 54 & 13l_{e1} & 156 & -22l_{e1} \\ -13l_{e1} & -3l_{e1}^2 & -22l_{e1} & 4l_{e1}^2 \end{bmatrix} \quad (3.2)$$

The lumped mass contribution of m_1 and m_c are (for complete computation refer to Appendix B. Lumped mass contribution):

$$[m_{\text{Lump},e1}] = \begin{bmatrix} m_1 & m_1 a_1 & 0 & 0 \\ m_1 a_1 & J_1 & 0 & 0 \\ 0 & 0 & m_c & m_c a_c \\ 0 & 0 & m_c a_c & J_c \end{bmatrix} \quad (3.3)$$

Where:

- $J_1 = J_{G1} + m_1 a_1^2$
- $J_c = J_{Gc} + m_c a_c^2$

The stiffness matrix for the messenger wire (element 1) can be obtained from the expression representing the potential energy of the beam [11]

$$[k_{\text{wire},e1}] = \int_0^{l_{e1}} EI(y)\{N''(y)\}\{N''(y)\}^T dy$$

And results in the following 4x4 matrix:

$$[k_{\text{wire},e1}] = \frac{EI}{l_{e1}^3} \begin{bmatrix} 12 & 16l_{e1} & -12 & 6l_{e1} \\ 6l_{e1} & 4l_{e1}^2 & -6l_{e1} & 2l_{e1}^2 \\ -12 & -6l_{e1} & 12 & -6l_{e1} \\ 6l_{e1} & 2l_{e1}^2 & -6l_{e1} & 4l_{e1}^2 \end{bmatrix} \quad (3.4)$$

Where:

- μ is the linear density
- A is the cross-sectional area
- l_{e1} is the length of the element 1
- EI is the flexural rigidity of messenger wire

3.3 Element 2

Figure 3.7 shows element 2 with 4 degrees of freedom. For element 2, only the mass contribution m_2 is considered because the mass contribution of the clamp m_c has already been incorporated into element 1.

In Figure 3.7 x_c and x_2 are vertical displacement and ϕ_c , ϕ_2 are rotations.

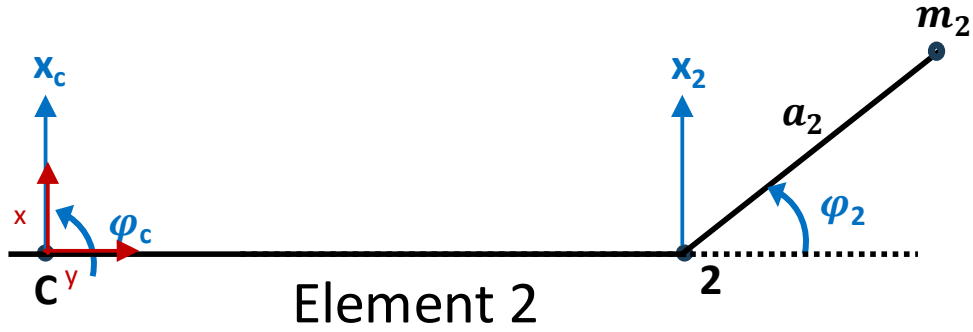


Figure 3.7. scheme diagram for element 2

Displacement vector:

$$\{x\} = \{x_c, \phi_c, x_2, \phi_2\}^T \quad (3.5)$$

The mass matrix for the messenger wire (element 2) can be obtained from the expression representing the kinetic energy of the beam [11]

$$[m_{\text{wire},e2}] = \int_0^{l_{e2}} \mu(y) \{N(y)\} \{N(y)\}^T dy \quad (3.6)$$

$$[m_{\text{wire},e2}] = \frac{\mu l_{e2}}{420} \begin{bmatrix} 156 & 22l_{e2} & 54 & -13l_{e2} \\ 22l_{e2} & 4l_{e2}^2 & 13l_{e2} & -3l_{e2}^2 \\ 54 & 13l_{e2} & 156 & -22l_{e2} \\ -13l_{e2} & -3l_{e2}^2 & -22l_{e2} & 4l_{e2}^2 \end{bmatrix}$$

The lumped mass contribution of m_2 is (for complete computation refer to Appendix B. Lumped mass contribution):

$$[m_{\text{Lump},e2}] = \begin{bmatrix} 0 & 0 & 0 & 0 \\ 0 & 0 & 0 & 0 \\ 0 & 0 & m_2 & m_2 a_2 \\ 0 & 0 & m_2 a_2 & J_2 \end{bmatrix} \quad (3.7)$$

Where:

- $J_2 = J_{G2} + m_2 a_2^2$

The stiffness matrix for the messenger wire (element 2) can be obtained from the expression representing the potential energy of the beam [11]:

$$[k_{\text{wire},e2}] = \int_0^{l_{e2}} EI(y)\{N''(y)\}\{N''(y)\}^T dy$$

And thus results in the following 4x4 matrix:

$$[k_{\text{wire},e2}] = \frac{EI}{l_{e2}^3} \begin{bmatrix} 12 & 16l_{e2} & -12 & 6l_{e2} \\ 6l_{e2} & 4l_{e2}^2 & -6l_{e2} & 2l_{e2}^2 \\ -12 & -6l_{e2} & 12 & -6l_{e2} \\ 6l_{e2} & 2l_{e2}^2 & -6l_{e2} & 4l_{e2}^2 \end{bmatrix} \quad (3.8)$$

Where:

- μ is the linear density
- A is the cross-sectional area
- l_{e2} is the length of the element
- EI is the flexural rigidity of messenger wire

3.4 Assembly

Generally, it is necessary to project (rotate) the local element matrices into the Global Reference System (GRS). Since for the considered case the GRS is horizontal like the local ones, the rotation matrix is identity.

The global matrix is of dimensions 6x6, corresponding to the six degrees of freedom (6DOF) of the system. The six rows and columns in the global matrix are associated with the nodal deformations $\{x_1, \varphi_1, x_c, \varphi_c, x_2, \varphi_2\}$. Element 1 is characterized by entries $\{x_1, \varphi_1, x_c, \varphi_c\}$. Similarly, Element 2 is linked to the entries $\{x_c, \varphi_c, x_2, \varphi_2\}$.

The Global Reference System is stated in upper-case letters and local reference system in lower-case letters.

Displacement vector:

$$\{X\} = \{x_1, \varphi_1, x_c, \varphi_c, x_2, \varphi_2\}^T \quad (3.9)$$

Mass matrix:

Mass matrix for element 1 in global coordinate system $[M_1]$:

$$[M_{\text{wire},e1}] = \frac{\mu l_{e1}}{420} \begin{bmatrix} 156 & 22l_{e1} & 54 & -13l_{e1} & 0 & 0 \\ 22l_{e1} & 4l_{e1}^2 & 13l_{e1} & -3l_{e1}^2 & 0 & 0 \\ 54 & 13l_{e1} & 156 & -22l_{e1} & 0 & 0 \\ -13l_{e1} & -3l_{e1}^2 & -22l_{e1} & 4l_{e1}^2 & 0 & 0 \\ 0 & 0 & 0 & 0 & 0 & 0 \\ 0 & 0 & 0 & 0 & 0 & 0 \end{bmatrix}$$

$$[M_{\text{Lump},e1}] = \begin{bmatrix} m_1 & m_1 a_1 & \dots & 0 \\ m_1 a_1 & J_{G1} + m_1 a_1^2 & \dots & \dots \\ \vdots & \vdots & m_c & m_c a_c \\ \vdots & \vdots & m_c a_c & J_{Gc} + m_c a_c^2 \\ 0 & 0 & \dots & \dots \\ \vdots & \vdots & \vdots & \vdots \\ 0 & 0 & 0 & 0 \end{bmatrix}$$

$$[M_1] = [M_{\text{wire},e1}] + [M_{\text{Lump},e1}]$$

Mass matrix for element 2 in global coordinate system $[M_2]$:

$$[M_{\text{wire},e2}] = \frac{\mu l_{e2}}{420} \begin{bmatrix} 0 & 0 & 0 & 0 & 0 & 0 \\ 0 & 0 & 0 & 0 & 0 & 0 \\ 0 & 0 & 156 & 22l_{e2} & 54 & -13l_{e2} \\ 0 & 0 & 22l_{e2} & 4l_{e2}^2 & 13l_{e2} & -3l_{e2}^2 \\ 0 & 0 & 54 & 13l_{e2} & 156 & -22l_{e2} \\ 0 & 0 & -13l_{e2} & -3l_{e2}^2 & -22l_{e2} & 4l_{e2}^2 \end{bmatrix}$$

$$[M_{\text{Lump},e2}] = \begin{bmatrix} 0 & 0 & \dots & & 0 \\ 0 & 0 & & & \\ \vdots & 0 & 0 & & \vdots \\ & 0 & 0 & & \\ 0 & \dots & m_2 & m_2 a_2 & \\ & & m_2 a_2 & J_{G2} + m_2 a_2^2 & \end{bmatrix}$$

$$[M_2] = [M_{\text{wire},e2}] + [M_{\text{Lump},e2}]$$

Global mass matrix $[M]$:

$$[M] = [M_1] + [M_2] \quad (3.10)$$

Stiffness matrix:

Stiffness matrix for element 1 in global coordinate system $[K_{\text{wire},e1}]$:

$$[K_{\text{wire},e1}] = EI \begin{bmatrix} 12/l_{e1}^3 & 6/l_{e1}^2 & -12/l_{e1}^3 & 6/l_{e1}^2 & 0 & 0 \\ 6/l_{e1}^2 & 4/l_{e1} & -6/l_{e1}^2 & 2/l_{e1} & 0 & 0 \\ -12/l_{e1}^3 & -6/l_{e1}^2 & 12/l_{e1}^3 & -6/l_{e1}^2 & 0 & 0 \\ 6/l_{e1}^2 & 2/l_{e1} & -6/l_{e1}^2 & 4/l_{e1} & 0 & 0 \\ 0 & 0 & 0 & 0 & 0 & 0 \\ 0 & 0 & 0 & 0 & 0 & 0 \end{bmatrix}$$

Stiffness matrix for element 2 in global co-ordinate system $[K_{\text{wire},e2}]$:

$$[K_{\text{wire},e2}] = EI \begin{bmatrix} 0 & 0 & 0 & 0 & 0 & 0 \\ 0 & 0 & 0 & 0 & 0 & 0 \\ 0 & 0 & 12/l_{e2}^3 & 6/l_{e2}^2 & -12/l_{e2}^3 & 6/l_{e2}^2 \\ 0 & 0 & 6/l_{e2}^2 & 4/l_{e2} & -6/l_{e2}^2 & 2/l_{e2} \\ 0 & 0 & -12/l_{e2}^3 & -6/l_{e2}^2 & 12/l_{e2}^3 & -6/l_{e2}^2 \\ 0 & 0 & 6/l_{e2}^2 & 2/l_{e2} & -6/l_{e2}^2 & 4/l_{e2} \end{bmatrix}$$

Global stiffness matrix [K]:

$$[K] = [K_{\text{wire},e1}] + [K_{\text{wire},e2}] \quad (3.11)$$

Load vector:

External load and momenta are at node c (clamp).

$$\{F\} = \{0, 0, F_c, M_c, 0, 0\}^T \quad (3.12)$$

Where:

- F_c is the load at clamp
- M_c is the moment at clamp

3.5 Equation of motion

The equation of motion of the system reads:

$$[M]\{\ddot{X}\} + [C]\{\dot{X}\} + [K]\{X\} = \{F\} \quad (3.13)$$

$$\{\ddot{X}\} = \{\ddot{x}_1, \ddot{\phi}_1, \ddot{x}_c, \ddot{\phi}_c, \ddot{x}_2, \ddot{\phi}_2\}^T$$

$$\{\dot{X}\} = \{\dot{x}_1, \dot{\phi}_1, \dot{x}_c, \dot{\phi}_c, \dot{x}_2, \dot{\phi}_2\}^T \quad (3.14)$$

$$\{X\} = \{x_1, \phi_1, x_c, \phi_c, x_2, \phi_2\}^T$$

Where:

- $[M]$, $[C]$, $[K]$ are global mass matrix, viscous damping matrix and stiffness matrix of the system, having dimension $[6 \times 6]$
- $\{\ddot{X}\}$, $\{\dot{X}\}$, $\{X\}$ are acceleration, velocity and displacement vector of dimension $\{6 \times 1\}$
- $\{F\}$ is the Global force vector Eq (3.12).

3.6 Damping matrix

Hysteretic damping:

The damping matrix is characterized as being proportionate to the stiffness matrix by a coefficient denoted as β , which is referred to as the hysteretic damping constant. The selection of hysteretic damping is substantiated by the observation that the behavior of numerous materials can be effectively delineated by a genuine hysteresis cycle when subjected to a load exhibiting a sinusoidal trend over time.

The stiffness of a structural element incorporating hysteretic damping can be represented in the form of complex stiffness [12]. The loss factor is intricately associated with the material properties, structural shape, curvature, and dimensions of the element.

$$[K_{eq}] = [K](1 + i\beta) \quad (3.15)$$

$$[C] = \frac{i\beta}{\omega} [K] \quad (3.16)$$

Where:

- β is the loss factor
- ω is the frequency
- $[K]$ is the system stiffness matrix
- $[K_{eq}]$ is equivalent stiffness matrix with hysteresis contribution
- $[C]$ is the equivalent viscous damping matrix in the frequency domain

Damping matrix global coordinate system:

The damping matrix in the global reference is assembled by considering the two wire elements and applying Eq. 3.15:

Loss factor is a function of length and curvature. Since the Stockbridge is asymmetric, two damping coefficients are considered different and identified by the subscripts 1 and 2.

$$[C_{wire,e1}] = \frac{i\beta_{wire,e1}}{\omega} [K_{wire,e1}] \quad (3.17)$$

$$[C_{wire,e2}] = \frac{i\beta_{wire,e2}}{\omega} [K_{wire,e2}]$$

Therefore, the damping matrix $[C]$ results in:

$$[C] = [C_{wire,e1}] + [C_{wire,e2}] \quad (3.18)$$

3.7 Dynamic stiffness and phase (Master/slave method)

Known parameters from the experimental data is net force transmitted to the moving base and displacement at clamp, hence the equation of motion is rearranged in this section to make these quantities explicit. This is done by separating the contribution of the clamp (bounded) and masses (free), respectively named with subscripts B and F [10].

Split force vector:

$$\begin{aligned} \{F\} &= \{F_F, F_B\}^T \\ \text{Free DOFs: } \{F_F\} &= \{0, 0, 0, 0\}^T_{\text{NULL VECTOR}} \\ \text{Bounded DOFs: } \{F_B\} &= \{F_C, M_C\}^T \end{aligned} \quad (3.19)$$

Split displacement vector:

$$\begin{aligned} \{X\} &= \{X_F, X_B\}^T \\ \text{Free DOFs: } \{X_F\} &= \{x_1, \varphi_1, x_2, \varphi_2\}^T \\ \text{Bounded DOFs: } \{X_B\} &= \{x_C, \varphi_C\}^T \end{aligned} \quad (3.20)$$

Split equation of motion:

$$\begin{aligned} [M_{FF}]\{\ddot{X}_F\} + [C_{FF}]\{\dot{X}_F\} + [K_{FF}]\{X_F\} &= -[M_{FB}]\{\ddot{X}_B\} + [C_{FB}]\{\dot{X}_B\} + [K_{FB}]\{X_B\} \\ [M_{BF}]\{\ddot{X}_F\} + [C_{BF}]\{\dot{X}_F\} + [K_{BF}]\{X_F\} &= \{F_B\} - [M_{BB}]\{\ddot{X}_B\} + [C_{BB}]\{\dot{X}_B\} + [K_{BB}]\{X_B\} \end{aligned} \quad (3.21)$$

The load vector is considered to be of harmonic type, and thus the response of the system:

$$\begin{aligned} \{X\} &= \{X_0\}e^{i\omega t} \\ \{\dot{X}\} &= i\omega\{X_0\}e^{i\omega t} \\ \{\ddot{X}\} &= -\omega^2\{X_0\}e^{i\omega t} \\ \{F\} &= \{F_0\}e^{i\omega t} \end{aligned} \quad (3.22)$$

Substituting Eq (3.22) in Eq. (3.21) yields:

$$\begin{aligned} [A]\{X_{F0}\} &= [B]\{X_{B0}\} \\ [C_1]\{X_{F0}\} &= \{F_{B0}\} + [D]\{X_{B0}\} \end{aligned} \quad (3.23)$$

Where:

$$\begin{aligned}
[A] &= -\omega^2 [M_{FF}] + i\omega [C_{FF}] + [K_{FF}] \\
[B] &= -(-\omega^2 [M_{FB}] + i\omega [C_{FB}] + [K_{FB}]) \\
[C_1] &= \omega^2 [M_{BF}] + i\omega [C_{BF}] + [K_{BF}] \\
[D] &= -(-\omega^2 [M_{BB}] + i\omega [C_{BB}] + [K_{BB}])
\end{aligned}
\tag{3.24}$$

From Eq.3.21

$$\begin{aligned}
\{X_{FO}\} &= [A]^{-1} [B] \{X_{BO}\} \\
\{F_{BO}\} &= ([C_1][A]^{-1} [B] - [D]) \{X_{BO}\}
\end{aligned}
\tag{3.25}$$

Force transmitted to the base: The matrix of forces and moments transmitted to the moving base can be derived from the previous equations. In particular, the matrix [H] is considered, that is the force transmitted per unit of clamp motion.

$$\begin{aligned}
[H(\omega)] &= \{F_{BO}\} \{X_{BO}\}^{-1} = [C_1][A]^{-1} [B] - [D] \\
[H(\omega)] &= \begin{bmatrix} f_{uu} & f_{u\phi} \\ f_{\phi u} & f_{\phi\phi} \end{bmatrix}
\end{aligned}
\tag{3.26}$$

The matrix [H] has four contributions, namely f_{uu} , $f_{u\phi}$, $f_{\phi u}$ and $f_{\phi\phi}$. Since the experiments involve a simple vertical motion of the base, only the first contribution f_{uu} will be considered in the following. This contribution will be referred to as “dynamic stiffness”, since it is defined as force (in [N]) over base vertical amplitude displacement (in [mm]). It is a complex function, and thus it will be represented in magnitude and phase.

$$\begin{aligned}
\text{Dynamic stiffness} &= \text{Modulus or Absolute of } f_{uu} \\
\text{Phase} &= \text{angle of } f_{uu}
\end{aligned}
\tag{3.27}$$

Utilizing the formulation presented in Eq. 3.26, one can generate plots depicting the dynamic stiffness for various frequency values, as illustrated in Figure 3.8. This is achieved under the assumption of specific parameters that represents the model of the Stockbridge damper. In the example of Figure 3.8, the loss factors are $\beta_1 = \beta_2 = 0.5$, the dimensions are $a_1 = 28.3\text{mm}$, $a_2 = 15.4\text{mm}$, the flexural rigidity is $EJ_{\text{static}} = 113 \text{ Nm}^2$, and the linear density of the messenger wire is $\mu = 14.67 \text{ kg/m}$.

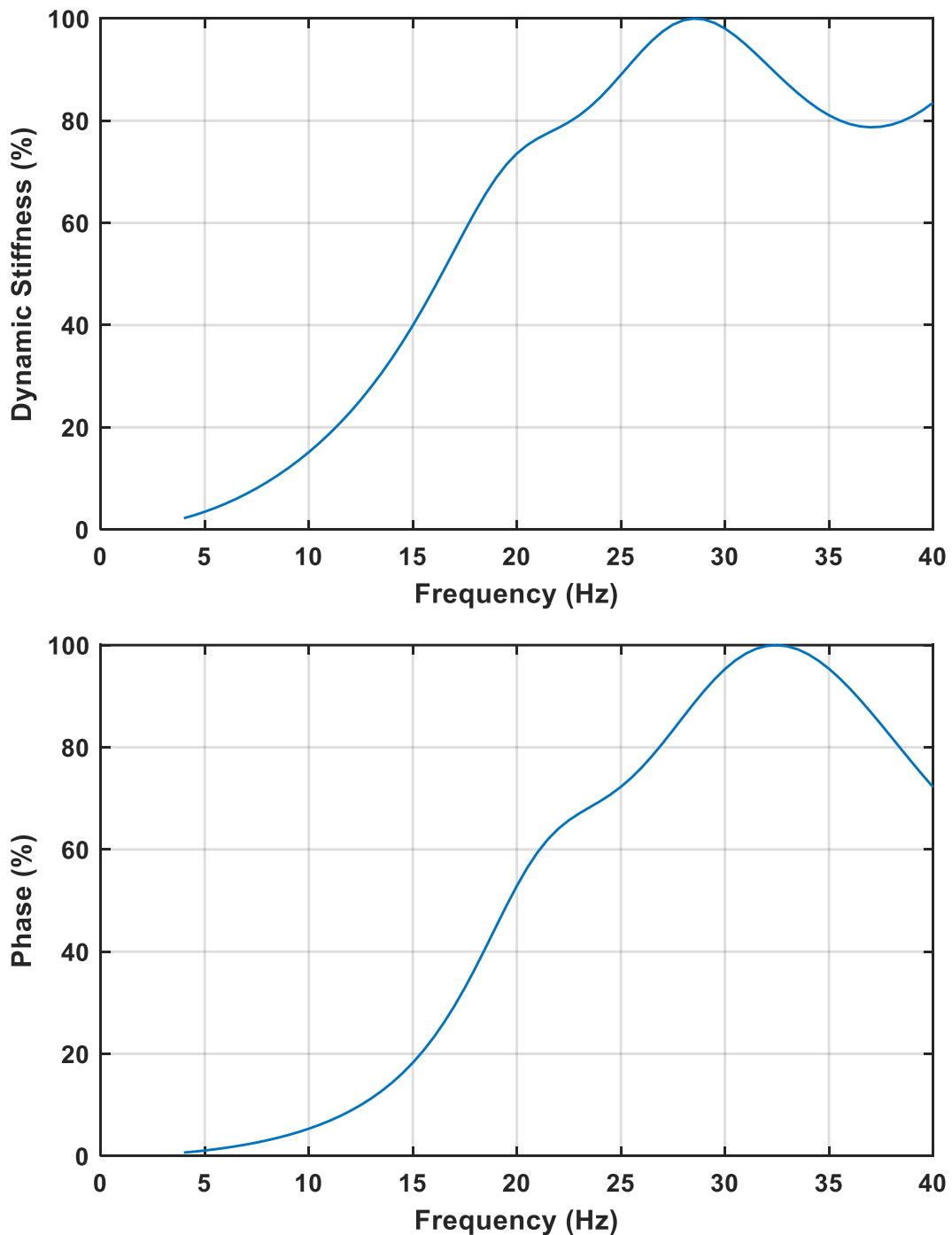


Figure 3.8. Dynamic stiffness and phase vs frequency plot from model

Chapter 4

Model fitting

The dynamic model of the system relies on a certain number of parameters that originate from geometrical, material and damping properties. Updating the model parameters to find the best fit to experimental measurements is a crucial step in the design and model validation of dynamic systems. In this work, this is done using Genetic Algorithms (GAs). Boundaries for each variable of the optimization problems are first established, and an endeavor is made to fit the model to the experimental curves. The objective is to obtain parameters that result in the best fit.

4.1 Introduction to genetic algorithm

The Genetic Algorithm (GA) is an optimization tool developed by using theory of nature's evolutionary mechanisms and used to find approximate solutions to optimization and search problems. Here are the typical steps involved in a genetic algorithm (Figure 4.1 shows flowchart of genetic algorithm).

- **Initialization:** Initiate process with a randomly generated population of individuals.
- **Selection:** Calculate the fitness of each individual in the population. The fitness is a measure of how good the solution is (Section 4.2).
- **Crossover (Reproduction):** Select pairs of individuals based on their fitness values and create new individuals by combining their features. This mimics the process of genetic recombination.
- **Mutation:** Introduce small random changes in some individuals. This introduces genetic diversity and helps in exploring the solution space.
- **Replacement:** Replace the old population with the new one.
- **Termination:** Repeat the selection, crossover, and mutation steps until a stopping criterion is met (e.g., a maximum number of generations, or a satisfactory fitness level is achieved).

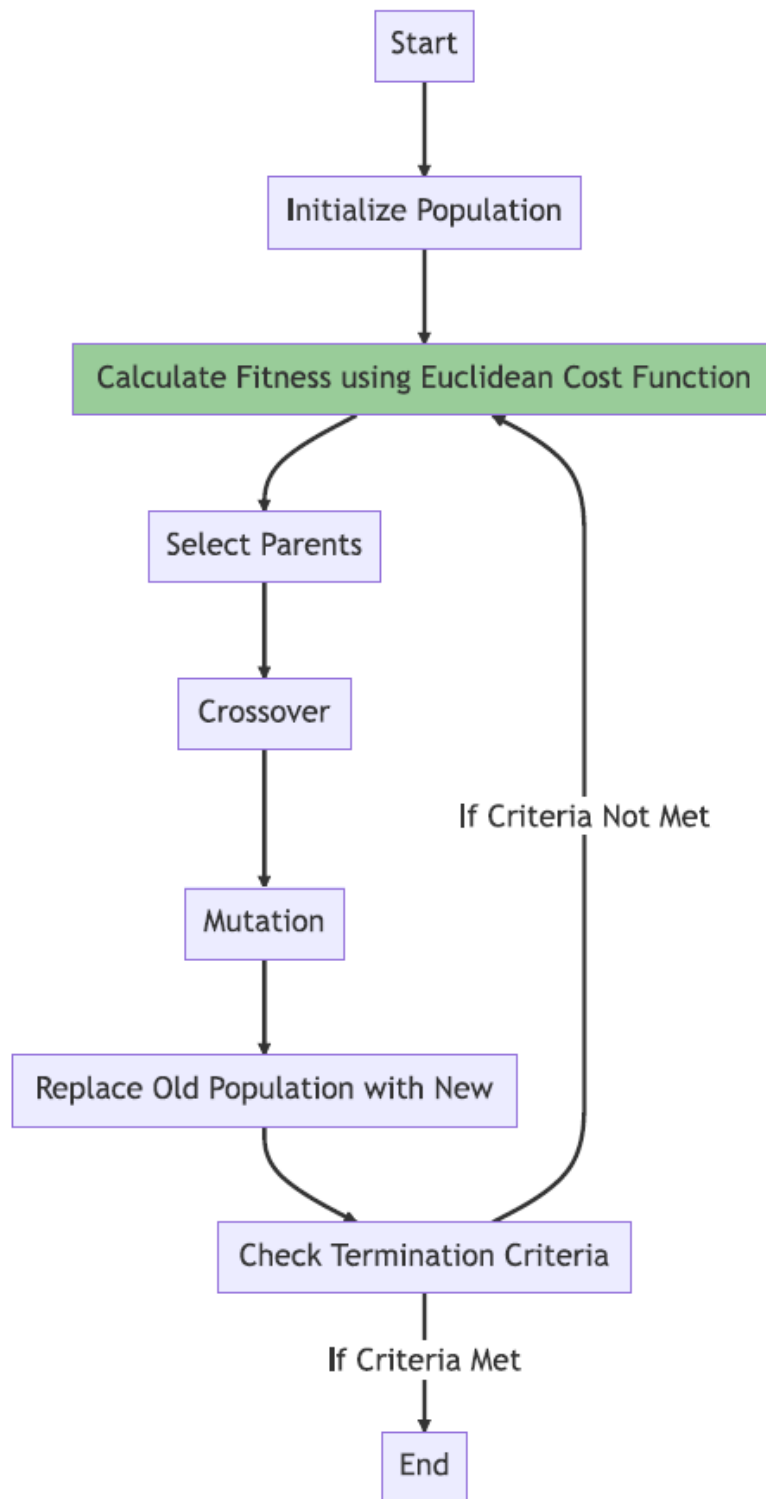


Figure 4.1. Genetic algorithm flowchart

The optimization problem can be solved in Matlab by using “ga” function (see Eq. (4.1)).

$$\begin{aligned} & [\mathbf{x}, \mathbf{fval}] \\ & = \text{ga}(\text{fun}, \text{nvars}, \mathbf{A}, \mathbf{b}, \mathbf{Aeq}, \mathbf{beq}, \text{lb}, \text{ub}, \text{nonlcon}, \text{intcon}, \text{options}) \end{aligned} \quad (4.1)$$

Here:

- fun is objective function to be minimized
- nvars is number of design variables
- A, b: Linear inequality constraints. The matrix A and vector b define constraints of the form $\mathbf{A} \cdot \mathbf{x} \leq \mathbf{b}$
- Aeq, beq: Linear equality constraints. The matrix Aeq and vector beq define constraints of the form $\mathbf{Aeq} \cdot \mathbf{x} = \mathbf{beq}$.
- lb and ub is lower and upper bounds of design variables
- nonlcon: Nonlinear constraint function.
- intcon: Integer constraint indices. If certain variables are constrained to take integer values, you specify their indices using this parameter.
- options: A structure containing optimization options and settings.

In this thesis, arguments A, b, Aeq, beq, nonlcon, and intcon will not be employed

User selected options can be defined using “optimoptions” function.

$$\begin{aligned} \text{options} &= \text{optimoptions}('ga', \dots \\ &'MaxGenerations', 500, \dots \\ &'FunctionTolerance', 1e - 6, \dots \\ &'PopulationSize', 500, \dots \\ &'InitialPopulationMatrix', \text{INIT}, \dots \\ &'PlotFcn', @gaplotbestf); \end{aligned} \quad (4.2)$$

Optimoptions('ga', ...): This initializes the options for the Genetic Algorithm ('ga').

MaxGenerations, 500: This sets the maximum number of generations or iterations the genetic algorithm will run. If the algorithm does not converge to a solution before 500 generations, it will stop.

FunctionTolerance, 1e-6: This sets the function tolerance to 1e-6. The algorithm will stop if the change in the best objective function value is less than this value.

PopulationSize, 500: This sets the size of the population for each generation to 500. A larger population might increase the chances of finding a global optimum but will also increase the computational time.

InitialPopulationMatrix, INIT: This sets the initial population matrix to the variable 'INIT'. The initial population matrix provides a starting point for the genetic algorithm. If a good guess for the solution is available, this can be set here to potentially speed up convergence.

PlotFcn, @gaplotbestf: This sets the plotting function to "gaplotbestf", which is one of the built-in plotting functions in MATLAB for genetic algorithms. When the algorithm runs, it will display a plot showing the best objective function value in each generation.

4.2 Euclidean fitness function

Euclidean distance represents the straight-line distance between two points in Euclidean space. The Euclidean distance can be used as a fitness function to measure the dissimilarity between predicted values and actual values (see Eq. (4.3)).

$$\text{Euclidean distance} = \sqrt{\sum_{i=1}^n (a_i - b_i)^2} \quad (4.3)$$

Where:

a_i is the i^{th} measured value

b_i is the i^{th} computed value

GA needs the output of the fitness function to be a scalar in order to find its global minimum. The measurements and the 6DOF model of the Stockbridge damper rely on the computation of the force transmitted to the base, that is a complex quantity function of the frequency. It is thus a vector of frequency lines, that can be split into its absolute value (dynamic stiffness) and its phase. The following cost (or fitness) functions is therefore defined in order to condense this information into a scalar error measure, using the Euclidian norm.

Cost function or fitness value:

$$\varepsilon = \sqrt{W_1 \sum_{i=1}^n \frac{(a_i - b_i)^2}{a_i^2} + W_2 \sum_{i=1}^n \frac{(x_i - y_i)^2}{x_i^2}} \quad (4.4)$$

Where:

- a_i and b_i are the measured (experimental) and computed values (6 DOF model) of dynamic stiffness
- x_i and y_i are the measured (experimental) and computed (6 DOF model) values of phase
- W_1 and W_2 are positive weights such that their sum is equal to one.

The dynamic stiffness vs. frequency curve fitting incorporates the weight W_1 , whereas the phase vs. frequency curve fitting incorporates the weight W_2 . As the phase curves exhibit greater distortion in comparison to the stiffness curves, a higher emphasis is placed on the weighting factor W_2 . The following values are therefore set: $W_2=0.7$, $W_1=1-0.7=0.3$.

It should be noted that the frequency increment step is not constant in the measured data (Figure 4.2 and Table 2.2). A weight vector $\{W_3\}$ is therefore introduced to account for this disparity, as a function of step change.

$$\varepsilon = \sqrt{W_1 \sum_{i=1}^n \frac{(a_i W_{3,i} - b_i W_{3,i})^2}{a_i^2 W_{3,i}} + W_2 \sum_{i=1}^n \frac{(x_i W_{3,i} - y_i W_{3,i})^2}{x_i^2 W_{3,i}}} \quad (4.5)$$

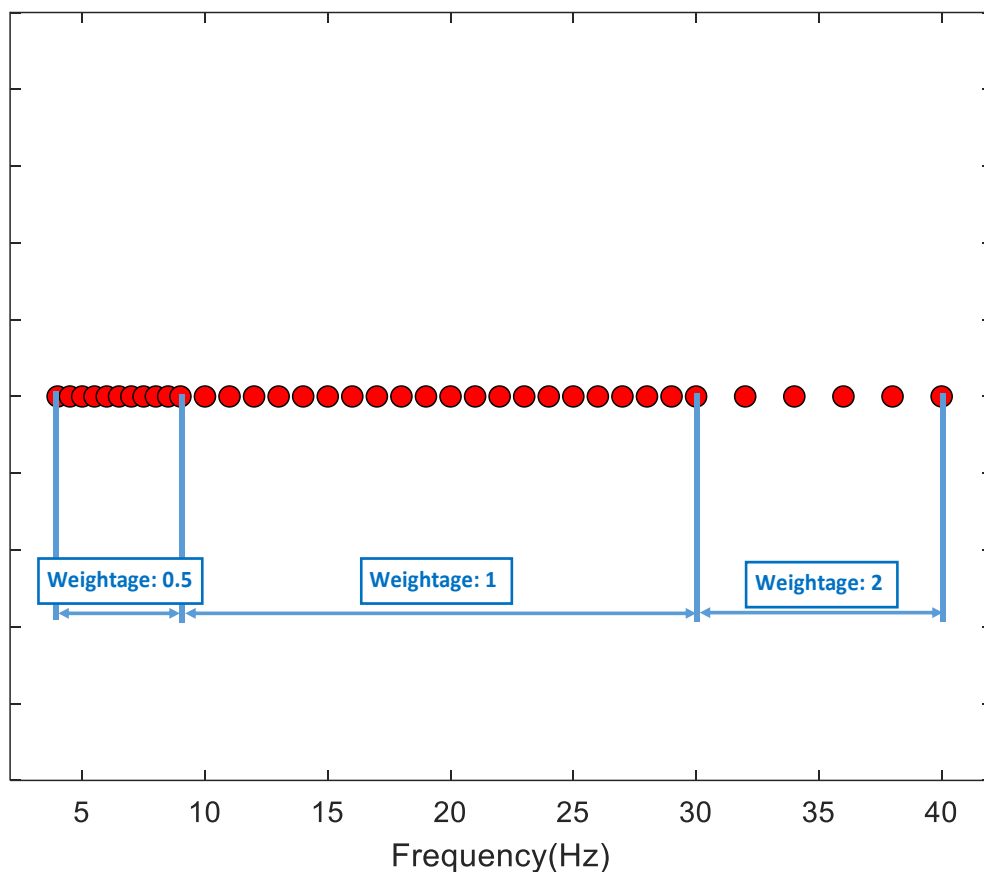


Figure 4.2. Frequency step

4.3 Parameters of Stockbridge damper

The Stockbridge damper consists of several components, including the masses (m_1 and m_2), clamp, and messenger cable whose dimensions (shown in Figure 4.3) and properties (listed in Table 4.1 and Table 2.2) are needed for curve fitting.

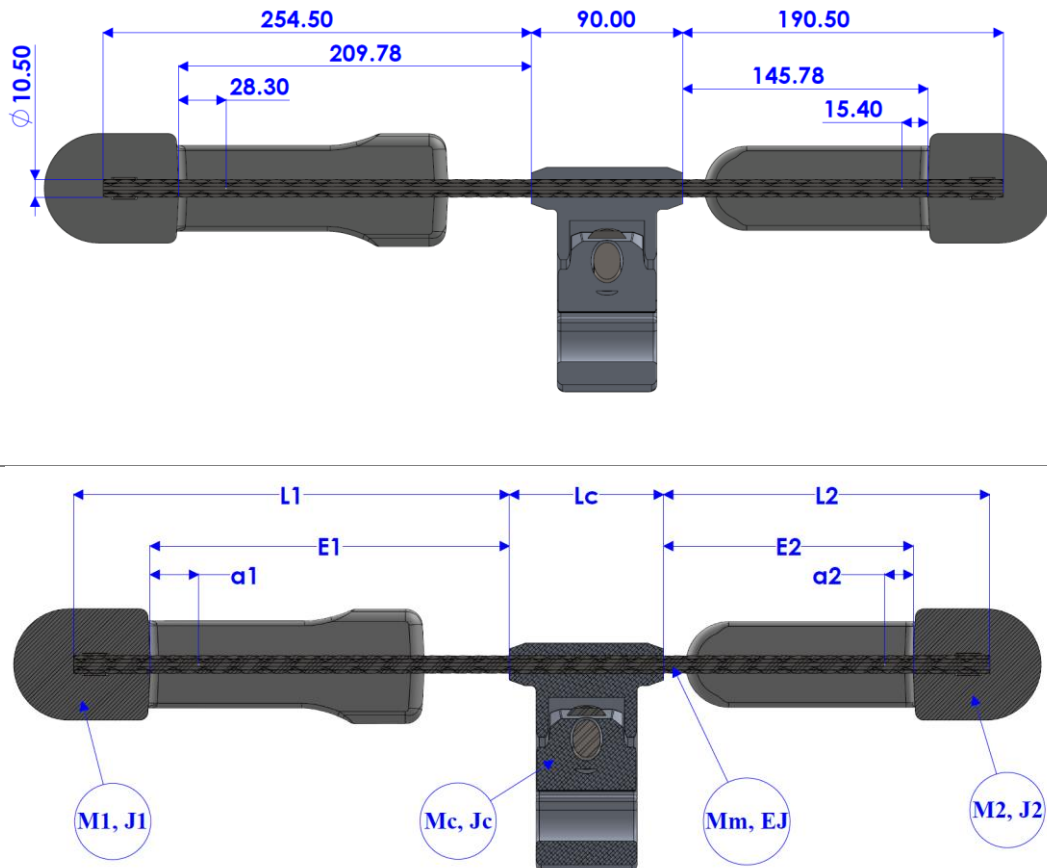


Figure 4.3. Stockbridge damper dimensions

Inertial properties of the masses:

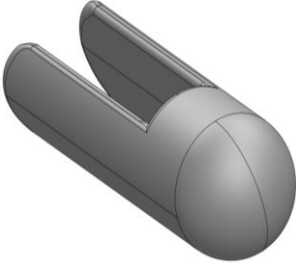
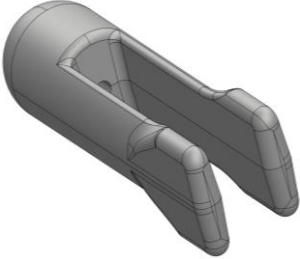
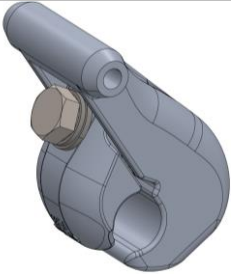
Element	Parameters		
	Mass (kg)	Moment of inertia (kg m ²)	Distance (mm)
 Mass m ₂	$m_2 = 2.4762$	$J_2 = 0.0082$	$a_2 = 15.4$
 Mass m ₁	$m_1 = 3.1005$	$J_1 = 0.0163$	$a_1 = 28.3$
 Clamp	$m_c = 1.05$	$J_c = 0.0015$	$a_c = 0$

Table 4.1. Inertial properties of masses

Inertial and stiffness properties of the messenger cable:

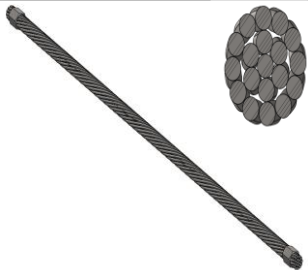
Element	Parameters		
	Linear density (Kg/m)	Modulus of elasticity (N/m ²)	Static flexural stiffness (N m ²)
 <p>Messenger cable (1-6/12)</p>	$\mu = 14.67$	$E = 2.07 \times 10^{11}$	$E_m J_{m,static} =$ $E J \cos^3 \alpha =$ 113 Helix angle (α) = 75° Diameter wire (D) = 10.5mm

Table 4.2. Inertial and stiffness properties of the messenger cable

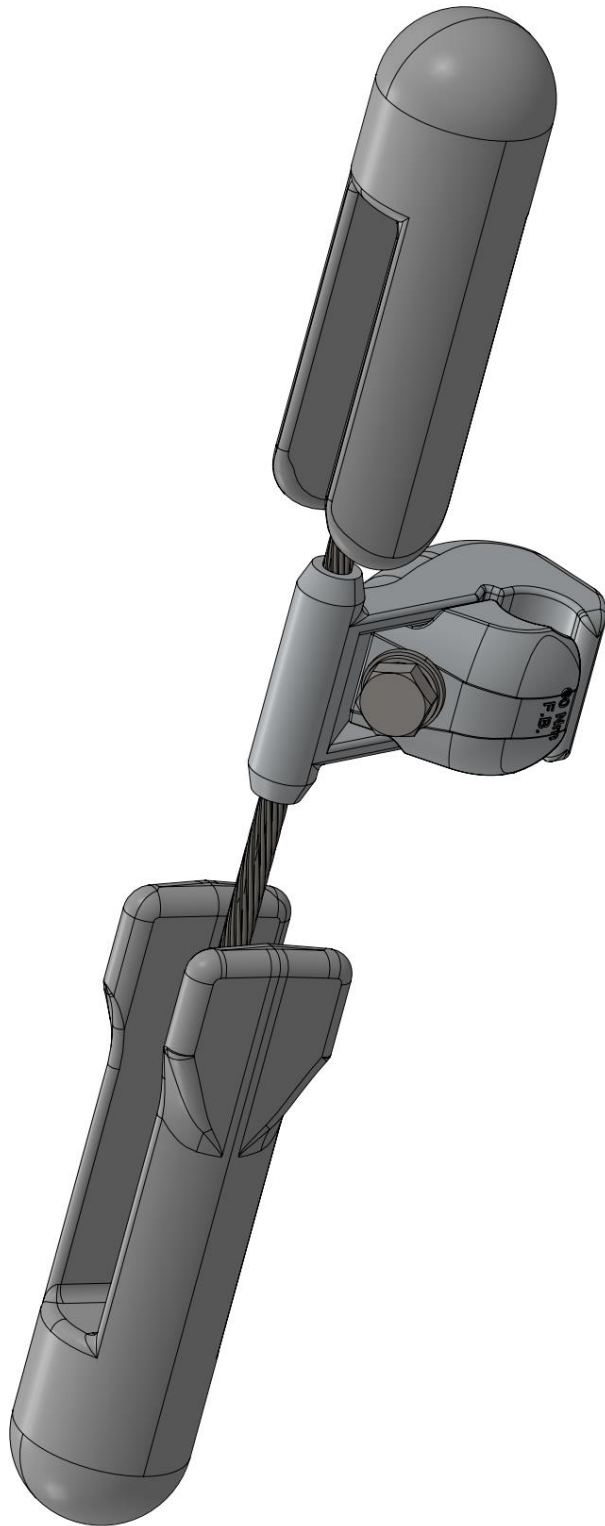


Figure 4.4. Stockbridge damper (3D)

Three distinct sets of vector parameters ($\{\theta_1\}$, $\{\theta_2\}$ and $\{\theta_3\}$) have been chosen for the purpose of curve fitting, which are listed in the Table 4.3, The first set $\{\theta_1\}$ encompasses parameters including β , a_1 , a_2 , and $E_m J_m$. The second set $\{\theta_2\}$ consists of β_1 , β_2 , a_1 , a_2 , and $E_m J_m$, while the third set $\{\theta_3\}$ encompasses β_1 , β_2 , a_1 , a_2 , $E_m J_m$, and ρ .

In this context, β_1 and β_2 denote the loss factors associated for the lengths $L_1+L_c/2$ and $L_2+L_c/2$ of the messenger wire (Figure 4.3) , β represents the loss factor of messenger wire (case $\beta_1 = \beta_2 = \beta$), and a_1 and a_2 correspond to the dimensions as illustrated in the Table 4.1. $E_m J_m$ stands for the flexural stiffness, and ρ represents the mass of the messenger cable.

Sets	Parameters
θ_1	$\beta, a_1, a_2, E_m J_m$
θ_2	$\beta_1, \beta_2, a_1, a_2, E_m J_m$
θ_3	$\beta_1, \beta_2, a_1, a_2, E_m J_m, \rho$

Table 4.3. Parameters sets to optimize

Optimizing parameters have bound conditions, where dimensions a_1 and a_2 cannot vary more than $\pm 5\%$. Messenger cable is highly damped and β is set not to exceed 2.5. Flexural stiffness value is less than static flexural stiffness and greater than zero.

Parameters	Boundaries
β, β_1, β_2	$0 \div 2.5$
a_1, a_2	$\pm 5\%$
$E_m J_m$	$0 < E_m J_m \leq E_m J_m \text{ static}$

Table 4.4. Limit box for the parameters

4.4 Curve fitting with different sets (θ_1, θ_2 and θ_3) of parameters

Parameters to optimize:

$$\begin{aligned} \{\theta_1\} &= \{\beta, a_1, a_2, E_m J_m\}^T \\ \{\theta_2\} &= \{\beta_1, \beta_2, a_1, a_2, E_m J_m\}^T \\ \{\theta_3\} &= \{\beta_1, \beta_2, a_1, a_2, E_m J_m, \rho\}^T \end{aligned} \quad (4.6)$$

Fitness function:

Refer to the section “4.2 Euclidean fitness function”

Genetic Algorithm:

Variables with upper and lower bounds	$\{\theta_1\}$	<pre> %Defining variable for optimization problem INIT = [beta a1 -a2 E_m J_m]; %Setting bounds %Lower boundaries for the variables lb = [0 a1*0.95 -a2*1.05 E_m J_m*0.01]; %Upper boundaries for the variables ub = [2.5 a1*1.05 -a2*0.95 E_m J_m]; </pre>
	$\{\theta_2\}$	<pre> INIT = [beta1 beta2 a1 -a2 E_m J_m]; lb = [0 0 a1*0.95 -a2*1.05 E_m J_m*0.01]; ub = [2.5 2.5 a1*1.05 -a2*0.95 E_m J_m]; </pre>
	$\{\theta_3\}$	<pre> INIT = [beta1 beta2 a1 -a2 E_m J_m rho]; lb = [0 0 a1*0.95 -a2*1.05 E_m J_m*0.01 rho*0.1]; ub = [2.5 2.5 a1*1.05 -a2*0.95 E_m J_m rho]; </pre>
Genetic Algorithm settings		<pre> % GA settings Eq (4.2) optga=optimoptions('ga',... 'MaxGenerations', 500 , ... 'FunctionTolerance', 1e-6,... 'PopulationSize', 500,... 'InitialPopulationMatrix', INIT,... 'PlotFcn', @gaplotbestf); </pre>

Optimized parameters:

The output of the genetic algorithm is the vector of optimized parameters θ^* . For the three cases considered here, it is therefore possible to set three optimization problems as in Eq. (4.7). The optimized parameters are listed in Table 4.5.

$$\begin{aligned}\operatorname{argmin}_{\theta_1} \varepsilon &= \{\theta_1^*\} = \{\beta_{\text{opt}}, a_{1 \text{ opt}}, a_{2 \text{ opt}}, E_m J_{m \text{ opt}}\}^T \\ \operatorname{argmin}_{\theta_2} \varepsilon &= \{\theta_2^*\} = \{\beta_{1 \text{ opt}}, \beta_{2 \text{ opt}}, a_{1 \text{ opt}}, a_{2 \text{ opt}}, E_m J_{m \text{ opt}}\}^T \\ \operatorname{argmin}_{\theta_3} \varepsilon &= \{\theta_3^*\} = \{\beta_{1 \text{ opt}}, \beta_{2 \text{ opt}}, a_{1 \text{ opt}}, a_{2 \text{ opt}}, E_m J_{m \text{ opt}}, \rho_{\text{opt}}\}^T\end{aligned}\quad (4.7)$$

Please refer to the following reference for the code: C. MATLAB - 6 DOF model

Figures Descriptions:

Figure 4.5, Figure 4.6 and Figure 4.7

β_1 and β_2 denote the loss factors associated with the lengths $L_1+L_c/2$ and $L_2+L_c/2$ of the messenger wire, β represents the loss factor of messenger wire (case $\beta_1 = \beta_2 = \beta$), and a_1 and a_2 correspond to the dimensions as illustrated in the Figure 4.4. $E_m J_m$ stands for the flexural rigidity, and ρ represents the mass of the messenger cable. Vertical redline in figure represents upper and lower bounds of parameters, red cross mark represents initial value of parameters and blue cross mark represents value of optimized value of the parameters.

As for the plots of the dynamic stiffness and phase vs frequency, black lines represent the locus of mean experimental data, dotted lines represent the locus of maximum and minimum experimental data and blue lines represent the optimized model output.

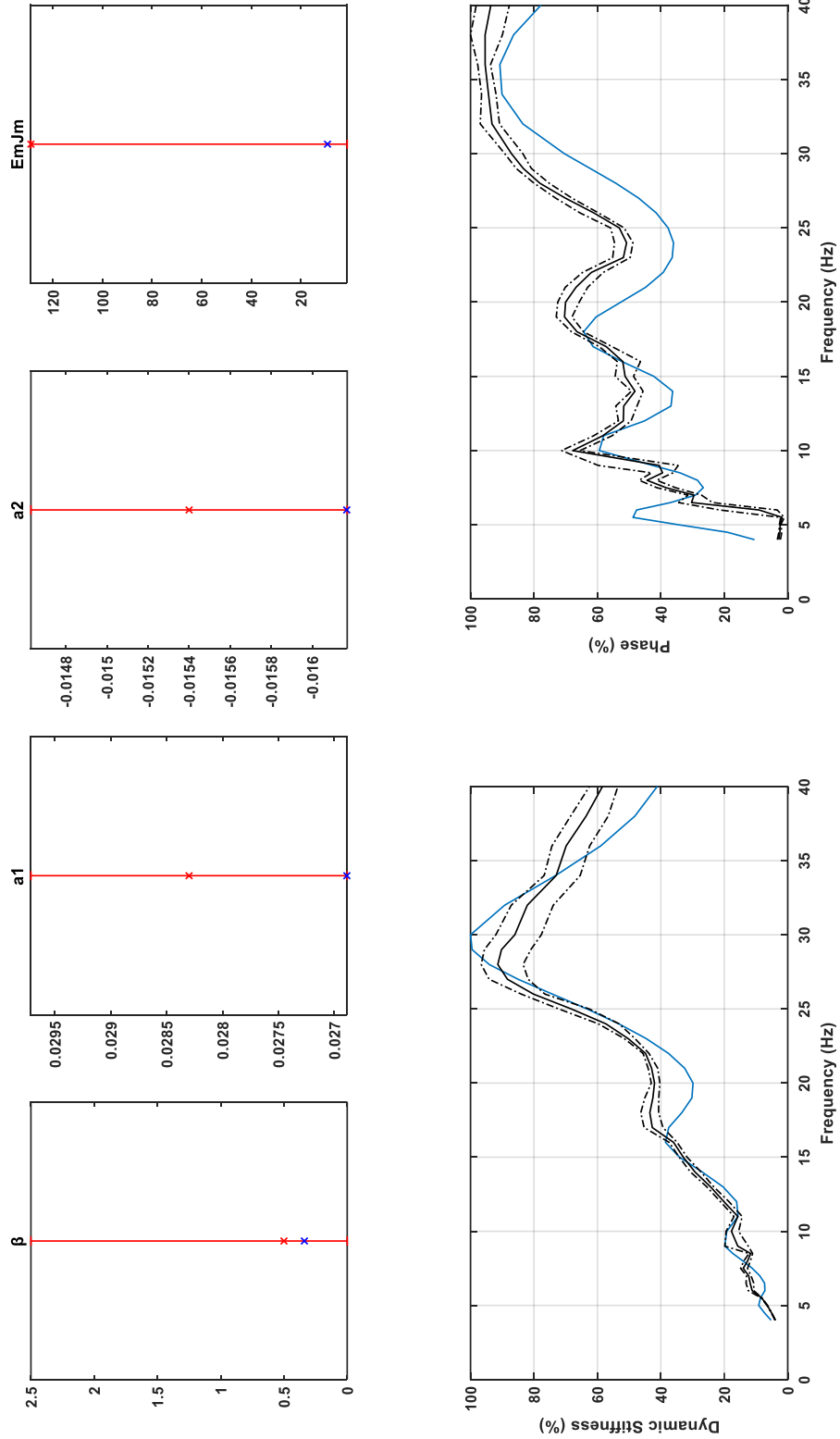


Figure 4.5. Output of genetic algorithm (Damper1, Test1-1, Set θ_1 parameters)

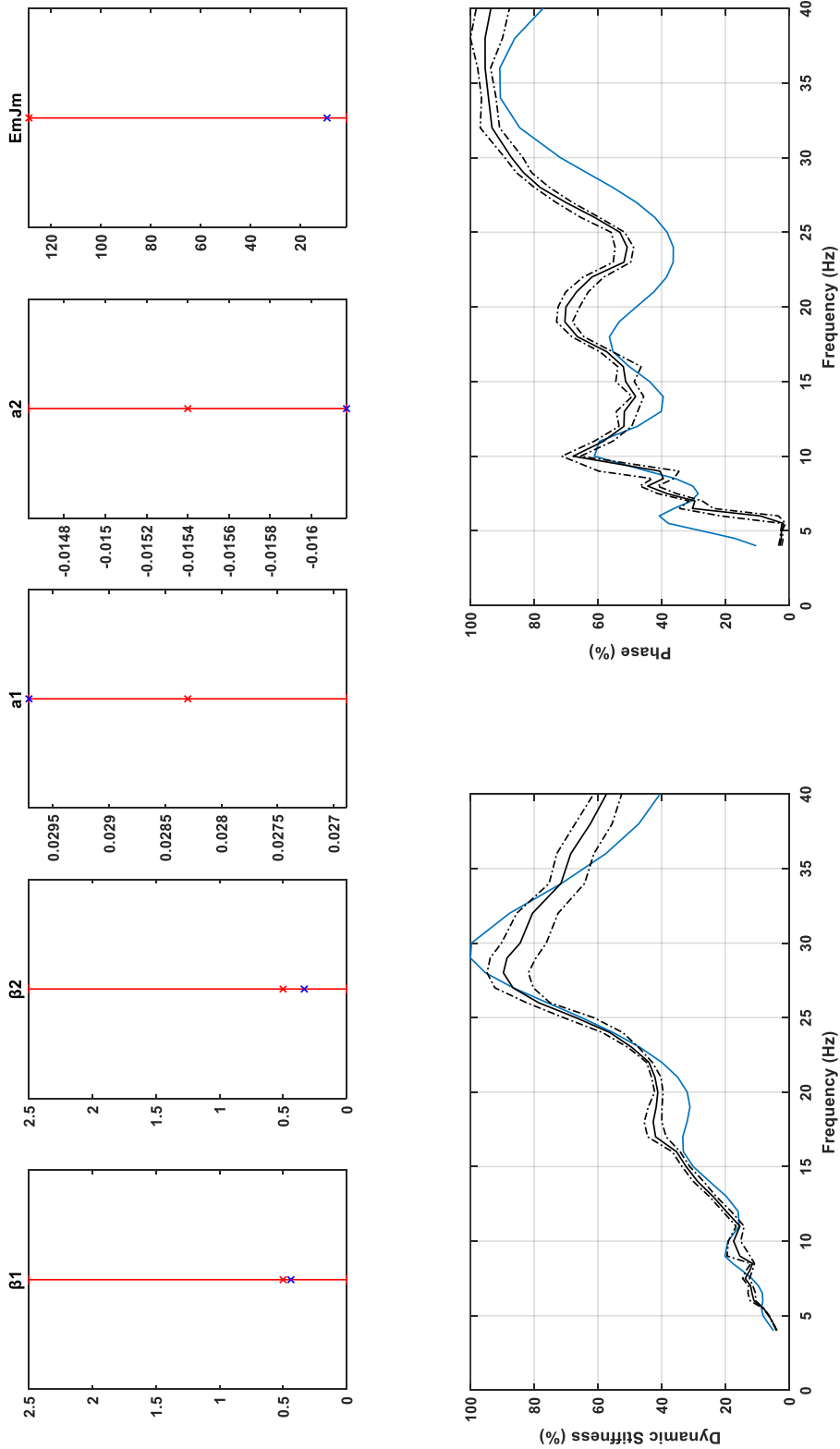


Figure 4.6. Output of genetic algorithm (Damper1, Test1-1, Set θ_2 parameters)

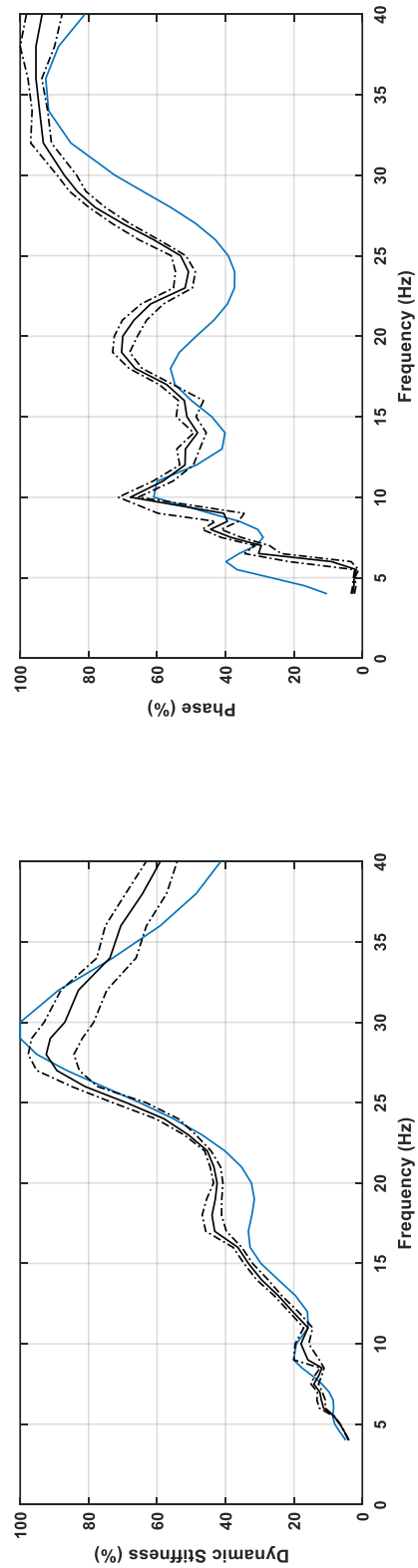
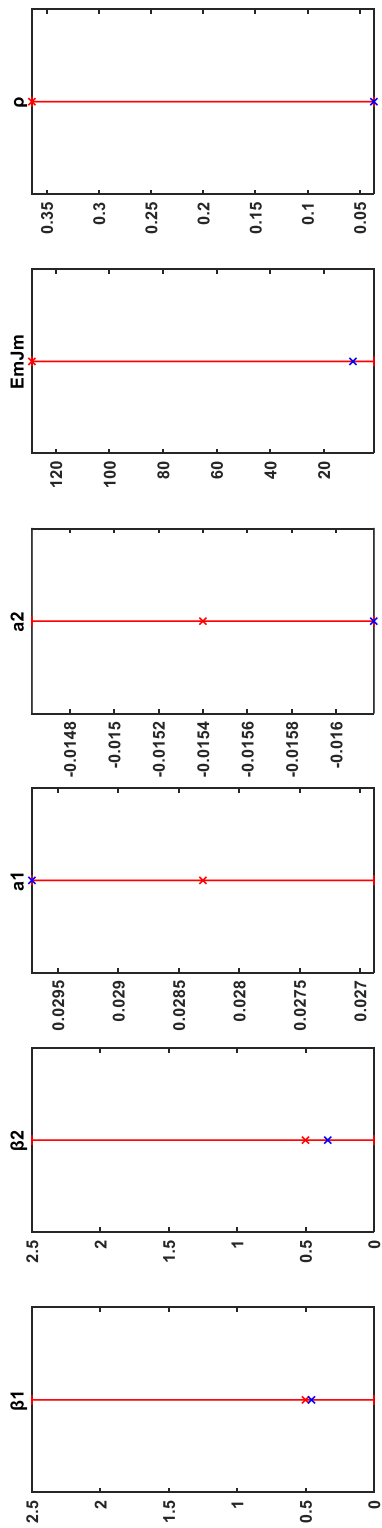


Figure 4.7. Output of genetic algorithm (Damper1, Test1-1, Set θ_3 parameters)

4.5 Optimized parameters from all tests

Damper-Test (Displacement p-p (mm))	Set θ_1 (β , a1, a2, EmJm)				Set θ_2 (β_1 , β_2 , a1, a2, EmJm)				Set θ_3 (β_1 , β_2 , a1, a2, EmJm, ρ)						
	β	a1	a2	EmJm	β_1	β_2	a1	a2	EmJm	β_1	β_2	a1	a2	EmJm	ρ
Damper1-T(0.1-0.1)	0.16	0.0297	-0.0146	28.69	0.15	0.27	0.0297	-0.0146	28.01	0.15	0.25	0.0297	-0.0146	27.88	0.0364
Damper1-T(0.2-0.2)	0.30	0.0297	-0.0162	23.34	0.22	0.42	0.0297	-0.0162	22.93	0.22	0.41	0.0297	-0.0162	22.56	0.0365
Damper1-T(0.3-0.3)	0.35	0.0287	-0.0162	15.29	0.23	0.37	0.0269	-0.0162	15.81	0.23	0.36	0.0269	-0.0162	15.74	0.0364
Damper1-T(0.4-0.4)	0.30	0.0269	-0.0162	13.00	0.31	0.30	0.0269	-0.0162	12.98	0.30	0.29	0.0269	-0.0162	12.95	0.0364
Damper1-T(0.5-0.5)	0.33	0.0269	-0.0162	11.05	0.40	0.32	0.0269	-0.0162	10.93	0.41	0.32	0.0269	-0.0162	10.91	0.0364
Damper1-T(1-1)	0.34	0.0269	-0.0162	9.23	0.44	0.33	0.0297	-0.0162	9.16	0.46	0.34	0.0297	-0.0162	9.10	0.0364
Damper1-T(2-2)	0.38	0.0274	-0.0162	6.98	0.49	0.37	0.0297	-0.0162	6.92	0.52	0.38	0.0297	-0.0162	6.81	0.0364
Damper1-T(1-1)-Oiled	0.35	0.0297	-0.0162	5.48	0.35	0.35	0.0297	-0.0162	5.48	0.37	0.35	0.0297	-0.0162	5.36	0.0364
Damper1-T(2-1)	0.35	0.0269	-0.0162	9.15	0.44	0.34	0.0269	-0.0162	9.06	0.45	0.34	0.0269	-0.0162	9.00	0.0364

Table 4.5. Optimized parameters for different sets

4.6 Conclusion on curve fitting

The optimization (dynamic stiffness and phase vs frequency) with different sets of parameters (θ_1 , θ_2 and θ_3), results in similar final curves. The values of parameters a_1 , a_2 and $E_m J_m$ are almost the same for the different sets of parameters (Table 4.5).

Decreasing the functional tolerance from $1e-6$ to $1e-10$ in GA settings (Eq. (4.2)), does not result in improvements in the optimized parameters, but only in increased computational time of the algorithm (Figure 4.8).

Furthermore, it has been found that the parameter ρ (density of the messenger wire) has poor influence in the system response, that thus its optimization is not meaningful. This can be justified by considering that the inertial contributions of the two lumped masses are way more important than the distributed inertia of the messenger wire. Also, using two different loss factors β_1 and β_2 , has no significant impact.

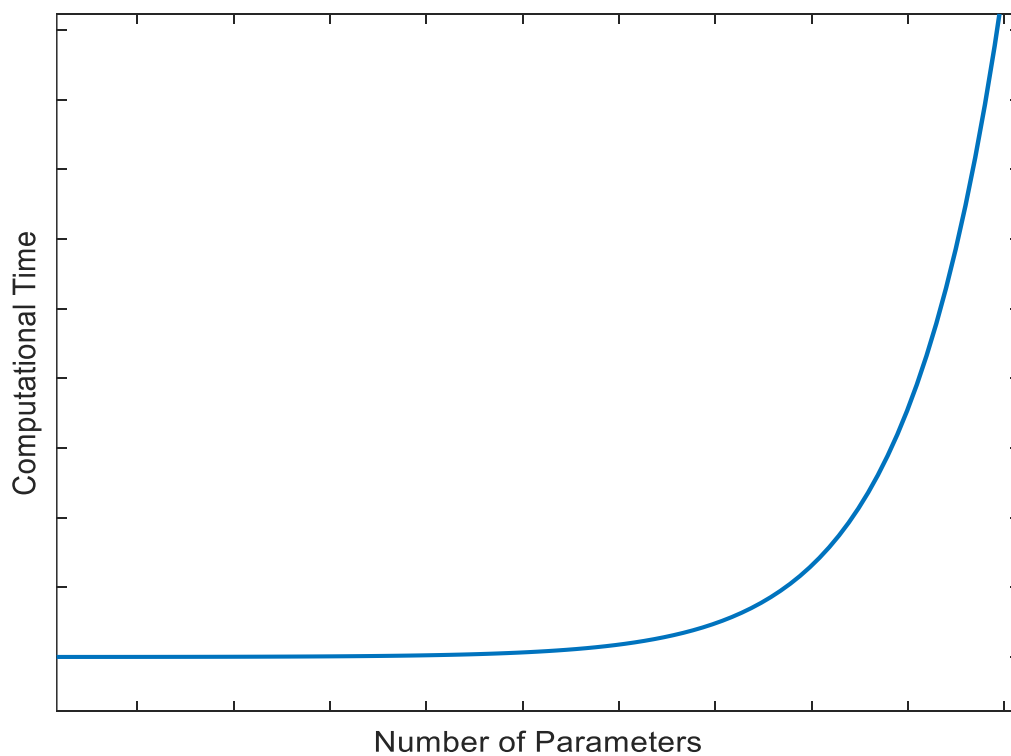


Figure 4.8. Number of parameters vs computational time

As a final comment, curve fitting is considered as satisfactory for Test1-1, Test2-1 and Test2-2 (base displacement ≥ 1 mm), but not satisfactory for Test0.5-0.5, Test 0.4-0.4, Test0.3-0.3, Test0.2-0.2 and Test0.1-0.1 (base displacement < 1 mm).

A deeper investigation of the different accuracies of the model for different base displacements can be done by inspecting the variation of the optimized flexural stiffness $E_m J_m$ across the different tests. The behavior of the flexural stiffness optimized parameter is plotted in Figure 4.9 as a function of the base displacement peak-peak amplitude. It can be observed that the flexural stiffness does not change much for the different sets of optimized parameters, but it is deeply affected by the vibration amplitude. In particular, it decreases for increasing values of amplitude vibrations.

Displacement p-p (mm)	$E_m J_m$ Set θ_1	$E_m J_m$ Set θ_2	$E_m J_m$ Set θ_3
0.1	28.69	28.01	27.88
0.2	23.34	22.93	22.56
0.3	15.29	15.81	15.74
0.4	13.00	12.98	12.95
0.5	11.05	10.93	10.91
1	9.23	9.16	9.10
2	6.98	6.92	6.81

Table 4.6. Flexural stiffness for different input displacement at the clamp.

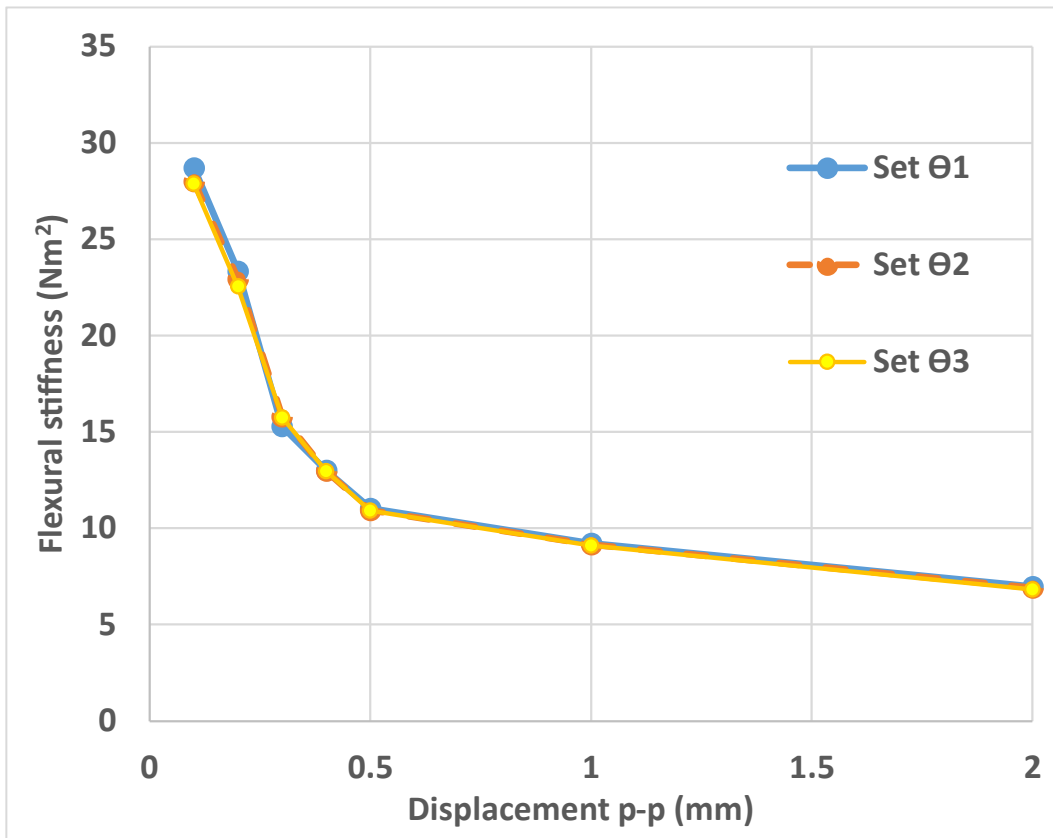


Figure 4.9. Flexural stiffness vs input displacement at the clamp (Damper1)

The behavior of the flexural stiffness is in agreement with the expectations, and also in accordance with the previous findings of the scientific literature.

A further analysis is conducted on the behavior of the optimized loss factor across the different values of the base displacement amplitude. Figure 4.10 illustrates the relationship between loss factor and base peak-peak amplitude with set θ_1 . The loss factor falls within the range of 0.3 to 0.38 for displacements ranging from 0.2 to 2 mm peak to peak. Notably, there is a sharp drop in the loss factor at a 0.1 mm peak to peak displacement. This could be explained by considering that at low amplitudes of excitation, the relative motion between the messenger wire and the base is minimized, and the flexural stiffness of the messenger cable is heightened, resulting in reduced friction. However, further analyses should be conducted to better understand this phenomenon.

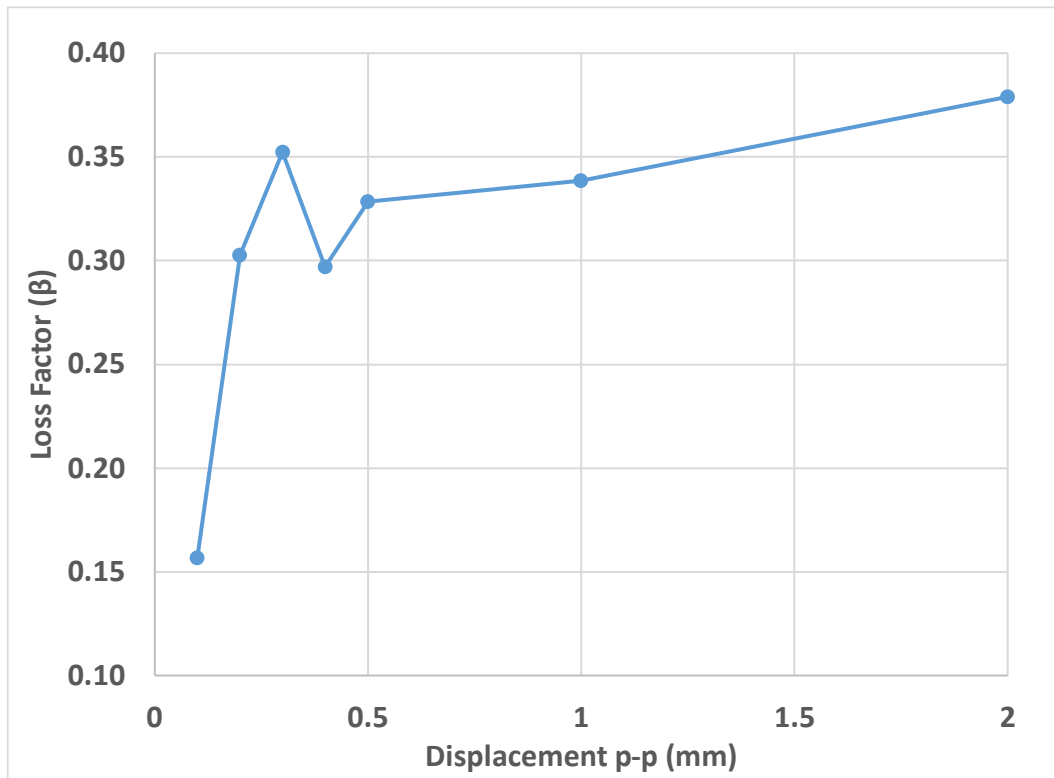


Figure 4.10. Loss factor vs displacement with set θ_1 .

4.7 Comparison of between different samples

To ensure the analysis's accuracy and reliability, all the tests previously discussed are repeated with a second sample. For the sake of clarity, the first sample will be referred to as “Damper1” and the second as “Damper2” in the following. A comprehensive list of all the tests can be found in the Appendix (A. Tests on dampers).

Figure 4.11 shows the relationship between flexural stiffness and displacement for both Damper1 and Damper2. They both exhibit a striking similarity (EJ reduces with increasing displacement) and adheres to a power law. It is noteworthy that the flexural stiffness, almost stabilizes after 0.5 mm peak-to-peak displacement.

Reduction factor: the reduction factor τ can be estimated as in the following.

$$\tau = \frac{EJ_{\text{static}}}{EJ_{\infty}} = 16.18 \div 18$$

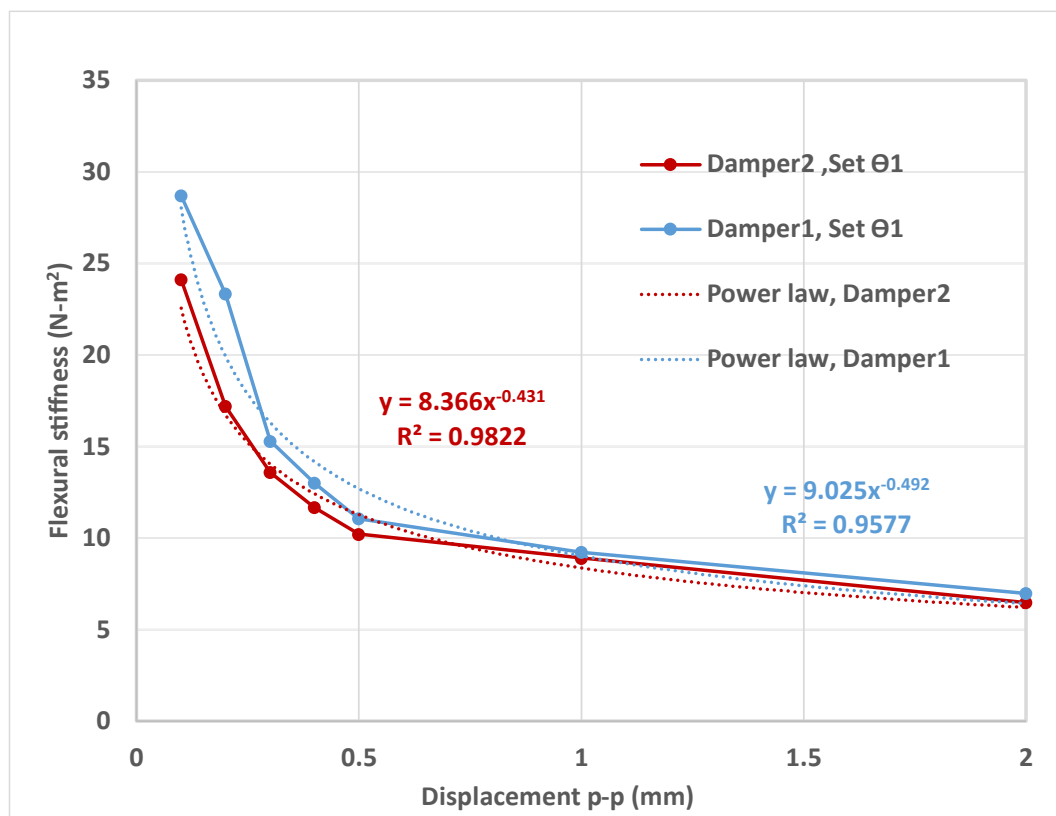


Figure 4.11. Flexural stiffness vs displacement (Damper1 and damper2)

As for the loss factor, its behavior differs between Damper1 and Damper2 below a displacement peak amplitude of 0.5 mm, as illustrated in Figure 4.12, with friction assuming a critical role. Nevertheless, beyond this value, the loss factor exhibits no significant variations.

It appears that the system must be excited beyond a specific threshold amplitude order to bring out effective damping. This phenomenon may be attributed to the increase in stiffness, resulting in restricted relative motion between wires in contact. In such instances, the messenger cable behaves more like to a rod than a rope.

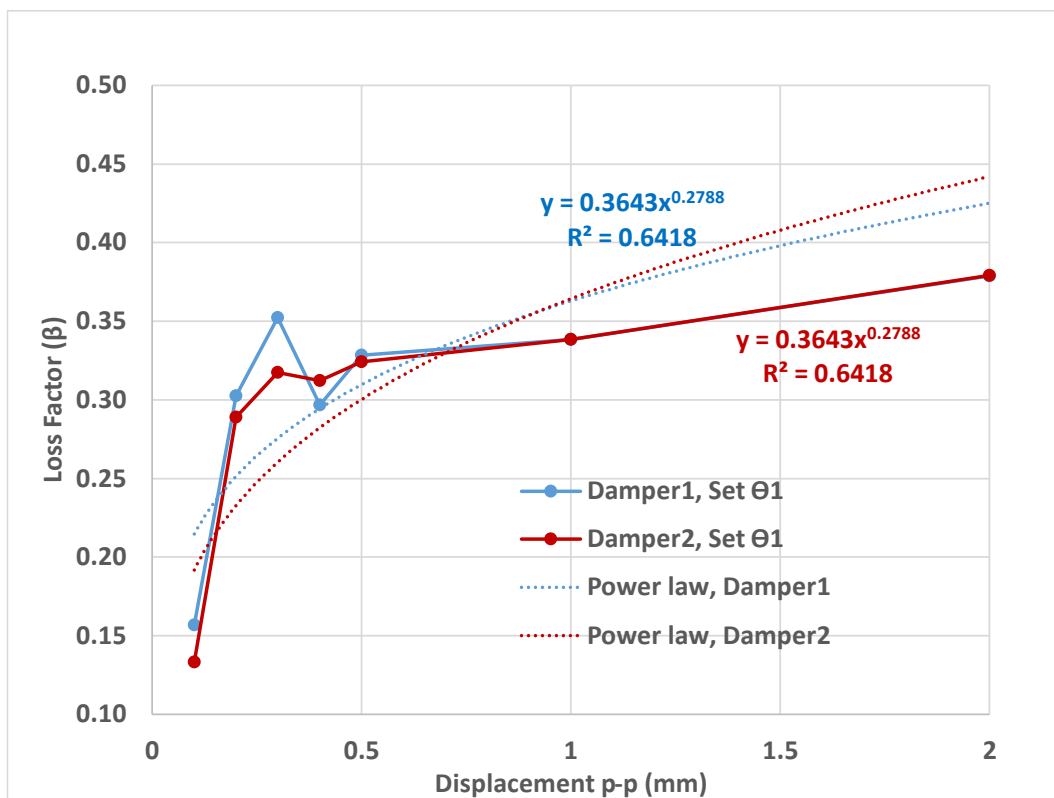


Figure 4.12. Loss factor vs displacement (Damper1 and damper2)

Chapter 5

Improved model

5.1 Non-constant flexural rigidity

It is assumed in this chapter that the flexural rigidity (EJ) of the messenger wire can be written as polynomial function of the excitation frequency (ω). This is intended to be a first step towards a comprehensive nonlinear model of the Stockbridge damper that includes the dependency of the flexural stiffness of the wire with respect to its curvature. The optimization problem is therefore solved using genetic algorithm with several polynomial orders of EJ (second, third and fourth orders) with condition $EJ > 0$.

In the below equations q_1, q_2, q_3, q_4, q_5 are the coefficients of the polynomial expansion and ω is the frequency of the excitation.

Polynomial equation :

$$EJ(\omega) = (q_1 + q_2\omega + q_3\omega^2 + q_4\omega^3 + q_5\omega^4 + \dots) \quad (5.1)$$

Condition:

$$EJ(\omega) > 0$$

Second order polynomial:

$$EJ(\omega) = (q_1 + q_2\omega + q_3\omega^2) \quad (5.2)$$

Third order polynomial:

$$EJ(\omega) = (q_1 + q_2\omega + q_3\omega^2 + q_4\omega^3) \quad (5.3)$$

Fourth order polynomial:

$$EJ(\omega) = (q_1 + q_2\omega + q_3\omega^2 + q_4\omega^3 + q_5\omega^4) \quad (5.4)$$

5.2 Curve fitting with θ_1 parameters (improved model)

Parameters to optimize:

In the equations below, the symbol $\{\theta_{1,2}\}$ represents vector of parameters corresponding to θ_1 set with $EJ(\omega)$ expressed as a second-order polynomial. The symbol $\{\theta_{1,3}\}$ represents parameters corresponding to $\{\theta_1\}$ with $EJ(\omega)$ expressed as a third-order polynomial. Similarly for $\{\theta_{1,4}\}$.

$$\begin{aligned}\{\theta_{1,2}\} &= \{\beta, a_1, a_2, q_1, q_2, q_3\}^T \\ \{\theta_{1,3}\} &= \{\beta, a_1, a_2, q_1, q_2, q_3, q_4\}^T \\ \{\theta_{1,4}\} &= \{\beta, a_1, a_2, q_1, q_2, q_3, q_4, q_5\}^T\end{aligned}\tag{5.5}$$

Fitness function:

The fitness function is the same of the previous chapter. The reader can refer to the section “4.2 *Euclidean fitness function*”.

Genetic Algorithm:

	<pre> %Defining variable for optimization problem INIT = [β a1 -a2 q1 q2 q3]; %Setting bounds %Lower boundaries for the variables lb = [0 a1*0.95 -a2*1.05 0 -0.5 -0.5e-3]; %Upper boundaries for the variables ub = [2.5 a1*1.05 -a2*0.95 113 0.5 0.5e-3]; </pre>
$\{\theta_{1,2}\}$	
	<pre> %Defining variable for optimization problem INIT = [β a1 -a2 q1 q2 q3 q4]; %Setting bounds %Lower boundaries for the variables lb = [0 a1*0.95 -a2*1.05 0 -0.5 -0.5e-3 -0.5e-6]; %Upper boundaries for the variables ub = [2.5 a1*1.05 -a2*0.95 113 0.5 0.5e-3 0.5e-6]; </pre>
$\{\theta_{1,3}\}$	
	<pre> %Defining variable for optimization problem INIT = [β a1 -a2 q1 q2 q3 q4 q5]; %Setting bounds %Lower boundaries for the variables lb = [0 a1*0.95 -a2*1.05 0 -0.5 -0.5e-3 -0.5e-6 -0.5e-9]; %Upper boundaries for the variables ub = [2.5 a1*1.05 -a2*0.95 113 0.5 0.5e-3 0.5e-6 0.5e-9]; </pre>
$\{\theta_{1,4}\}$	

Variables
with upper
and lower
bounds

Genetic Algorithm settings	<pre> % GA settings Eq:(4.2) optga=optimoptions('ga',... 'MaxGenerations', 500 , ... 'FunctionTolerance', 1e-6,... 'PopulationSize',500,... 'InitialPopulationMatrix',INIT,... 'PlotFcn',@gaplotbestf); </pre>
-----------------------------------	--

Optimized parameters:

The output from the genetic algorithm solver is the optimized vector of parameters $\{\theta_{1,k}^*\}$, where $k = 1,2,3,4$ refers to the polynomial order chosen for EJ. These optimized parameters are listed in Table 5.1. The optimization problems read:

$$\begin{aligned}
\underset{\theta_{1,2}}{\operatorname{argmin}} \varepsilon = \{\theta_{1,2}^*\} &= \{\beta_{\text{opt}}, a_{1 \text{ opt}}, a_{2 \text{ opt}}, q_{1 \text{ opt}}, q_{2 \text{ opt}}, q_{3 \text{ opt}}\}^T \\
\underset{\theta_{1,3}}{\operatorname{argmin}} \varepsilon = \{\theta_{1,3}^*\} &= \{\beta_{\text{opt}}, a_{1 \text{ opt}}, a_{2 \text{ opt}}, q_{1 \text{ opt}}, q_{2 \text{ opt}}, q_{3 \text{ opt}}, q_{4 \text{ opt}}\}^T \\
\underset{\theta_{1,4}}{\operatorname{argmin}} \varepsilon = \{\theta_{1,4}^*\} &= \{\beta_{\text{opt}}, a_{1 \text{ opt}}, a_{2 \text{ opt}}, q_{1 \text{ opt}}, q_{2 \text{ opt}}, q_{3 \text{ opt}}, q_{4 \text{ opt}}, q_{5 \text{ opt}}\}^T
\end{aligned} \tag{5.6}$$

Diagram Descriptions:

Figure 5.1, Figure 5.2 and Figure 5.3

β represents the loss factor of messenger wire (case $\beta_1 = \beta_2 = \beta$), and a_1 and a_2 correspond to the dimensions illustrated in Figure 4.4. Vertical redlines in figure represent upper and lower bounds of parameters, red cross mark represents initial value of parameters and blue cross mark represents value of optimized parameters.

As for the plots of the dynamic stiffness and phase vs frequency, black lines represent the locus of mean experimental data, dotted lines represent the locus of maximum and minimum experimental data and blue lines represent the optimized model output.

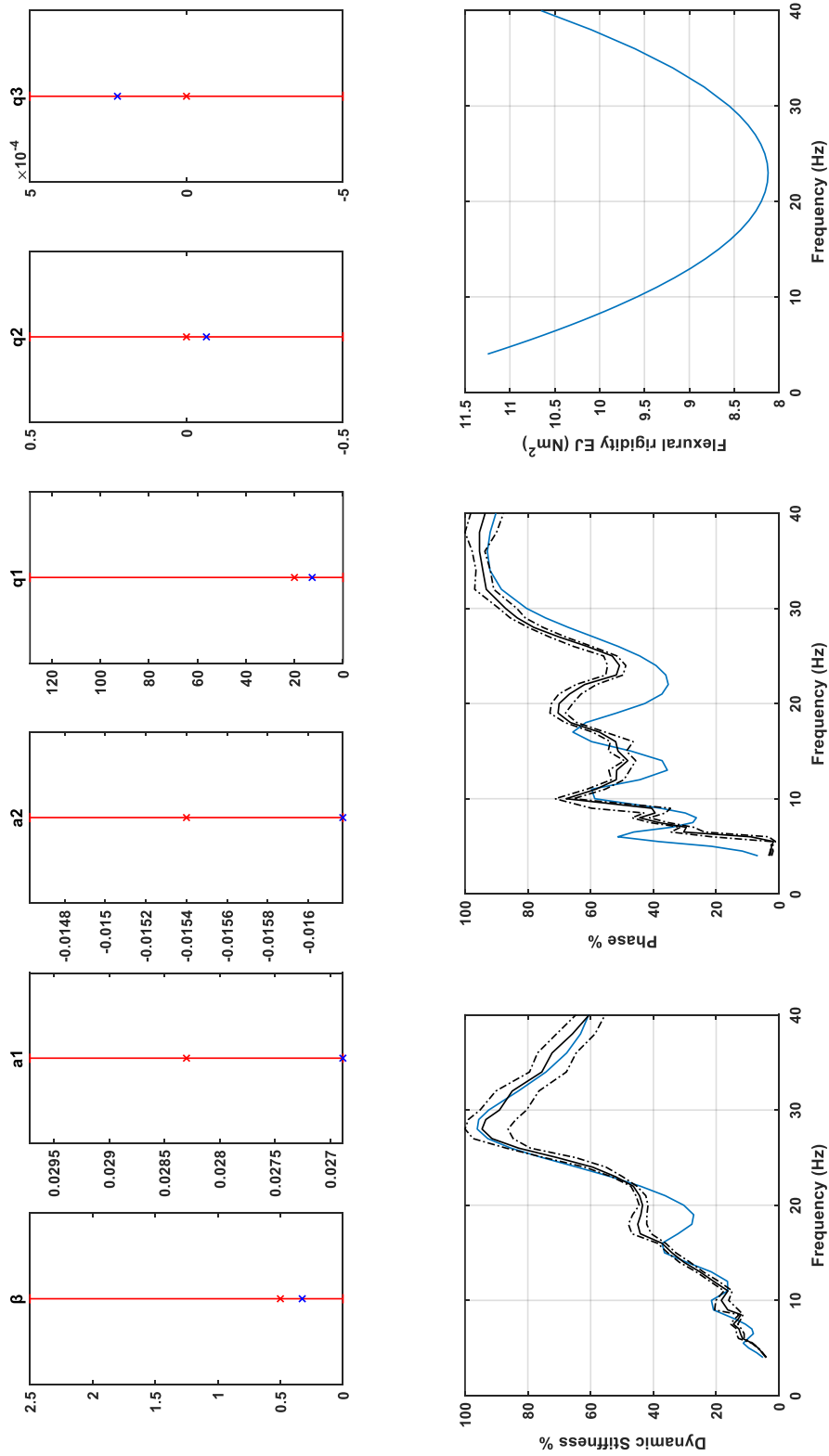


Figure 5.1. Output of genetic algorithm (Damper1, Test1-1, Second order polynomial)

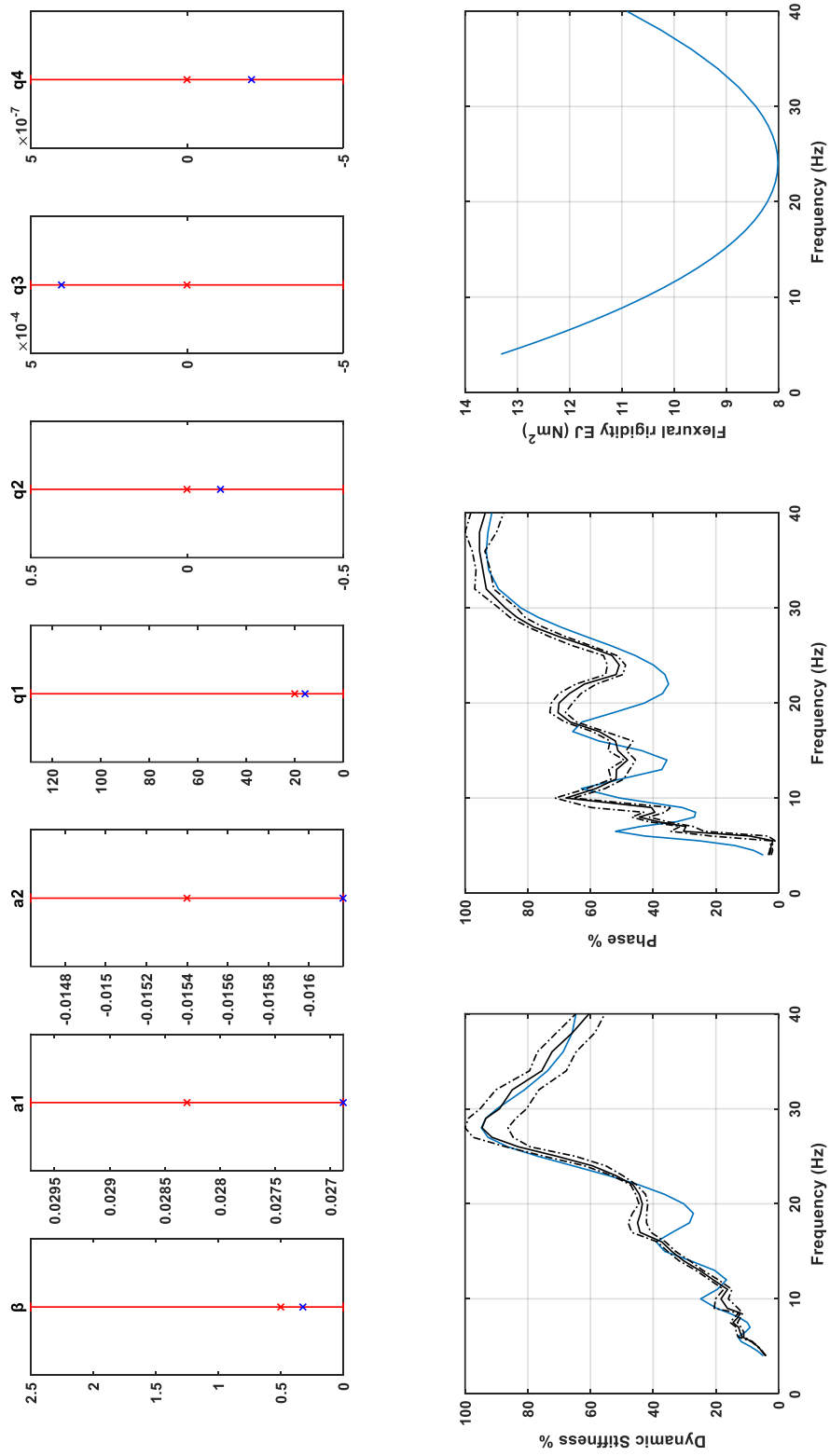


Figure 5.2. Output of genetic algorithm (Damper1, Test1-1, Third order polynomial)

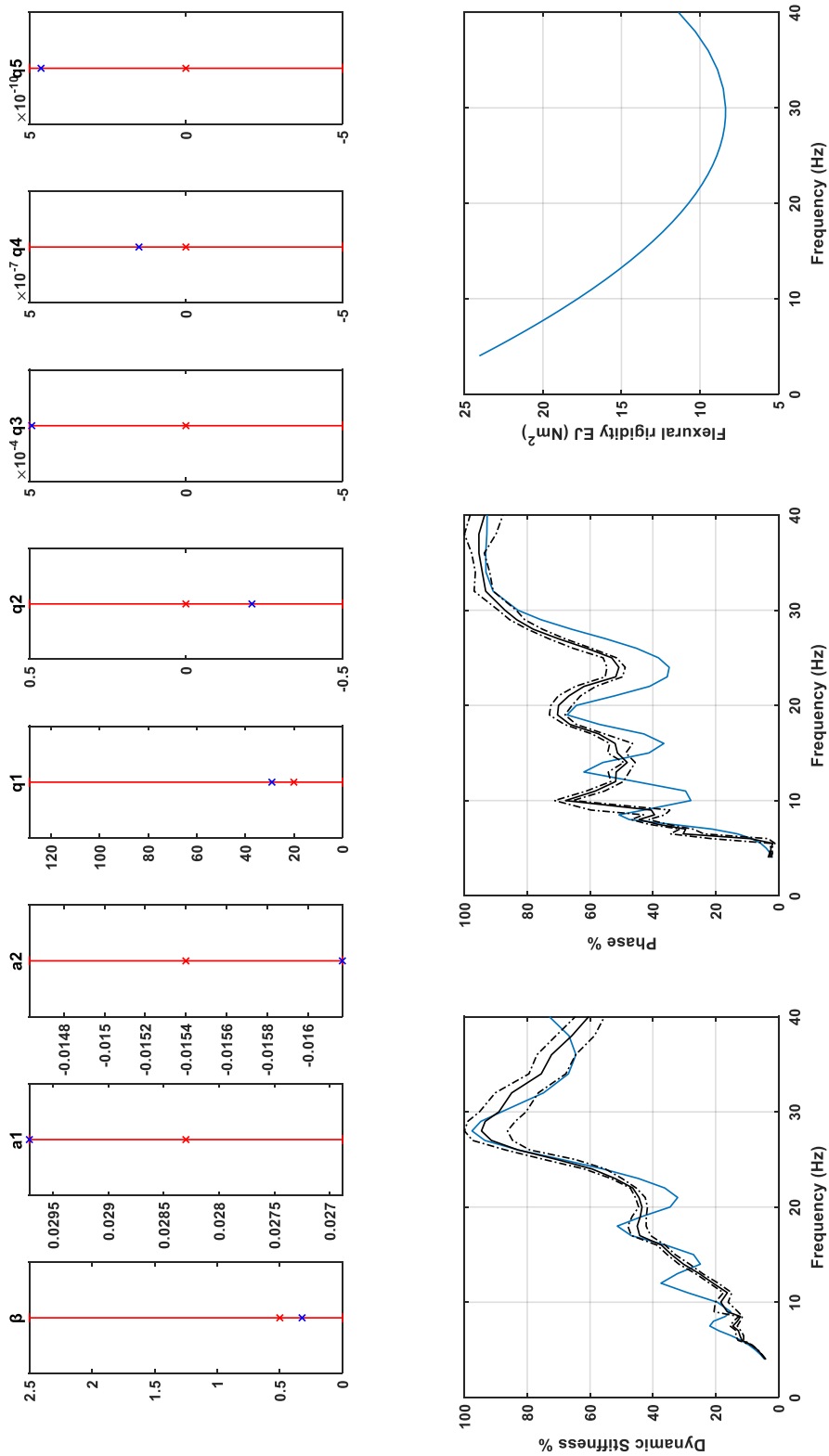


Figure 5.3. Output of genetic algorithm (Damper1, Test1-1, Fourth order polynomial)

5.3 Optimized parameters for improved model

Damper - Test - Displacement p-p (mm)	Set θ_1 , $E(\omega)$ is 2nd order polynomial of frequency						Set θ_1 , $E(\omega)$ is 3rd order polynomial of frequency						Set θ_1 , $E(\omega)$ is 4th order polynomial of frequency								
	β	a1	-a2	q1	q2	q3	β	a1	-a2	q1	q2	q3	q4	β	a1	-a2	q1	q2	q3	q4	q5
Damper1-T(0.1-0.1)	0.15	0.0269	-0.0162	11.99	-2.52E-02	-4.14E-07	0.14	0.0297	-0.0146	39.94	-1.63E-01	5.00E-04	1.20E-07	0.14	0.0297	-0.0151	37.22	-1.33E-01	4.24E-04	6.22E-08	2.50E-10
Damper1-T(0.2-0.2)	0.25	0.0297	-0.0146	38.56	-6.29E-02	-1.32E-04	0.25	0.0297	-0.0146	40.92	-1.15E-01	1.25E-04	-3.48E-07	0.24	0.0297	-0.0146	27.01	6.52E-02	-4.32E-04	0.00E+00	-4.76E-10
Damper1-T(0.3-0.3)	0.27	0.0297	-0.0150	42.54	-2.38E-01	4.97E-04	0.28	0.0297	-0.0162	28.97	-6.94E-02	8.54E-05	-1.98E-07	0.27	0.0297	-0.0153	40.35	-1.98E-01	2.47E-04	4.69E-07	1.61E-10
Damper1-T(0.4-0.4)	0.25	0.0297	-0.0162	32.33	-1.65E-01	3.47E-04	0.26	0.0297	-0.0162	28.13	-1.15E-01	2.44E-04	-1.31E-07	0.26	0.0297	-0.0162	22.95	-2.90E-02	-1.93E-04	4.70E-07	3.74E-10
Damper1-T(0.5-0.5)	0.32	0.0269	-0.0162	17.17	-7.45E-02	2.10E-04	0.33	0.0269	-0.0162	12.80	-2.97E-02	9.13E-05	3.05E-08	0.32	0.0269	-0.0162	14.10	-1.75E-02	-9.59E-05	4.00E-07	4.54E-10
Damper1-T(1-1)	0.33	0.0269	-0.0162	12.71	-6.36E-02	2.21E-04	0.32	0.0269	-0.0162	15.76	-1.07E-01	4.02E-04	-2.06E-07	0.32	0.0297	-0.0162	29.04	-2.11E-01	4.92E-04	1.50E-07	4.63E-10
Damper1-T(2-2)	0.38	0.0297	-0.0162	24.86	-1.91E-01	4.98E-04	0.36	0.0283	-0.0162	10.58	-5.20E-02	1.00E-04	3.12E-07	0.36	0.0276	-0.0162	8.63	-2.03E-02	-4.40E-05	4.51E-07	1.87E-10
Damper1-T(1-1)-Oiled	0.35	0.0297	-0.0162	17.61	-1.56E-01	4.69E-04	0.32	0.0297	-0.0162	10.79	-8.44E-02	3.06E-04	-8.35E-08	0.35	0.0297	-0.0162	16.80	-1.34E-01	2.99E-04	4.87E-07	-3.56E-10
Damper1-T(2-1)	0.34	0.0269	-0.0162	9.72	-3.18E-02	1.36E-04	0.33	0.0269	-0.0162	17.24	-1.24E-01	4.47E-04	-2.16E-07	0.34	0.0269	-0.0162	8.54	-9.77E-04	-6.39E-05	3.80E-07	-8.49E-12

Table 5.1. Optimized parameters from improved model

5.4 Conclusion on improved model

The curve fitting is consistent across Test1-1, Test2-1, and Test2-2 when using set $\{\theta_1\}$ parameters with EJ as a constant and $EJ(\omega)$. However, there is an enhancement in curve fitting for Test0.5-0.5, Test0.4-0.4, Test0.3-0.3, Test0.2-0.2, and Test0.1-0.1, addressing the previous limitation of EJ remaining constant.

Figure 5.4 illustrates how flexural stiffness varies with frequency for different polynomial orders of $EJ(\omega)$. It is worth noting that the second and third-order polynomials of $EJ(\omega)$ exhibit slight variations around a constant EJ.

For displacements greater than or equal to 1mm (p-p), curve fitting using set $\{\theta_1\}$ parameters with a constant EJ is appropriate. If the displacement is less than 1mm (p-p), using set $\{\theta_1\}$ parameters where $EJ(\omega)$ is second or third-order polynomial provides a better fit. No significant improvement has been found instead when using a fourth-order polynomial representation.

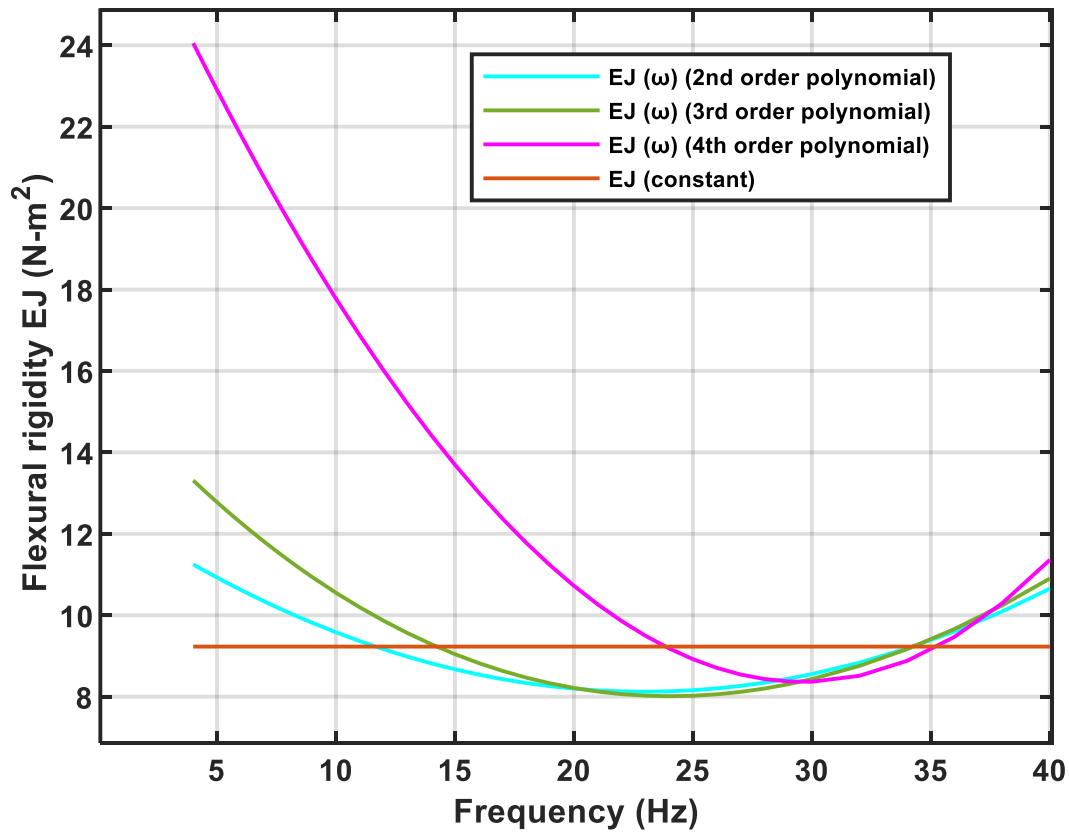
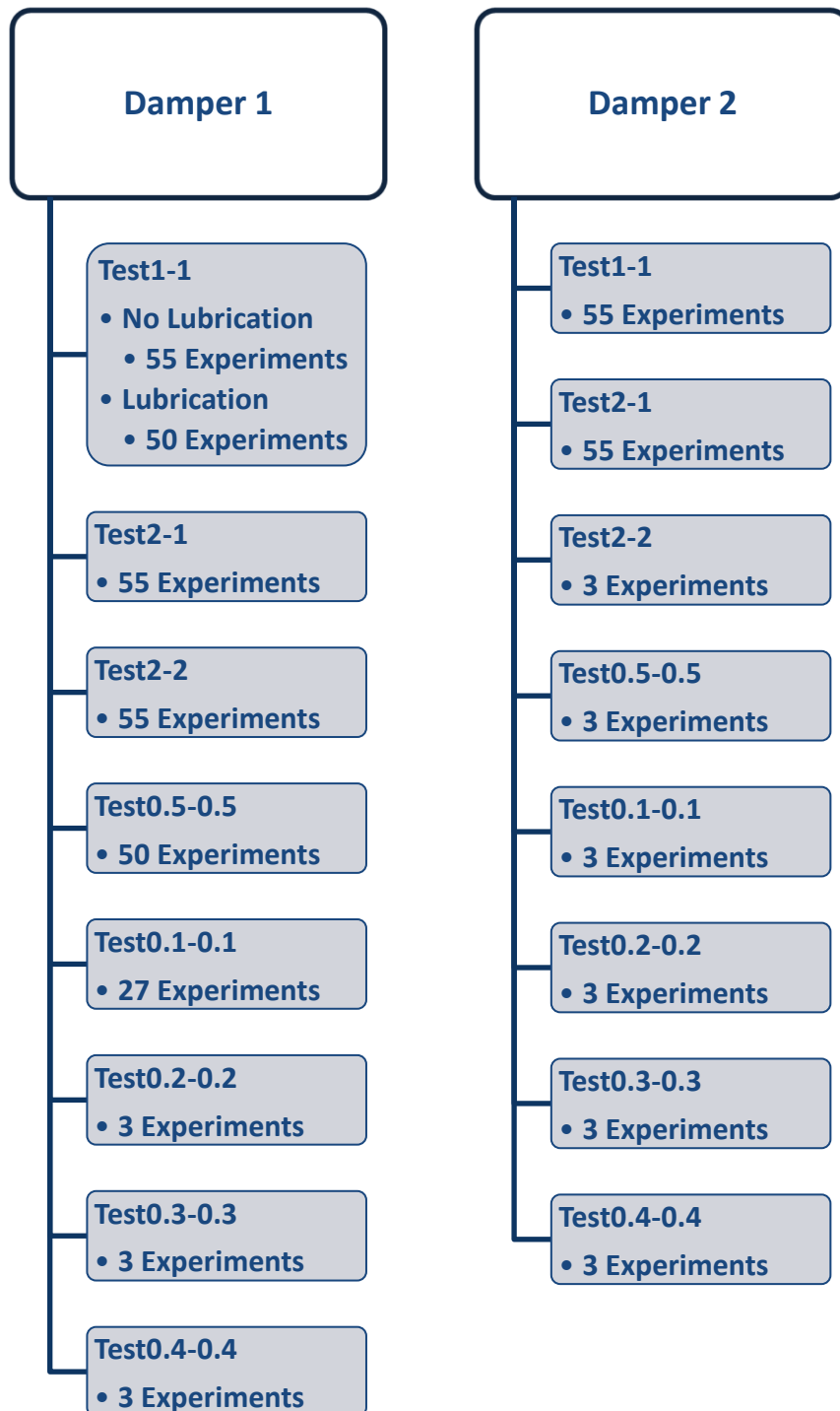


Figure 5.4. Flexural rigidity (EJ) vs frequency

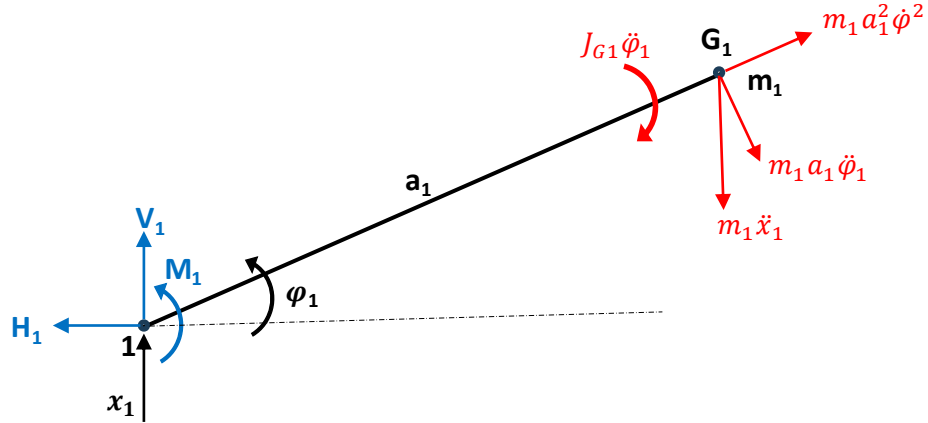
Appendix

A. Tests on dampers

A total of 429 experiments have been conducted, here summarized.



B. Lumped mass contribution



Free body diagram for mass

Forces and moments at node 1

$$(m_1 a_1^2 + J_{G1}) \ddot{\phi}_1 + m_1 a_1 \ddot{x}_1 \cos \phi_1 = M_1$$

$$m_1 \ddot{x}_1 + m_1 a_1 \ddot{\phi}_1 \cos \phi_1 - m_1 a_1 \dot{\phi}_1^2 \sin \phi_1 = V_1$$

$$m_1 a_1 \ddot{\phi}_1 \sin \phi_1 + m_1 a_1 \dot{\phi}_1^2 \cos \phi_1 = H_1$$

For small angle $\cos \phi_1 \sim 1$ and $\sin \phi_1 \sim \phi_1$

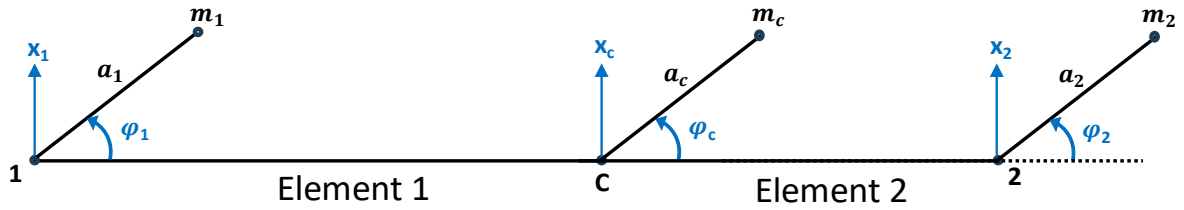
$$J_1 \ddot{\phi}_1 + m_1 a_1 \ddot{x}_1 = M_1$$

$$m_1 \ddot{x}_1 + m_1 a_1 (\ddot{\phi}_1 - \phi_1 \dot{\phi}_1^2) = V_1$$

$$m_1 a_1 (\ddot{\phi}_1 \phi_1 + \dot{\phi}_1^2) = H_1$$

Eq: 1

Where $J_1 = J_{G1} + m_1 a_1^2$



Finite element model for stockbridge (Euler Bernoulli)

Shape functions:

$$N_1 = 1 - \frac{3y^2}{l^2} + \frac{2y^3}{l^3}$$

$$N_2 = y - \frac{2y^2}{l} + \frac{y^3}{l^2}$$

$$N_3 = \frac{3y^2}{l^2} - \frac{2y^3}{l^3}$$

$$N_4 = -\frac{y^2}{l} + \frac{y^3}{l^2}$$

Displacement and rotation at node 1

$$x(y, t) = \{N(y)\}^T \{X(t)\}$$

$$\varphi(y, t) = \frac{\partial x(y, t)}{\partial y} = \{N'(y)\}^T \{X(t)\}$$

Initial condition: $y = 0$ (node 1)

$$x(0, t) = x_1(t) = \{N(0)\}^T \{X(t)\}$$

$$\varphi(0, t) = \varphi_1(t) = \{N'(0)\}^T \{X(t)\}$$

$$x_1 = \{N(0)\}^T \{X\}$$

$$\varphi_1 = \{N'(0)\}^T \{X\}$$

$$\dot{x}_1 = \{N(0)\}^T \{\dot{X}\}$$

$$\dot{\varphi}_1 = \{N'(0)\}^T \{\dot{X}\}$$

$$\ddot{x}_1 = \{N(0)\}^T \{\ddot{X}\}$$

$$\ddot{\varphi}_1 = \{N'(0)\}^T \{\ddot{X}\}$$

Computing work at node 1 and neglecting H_1 (No work produced) and substituting $x(y, t)$, $\varphi(y, t)$, $\dot{x}(y, t)$, $\dot{\varphi}(y, t)$, and $\ddot{x}(y, t)$, $\ddot{\varphi}(y, t)$ in Eq: 1.

Work produced by moment at node 1:

$$M_1 \delta \varphi_1 = (J_1 \ddot{\varphi}_1 + m_1 a_1 \ddot{x}_1) \delta \varphi_1$$

$$\delta \varphi_1 = \{N'(0)\}^T \{\delta X\}$$

$$M_1 \delta \varphi_1 = J_1 \{\ddot{X}\}^T \{N'(0)\} \{N'(0)\} \{\delta X\} + m_1 a_1 \{\ddot{X}\}^T \{N(0)\} \{N'(0)\} \{\delta X\}$$

$$M_1 \delta \varphi_1 = \{\ddot{X}\}^T \left(\begin{bmatrix} 0 & 0 & 0 & 0 \\ 0 & J_1 & 0 & 0 \\ 0 & 0 & 0 & 0 \\ 0 & 0 & 0 & 0 \end{bmatrix} + \begin{bmatrix} 0 & m_1 a_1 & 0 & 0 \\ 0 & 0 & 0 & 0 \\ 0 & 0 & 0 & 0 \\ 0 & 0 & 0 & 0 \end{bmatrix} \right) \{\delta X\}$$

Work produced by force at node1:

$$V_1 \delta X_1 = (m_1 \ddot{x}_1 + m_1 a_1 (\ddot{\varphi}_1 - \varphi_1 \dot{\varphi}_1^2)) \delta X_1$$

$$\delta W_1 = \{N(0)\}^T \{\delta X\}$$

$$V_1 \delta X_1 = m_1 \{\ddot{X}\}^T \{N(0)\} \{N(0)\}^T \{\delta X\} + m_1 a_1 \{\ddot{X}\}^T \{N'(0)\} \{N(0)\}^T \{\delta X\} \\ - m_1 a_1 \{X\}^T \{N'(0)\} \{\dot{X}\}^T \{N'(0)\} \{N'(0)\}^T \{\dot{X}\} \{N'(0)\}^T \{\delta X\}$$

$$V_1 \delta X_1 = \{\ddot{X}\}^T \left(\begin{bmatrix} m_1 & 0 & 0 & 0 \\ 0 & 0 & 0 & 0 \\ 0 & 0 & 0 & 0 \\ 0 & 0 & 0 & 0 \end{bmatrix} + \begin{bmatrix} 0 & 0 & 0 & 0 \\ m_1 a_1 & 0 & 0 & 0 \\ 0 & 0 & 0 & 0 \\ 0 & 0 & 0 & 0 \end{bmatrix} \right) \{\delta X\}$$

Total work produced at node1 by forces and moments:

$$M_1 \delta \varphi_1 + V_1 \delta X_1 = \{\ddot{X}\}^T \left(\begin{bmatrix} m_1 & m_1 a_1 & 0 & 0 \\ m_1 a_1 & J_1 & 0 & 0 \\ 0 & 0 & 0 & 0 \\ 0 & 0 & 0 & 0 \end{bmatrix} \right) \{\delta X\}$$

Similarly for node c.

$$M_c \delta \varphi_c + V_c \delta X_c = \{\ddot{X}\}^T \left(\begin{bmatrix} 0 & 0 & 0 & 0 \\ 0 & 0 & 0 & 0 \\ 0 & 0 & m_c & m_c a_c \\ 0 & 0 & m_c a_c & J_c \end{bmatrix} \right) \{\delta X\}$$

Lumped mass contribution from element 1:

$$[M_{Lump,e1}] = \begin{bmatrix} m_1 & m_1 a_1 & 0 & 0 \\ m_1 a_1 & J_1 & 0 & 0 \\ 0 & 0 & m_c & m_c a_c \\ 0 & 0 & m_c a_c & J_c \end{bmatrix}$$

Lumped mass contribution from element 2, node 2

$$[M_{Lump,e2}] = \begin{bmatrix} 0 & 0 & 0 & 0 \\ 0 & 0 & 0 & 0 \\ 0 & 0 & m_2 & m_2 a_2 \\ 0 & 0 & m_2 a_2 & J_2 \end{bmatrix}$$

C. MATLAB - 6 DOF model

%Mass Matrix Element-1 6x6

```
M1= mm1/420*
    [156      22*l1      54      -13*l1      0      0;
     22*l1     4*l1^2     13*l1     -3*l1^2     0      0;
      54      13*l1     156     -22*l1      0      0;
     -13*l1    -3*l1^2    -22*l1     4*l1^2     0      0;
      0         0         0         0         0      0;
      0         0         0         0         0      0];
```

%Mass Matrix Element-2 6x6

```
M2= mm2/420*
    [0      0      0      0      0      0;
     0      0      0      0      54      0;
     0      0     156     22*l2     13*l2    -13*l2;
     0      0     22*l2     4*l2^2     156    -3*l2^2;
     0      0      54     13*l2    -22*l2    -22*l2;
     0      0    -13*l3    -3*l3^2   -22*l2^4*l2^2;  4*l2^2];
```

%Lumped Mass Contribution 6x6

```
Mmass= diag([m1 J1+m1*a1^2 mc Jc m2 J2+m2*a2^2])+
        diag([m1*a1 0 0 0 m2*a2],1)+
        diag([m1*a1 0 0 0 m2*a2],-1);
```

%Global Mass Matrix

```
M= M1 + M2+ Mmass;
```

%Decomposition of mass matrix

```
MLL= [M(1:2,1:2) M(1:2,5:6) ; M(5:6,1:2) M(5:6,5:6)];
MVL= [M(3:4,1:2) M(3:4,5:6)];
MLV= [M(1:2,3:4) ;M(5:6,3:4)];
MVV= [M(3:4,3:4)];
```

%Stiffness Matrix Element-1 6x6

```
K1=EmJm*
    [12/l1^3      6/l1^2     -12/l1^3      6/l1^2      0      0;
     6/l1^2       4/l1       -6/l1^2       2/l1      0      0;
    -12/l1^3     -6/l1^2     12/l1^3     -6/l1^2     0      0;
     6/l1^2       2/l1       -6/l1^2       4/l1      0      0;
      0           0           0           0         0      0;
      0           0           0           0         0      0];
```

%Stiffness Matrix Element-2 6x6

```
K2=EmJm*
    [0      0      0      0      0      0;
     0      0      0      0; 0      0;
     0      0     12/l2^3     6/l2^2    -12/l2^3     6/l2^2;
     0      0     6/l2^2      4/l2     -6/l2^2      2/l2;
     0      0    -12/l2^3    -6/l2^2     12/l2^3    -6/l2^2];
```

0 0 6/l2^2 2/l2 -6/l2^2 4/l2]

%Global Stiffness Matrix

K= K1 + K2

%Decomposition of stiffness matrix

KLL= [K(1:2,1:2) K(1:2,5:6) ; K(5:6,1:2) K(5:6,5:6)];
KVL= [K(3:4,1:2) K(3:4,5:6)];
KLV= [K(1:2,3:4) ;K(5:6,3:4)];
KVV= [K(3:4,3:4)];

% Cycle: Damping is a function of ω (frequency)

forceOverDisp=zeros(1,length(f));

for j=1:length(f)
w=wtot(j);

%Damping matrix (Structural damping) C = (β/ω)*K 6x6

C = $\beta_1/w*[K1] + \beta_2/w*[K2]$;

% Decomposition of damping matrix

CLL= [C(1:2,1:2) C(1:2,5:6);C(5:6,1:2) C(5:6,5:6)];
CVL= [C(3:4,1:2) C(3:4,5:6)];
CLV= [C(1:2,3:4) ; C(5:6,3:4)];
CVV= [C(3:4,3:4)];

%A,B,C,D coefficients

A=-w^2*MLL+1i*w*CLL+KLL;
B=-(-w^2*MLV+1i*w*CLV+KLV);
C1=-w^2*MVL+1i*w*CVL+KVL;
D=-(-w^2*MVV+1i*w*CVV+KVV);

% Impedance Matrix

H=C1*(A\B)-D;
forceOverDisp(j)=H(1,1);

end

References

- [1] Patent Number 1,675,391, "Vibration Damper."
- [2] Laneville, "An Experimental Study of the Aeolian Vibrations of a Flexible Circular Cylinder at Different Incidences," *Journal of Fluids and Structures*, vol. 9, pp. 371-391, May 1995.
- [3] Strouhal, E. (1878). "Über die periodischen Erscheinungen in den Bewegungen der in der Luft schwingenden Stäbe." *Annalen der Physik*, vol. 234, no. 12, pp. 507-528.
- [4] R. Claren and G. Diana's research on mathematical analysis of transmission line vibration was published in "IEEE Trans Power Apparatus Syst" in 1969. Their additional work on tests conducted on span and on the shaker is documented in "IEEE Transactions on Power Delivery," vol. 18, no. 4, October 2003.
- [5] Barbieri, N., et al. "Dynamical Analysis of Transmission Lines Cables: Part 1 – Linear Theory," *Mecha Syst Sig Process*, 2004
- [6] Diana, G., Falco, M., Cigada, A., et al. "On the Measurement of Overhead Transmission Lines Conductor Self-Damping," *IEEE Trans Power Apparatus Sys*, 2000, pp. 285–292.
- [7] Kim, C-J. "Design Sensitivity Analysis of a Stockbridge Damper to Control Resonant Frequencies," Department of Mechanical Design Engineering, Pukyong National University, March 2017.
- [8] Leblond, A., Hardy, C. "On the Estimation of a 2 x 2 Complex Stiffness Matrix of Symmetric Stockbridge-Type Dampers," *proc. 3rd Int. Symp. Cable Dynamics*, Trondheim, Norway, Aug. 1999.
- [9] Diana, G., et al. "Stockbridge-Type Damper Effectiveness."
- [10] Marco Onore. "Smorzatore Stockbridge e Soppressione Delle Vibrazioni Dei Cavi Tesi: Analisi Numerica e Sperimentale."
- [11] Meirovitch, Leonard. *Elements of Vibration Analysis – Finite Element Method*.
- [12] Genta, G. *Vibration Dynamics and Control*.